THE RELATIONSHIP OF MICROSTRUCTURE TO MONOTONIC AND CYCLIC STRAINING IN TWO ALUMINUM-ZINC-MAGNESIUM PRECIPITATION HARDENING ALLOYS

A THESIS

Presented to

The Faculty and Graduate Division

by

Thomas Henry B. Sanders, Jr.

In Partial Fulfillment

of the Requirements for the Degree

Doctor of Philosophy

in the School of Chemical Engineering

Georgia Institute of Technology

November, 1974

THE RELATIONSHIP OF MICROSTRUCTURE

TO MONOTONIC AND CYCLIC STRAINING

IN TWO ALUMINUM-ZINC-MAGNESIUM

PRECIPITATION HARDENING ALLOYS

Approved:

Dr. Edgar A. Starke, Jr.
Chairman

Date Approved: February 14, 1975

ACKNOWLEDGMENTS

The author wishes to express his sincere appreciation to his thesis advisor, Dr. Edgar A. Starke, Jr., without whom this work could not have been completed. He is indebted to Professor Starke for suggesting the problem, the numerous stimulating discussions, and his constant encouragement throughout the investigation.

He would also like to thank Dr. B. G. LeFevre and Dr. P. Muije for their helpful discussions and for having taken the time to review this work. He also wishes to thank Dr. W. E. Moody, Jr., Dr. R. F. Hochman and Dr. D. Kalish for participating on the oral examining committee. The discussion with Dr. M. Marek while the work was in progress is also greatly appreciated.

The author would like to thank the Alcoa Technical Center for preparing the alloys used in this research and for the numerous discussions with the members of the staff, particularly, Mr. J. T. Staley and Mr. H. Y. Hunsicker.

Mr. Charles Blackwood of the Chemical Engineering and Metallurgy Machine Shop deserves much credit for the construction of apparatus and preparation of samples. The capable typing of Mrs. D. Rakestraw is gratefully acknowledged.

The author would also like to thank his colleagues and friends Messrs. J. G. Rinker and H. G. Paris and Dr. S. B. Chakrabortty for their assistance and support during this investigation.

The financial support of the Alcoa Foundation, the Air Force

Office of Scientific Research, under contract Number F4-2614, and the Financial Aid Office of the Georgia Institute of Technology are gratefully acknowledged.

TABLE OF CONTENTS

TABLE OF CONTENTS (continued)

LIST OF FIGURES

LIST OF FIGURES (continued)

LIST OF FIGURES (continued)

LIST OF FIGURES (continued)

LIST OF FIGURES (continued)

LIST OF FIGURES (continued)

LIST OF FIGURES (continued)

LIST OF TABLES

SUMMARY

The effect of microstructure on the monotonic and low cycle fatigue properties of a high purity, large grain, ternary aluminum-zinc-magnesium (Al-Zn-Mg) alloy and a high strength 7050 aluminum alloy was investigated.

The number of steps in the precipitation sequence: super-saturated, solid solution → Guinier Preston (G.P.) zones → η' → η ($MgZn_2$) were unaltered by the presence of copper in the 7050 alloy. Copper and aluminum were thought to enter directly into the zone formation. The presence of copper and aluminum in the zones were justified on the basis of the electron:atom stability of the Friauf-Laves $MgZn_2$ structure. The presence of copper in the alloys increased the G.P. solvous temperature, presumably by a reduction in the barrier to nucleation.

The microstructure that produced the highest static strength while maintaining good ductility occurred when the ternary alloy was aged at 150°C to produce a maximum number of semicoherent η' precipitates which had a Guinier radius of approximately 65A. Aging at 120°C increased the frequency of nucleation and a greater tendency toward brittle fracture as shown by the brittle nature when the ternary alloy was aged at 120°C. The highest static yield strength was obtained when 7050 was double aged to produce a high density of small, semicoherent (40 A) η' precipitates.

The monotonic fracture behavior of the ternary alloy progressively changed with aging from ductile microvoid coalesence to brittle, low energy intergranular separation. This contrasted to the ductile, transgranular fracture nature of 7050 alloy under similar aging conditions. The brittle nature of the ternary alloy was related to the large grain size. The nonhomogeneous deformation associated with the large grain ternary alloy produced large slip steps at the grain boundaries which induced large stress concentrations across the grain boundaries.

Fatigue behavior was found to be sensitive to aging in both alloys investigated. The best combination of fatigue life, strength and ductility for the ternary alloy resulted when aged to produce a microstructure containing predominately η' having a Guinier radius of approximately 70 A and a small amount of incoherent η ($MgZn_2$). Superior fatigue life, strength and ductility were found when the 7050 alloy was aged to produce the maximum number of partially coherent η' precipitates having a Guinier radius approximately 35 A. Aging the 7050 alloy to produce particles of about 50 A gave a microstructure that had poor fatigue properties at the low plastic strain amplitudes, $\frac{\Delta\varepsilon_p}{2}$ <1.0 per cent.

The empirical Coffin-Manson relation was found to adaquately describe the fatigue behavior when the deformation process did not depend upon the plastic strain amplitude.

CHAPTER I

INTRODUCTION

The discovery of age hardening in 1905[1] has been followed by numerous investigations of the kinetics, growth and distribution of the precipitates with the ultimate goal being the production of high strength alloys. These studies have produced many aluminum alloy systems which have found great usage in the aircraft industry where a high strength to weight ratio is of paramount importance. The application of these alloys in aircraft structures, however, has shown that the aluminum alloys which show the highest static strength are inherently susceptible to stress corrosion cracking[2,3,4], have poor fracture toughness properties[5], and typically exhibit poor fatigue performance, all of which are acute problems in aircraft structures[6].

The prospect for improving the stress corrosion resistance, and fracture toughness without sacrificing the initial high static strength appears promising[7,8,9]. There have been limited improvements in fatigue properties obtained by thermo-mechanical processing[10,11,12] of the precipitation hardening alloys. These small gains, however, have been generally the result of metallurgical processing changes for other reasons[13]. The actual mechanisms associated with fatigue are not well understood. The subtle interactions of the precipitates, grain boundaries, inclusions, alloy composition, and grain size and morphology under reversed loading have not been clearly established.

It was the purpose of this study to investigate the fatigue behavior of two 7XXX aluminum alloys by varying the aging temperature, time and composition, to systematically determine the microstructure that is best suited for reversed loading, through the understanding of the phenomena of fatigue in terms of basic principles.

CHAPTER II

REVIEW OF THE LITERATURE

The Phase Relations

The equilibrium phase relations in the aluminum rich Al-Zn-Mg system have been established by previous investigators[14-22]. Figure 1 shows the binary phase diagrams of the Al-Zn, Al-Mg, and Mg-Zn systems, along with the room temperature isotherm of the ternary system. The phase boundaries at 200°C are shown in Figure 2. Superimposed on this are the limits of solid solubility at 300, 350, and 400°C. Also indicated on the diagram is one of the compositions to be investigated. It can easily be seen from Figure 2 that homogenization of the alloy can be accomplished at 400°C.

The Decomposition Process

Precipitation reactions in the Al-Zn-Mg system can be summarized by the following sequence of events after the quench[23-29]:

$$\text{Super saturated, solid solution} \xrightarrow[\text{Temp. } <200^\circ\text{C}]{\eta} \text{G-P zones} \rightarrow \text{G-P Compounds } (\eta') \xrightarrow[\text{Temp. } > 200^\circ\text{C}]{T}$$

where, η is the incoherent, intermetallic compound $MgZn_2$ and T the ternary $(Al,Zn)_{49}Mg_{32}$ compound.

As the temperature of an alloy is raised, the solubility of the solutes increases until a temperature is reached when all are com-

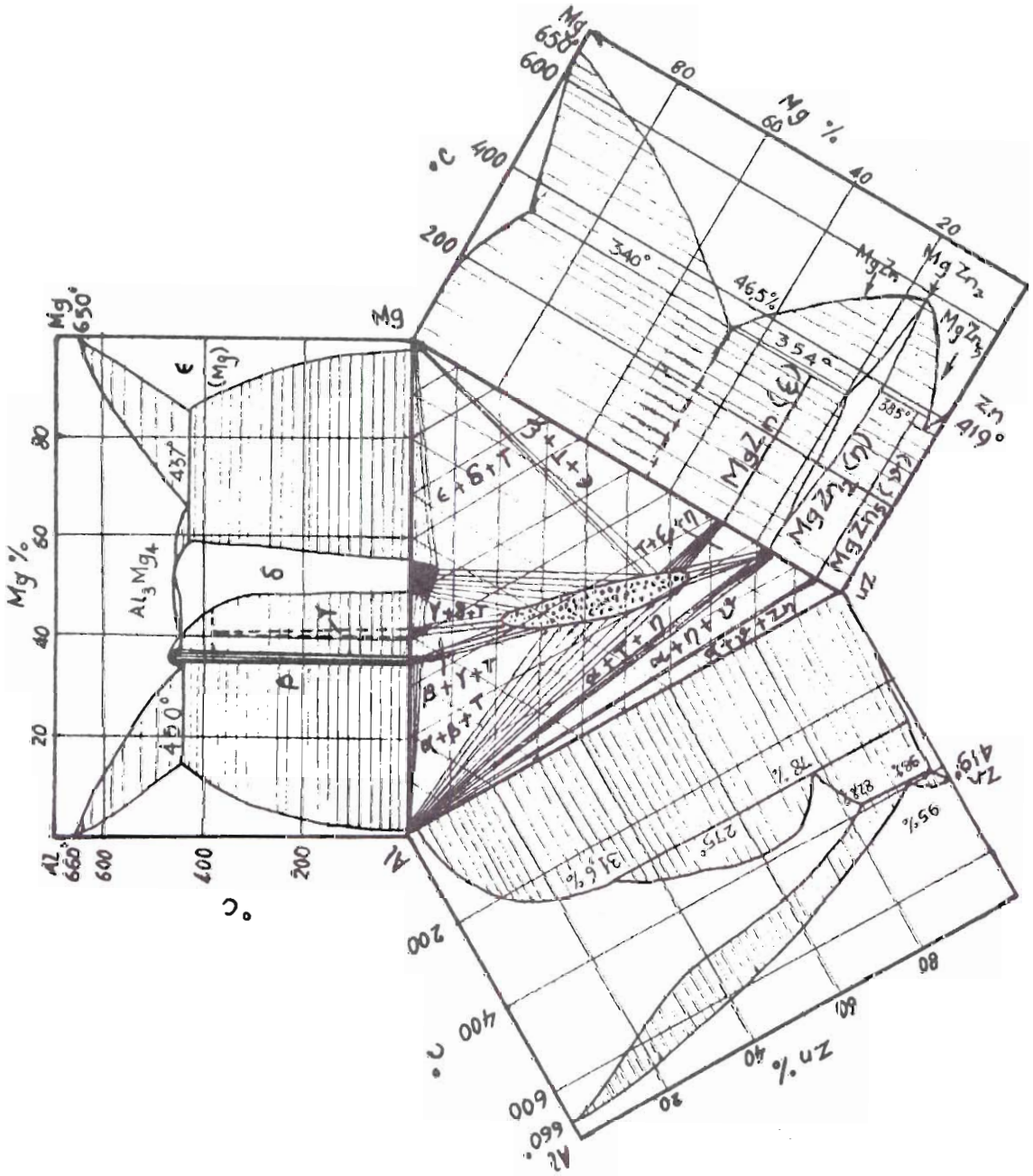

Figure 1. Equilibrium Phase Relationships in the Ternary Al-Zn-Mg System[16].

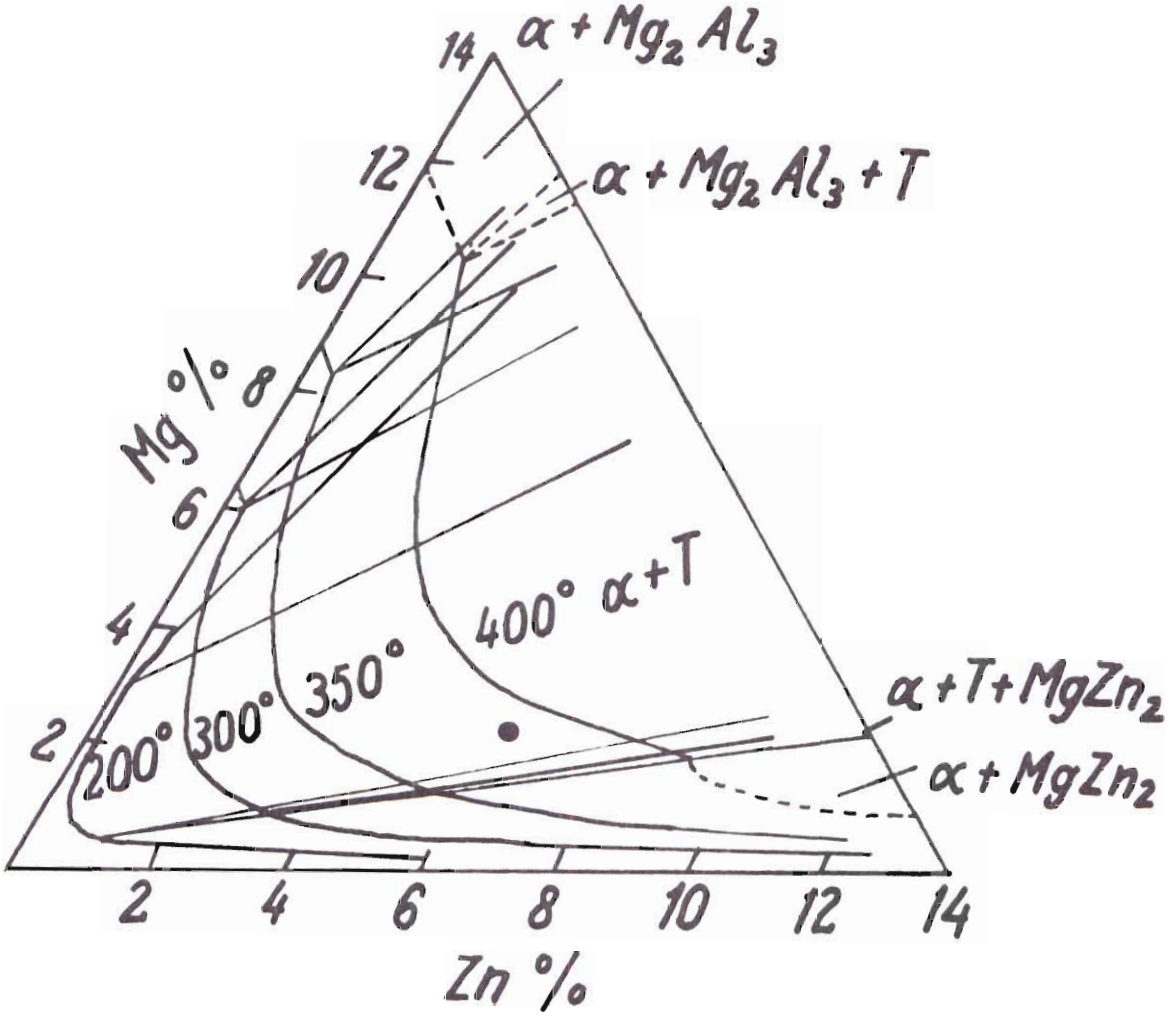

Figure 2. Constitution Diagram of the Ternary Al-Zn-Mg System at Various Temperatures[16].

pletely in solution, as predicted by the phase diagram. However, there are statistical fluctuations of concentration in the matrix which aid in the formation of nuclei[30,31] upon quenching to low temperature. The statistical fluctuations are due to regions of short-range-order (SRO) which arise out of a preference for like neighbors. Additionally, there is an increase in vacancy concentration as the temperature is raised and upon rapid quenching a supersaturation of vacancies can be obtained.

Quenching from above the solvus temperature and holding at room temperature (natural aging) or elevated temperature (artifical aging) produces a transition structure called Guinier-Preston (G-P) zones. The zones are initally spherical in Al-Zn-Mg alloys and increase in size with aging. There is an increase in hardness which accompanies the increase in size. Continued aging of the alloy below a critical temperature[24] transforms the zones into platelets called η'. The structure belongs to the space group $P2_1/m$[32] and has the lattice parameters:

$$a = b = 4.97A,\ c = 5.54A,\ \text{and}\ \gamma = 120°$$

The orientation of the monoclinic unit cell is related to the matrix by:

$$(001)_{\eta'} \,||\, (1\bar{1}\bar{1})_{Al},\ (100)_{\eta'} \,||\, (110)_{Al}.$$

The precipitates are partially coherent along the basal planes, but incoherent along the c direction of the precipitate, since there is a misfit of approximately 7 per cent. The structure of η' is composed

of alternate layers of zinc and magnesium and an atomic ratio of zinc to magnesium of 2:1. If the alloy is such that $N_{Mg} \neq 0.5N_{Zn}$, then the species in excess will cluster and contribute to the overall hardening of the α phase[23]. This two zone hypothesis has been used by Gould and Starke[33] to explain diffraction effects after reversion in 12.9 per cent Zn 0.66 per cent Mg alloys. They found that an unreverted portion persisted in the small angle scattering (SAS) curves long after reversion.

Persistent aging produces an incoherent precipitate η[34]. The η grows at the expense of η' and forms the stable, $MgZn_2$ compound. The reduction of partial coherency between the matrix and the precipitate results in a drop in hardness with time. Extended periods of aging produces a Widemanstätten structure of η on the {111} planes of primary α.

Friauf-Laves Phases of Magnesium Zinc, Copper and Aluminum

The Friauf-Laves phases denote a large class of related close-packed, intermetallic compounds approximated by the formula AB_2[35-38]. The stacking sequence is based upon the six possible compound layers of the Friauf-Laves phases as shown in Figure 3. The phases crystallize into one of the three structural types. The $MgCu_2$ structure (C15) is cubic, space group Fd3m with ABCABC...packing sequence, $MgZn_2$ (C14) and $CuMg_2Zn_3$ (C36) structures are hexagonal, space group $P6_3/mmc$ with packing sequences AB'AB'... and AB'A'C..., respectively. Figure 4 shows the arrangement of the A and B atoms in the three Friauf-Laves

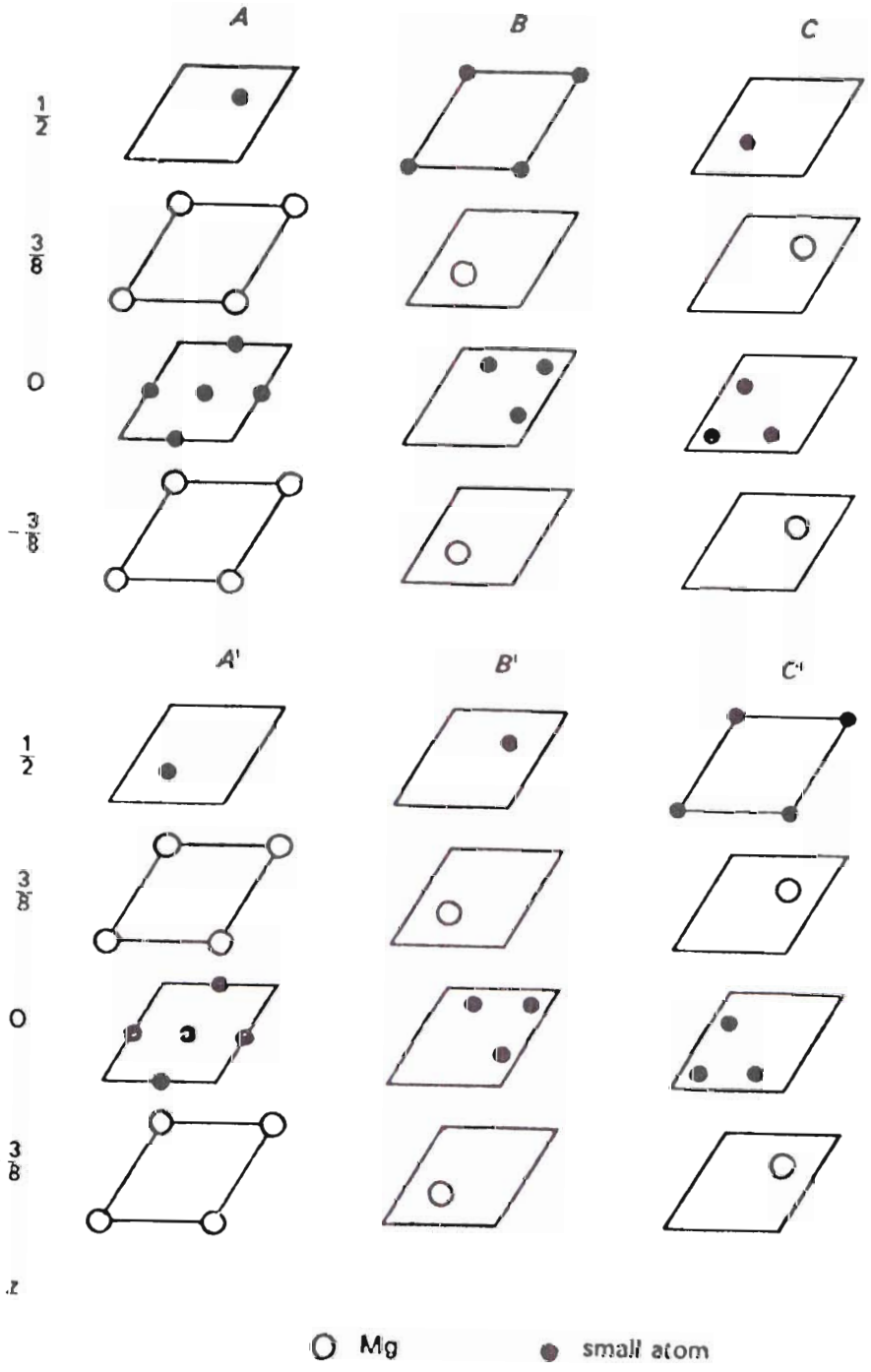

Figure 3. Six Types of Compound Layers of the Friauf-Laves Phases[39].

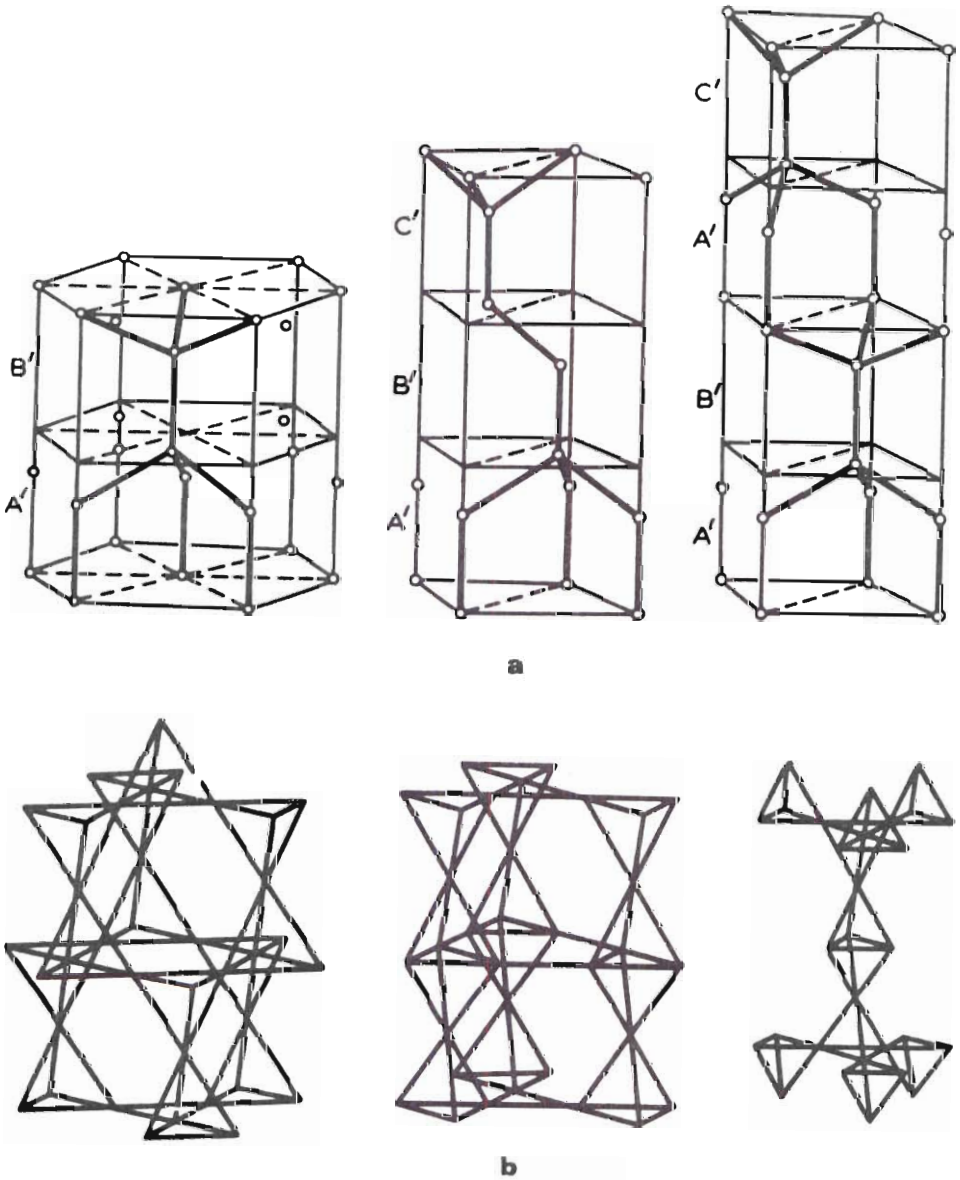

Figure 4. (a) The Arrangement of Atoms in the Three Friauf-Laves Phases[40].

(b) The Tetrahedral Arrangement of the B Atoms in the Friauf-Laves Phases[40].

phase structures[40].

Tabulated values of the Laves phases[40] have shown that in most cases the formation and stability of a particular structure will depend in part on the d_A/d_B ratio (atomic diameters). If the deviation is either greater or less than 1.225 (ideal hard sphere packing) the C15 ($MgCu_2$) structure predominates. Research[38,41] on the progressive replacement of copper in $MgCu_2$ and zinc in $MgZn_2$ structures by elements of lower and higher electron:atom ratio indicated the structure progression:

$$C36 \rightarrow C15 \rightarrow C36 \rightarrow C14$$

occured as the electron:atom ratio increased from:

$$0.92 \rightarrow (1.08 - 1.76) \rightarrow (1.81 - 1.92) \rightarrow > 2.0.$$

For example, when zinc is replaced by Al[38], the size effect favors the formation of $MgCu_2$ type structure, but is opposed by an increase in the electron:atom ratio, thus $MgZn_2$ is stable. However, it has also been observed that when replacing zinc with copper, both a size effect and electron:atom ratio favors a change in the $MgZn_2$ to $MgCu_2$ structure.

Addition of Copper to the Ternary System

Previous work[42-45] on the system Al-Zn-Mg-Cu indicated that additions of copper reduced the intercrystalline weakness and improved the stress-corrosion resistance of Al-Zn-Mg alloys and consequently copper became an important alloying addition. The implied effect of copper is that it stimulates the precipitation throughout the grains resulting in a significant reduction of the precipitate

free zone (PFZ) and therefore a reduction in the electrode potential difference between the grains and the free boundaries[46].

Comparatively little is known concerning the exact mechanisms involved in the precipitation reactions in the quarternary alloys but the following generalities based on experimental observations concerning microstructural effects are noteworthy[47-52]:

1. The quenched hardness is greater in copper containing alloys than in the simpler Al-Zn-Mg ternary alloys.

2. The onset of hardening below 50°C aging temperature is delayed when copper is present as compared to the simpler Al-Zn-Mg alloys.

3. The copper appears to have its greatest effect during the first stages of aging.

4. The presence of copper does not seem to alter the number of stages that exist during the aging of the simpler ternary Al-Zn-Mg alloys.

Undissolved copper-rich particles of the type $CuMgAl_2$ have been shown by Hyatt and Quist[10] to exist in Al-Zn-Mg-Cu alloys. Microprobe results[53] have demonstrated that during the early stages of solution treatment, magnesium diffuses rapidly from the second phase leaving nearly pure $CuAl_2$. The presence of the copper rich intermetallic is associated with the zinc:magnesium ratio and copper content. Figure 5 is a 460°C isotherm for 90 per cent aluminum showing the location of solubility limits. As the zinc:magnesium ratio increases, the solubility increases. It has been found[10,53] that in order to dissolve the $CuAl_2$ phase, extensive cold work is necessary prior to solutionizing, to break-up the copper intermetallics.

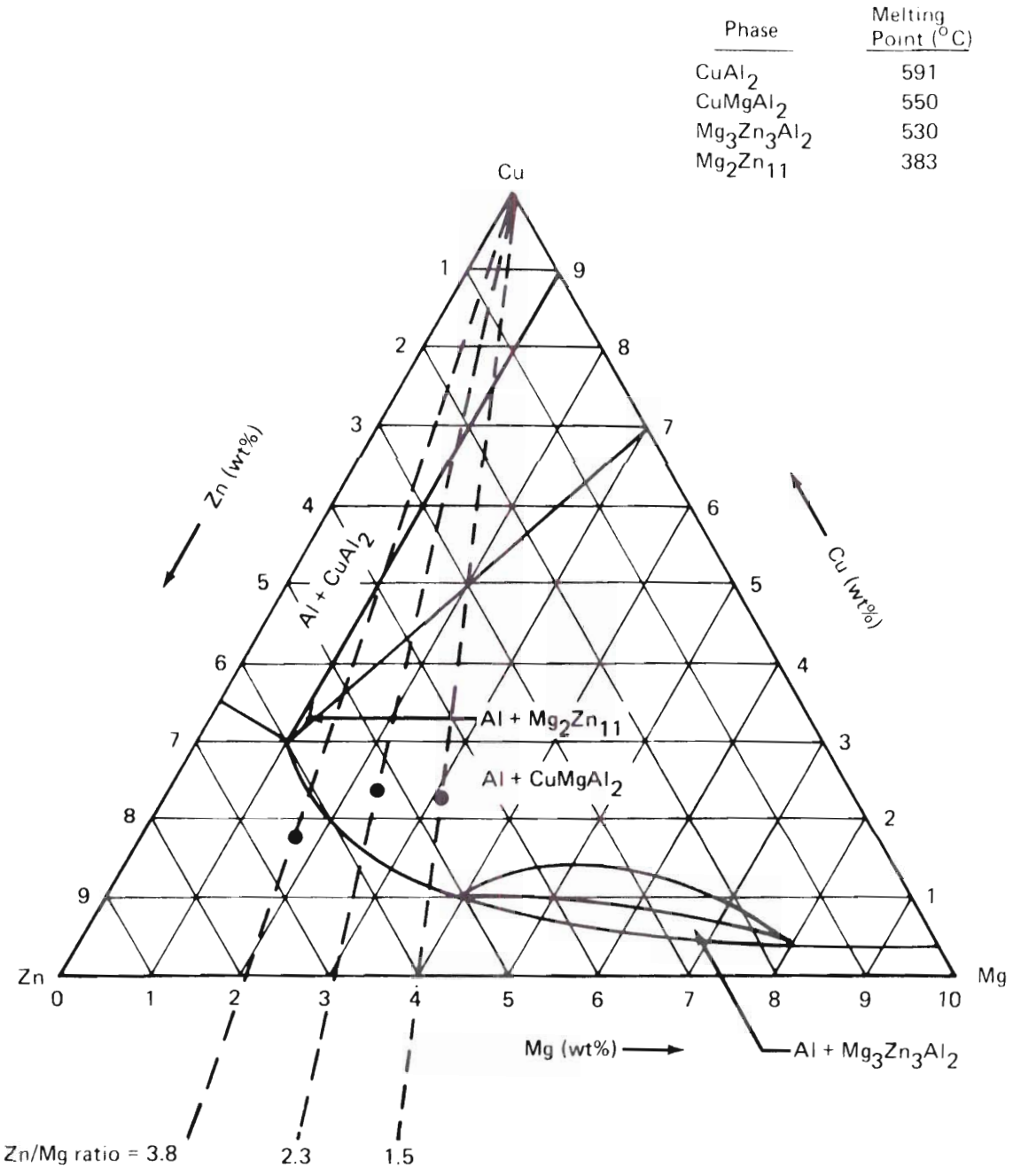

Figure 5. 460°C Isotherm Section of the 90 Per Cent Aluminum Phase Diagram[10].

Mechanical Properties

The increase in critical resolved shear stress, $\Delta\tau_o$, over the pure matrix, is due to the interaction of the dislocations with the preprecipitates and precipitates. Coherent, and partially coherent particles may be penetrated by dislocations, since, generally, the slip systems of the precipitate and the matrix are coincident. Precipitates of this type deform plastically and are sheared by the dislocations. In contrast, the intermetallic phases and dispersed oxides have an incoherent interface, and normally are not penetrated by the dislocations. The particles are looped by the dislocations and the process has been described by Orowan[55,56].

Mathematical expressions can be written[57] for the two processes. For looping, the expression:

$$\Delta\tau_o = \frac{2T}{bR} \cdot \frac{f}{2}^{\frac{1}{2}}, \quad \text{and} \tag{1}$$

for a cutting mechanism,

$$\Delta\tau_o = \frac{F}{b^2} \frac{F'}{2T} \cdot \frac{f}{2} \cdot \frac{R}{b}^{\frac{1}{2}}, \tag{2}$$

describe the motion of the dislocations in the dispersed particle system, where

$\Delta\tau_o$ - is the increase in shear stress due to the particles

F - is the average maximum force which a particle can withstand before shearing

F' - is a measure of the relative strength of the particle, with $F = F'R/b$

T - is the dislocation line tension

f - is the volume fraction, and

R - is the particle radius.

Equations (1) and (2) can be normalized by the factor $\Delta\tau_o\ b^2/2T\sqrt{f}$[57] and plotted as a function of R/b on a log-log scale. Figure 6 is a plot of this type, showing data from different types of precipitates[57-63]. The Orowan mechanism shows a linear dependence (when plotted in a log-log fashion) with a negative slope, and the cutting mechanism shows a linear behavior with a positive slope. The intersection of these two curves is a measure of the critical radius for looping. The position of the intersection along the Orowan curve is a measure of the particle strength, or its inability to deform.

Fatigue Properties

The fatigue ratio (fatigue strength/ultimate tensile strength) of high purity 2XXX and 7XXX series alloys is about 0.3[10]. There have been numerous attempts to account for the poor fatigue properties of these alloys. Four general hypotheses have been proposed to account for the premature failure during reversed loading: reversion, destruction of precipitate order, overaging and aging inhomogeneities.

The reversion mechanism is considered to operate as a result of repeated cutting of precipitates by dislocations[6,70-77]. Each time the preprecipitate is sheared by dislocations the radius is decreased. Eventally, the radius is reduced by the diffusion of the solute atoms away from the zone and once a critical value of the zone radius is reached, it becomes unstable and dissolves.

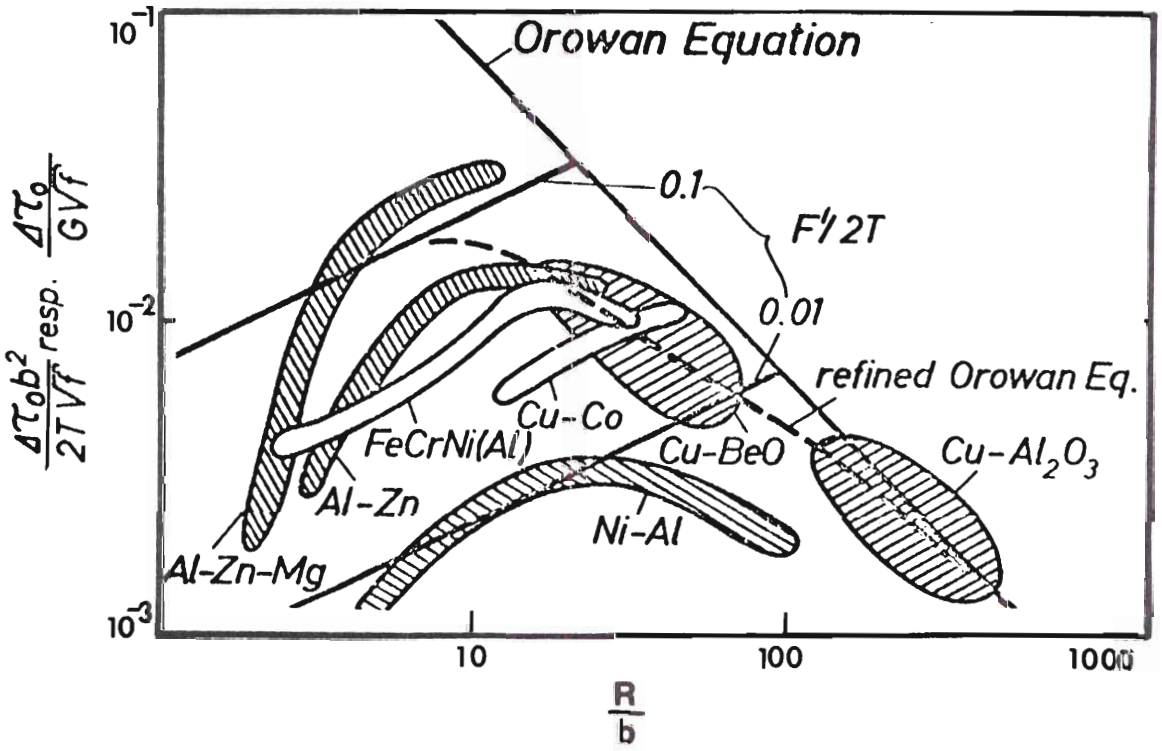

Figure 6. Normalized CRSS Versus Particle Radius. Theoretical Estimates and Experimental Results[57].

Calabrese and Laird[78] have studied the fatigue properties of Al-4 per cent Cu, aged to produce a finely dispersed coherent or partially coherent preprecipitate. Cyclic softening (reduction in stress amplitude with cycles) was found to occur after initial cyclic hardening (increase in stress amplitude with cycles). Cyclic hardening was thought to be the result of the interaction of the mobile dislocations with the zones. The softening was related to the to and fro motion of the dislocations, reducing the atomic order of the zones.

There have been numerous investigations[77,79-87] which have reported results that appear to support overaging as a mechanism for cyclic instability. In overaging, the mobile dislocations interact with the dislocations that form the boundaries of the coherent and semi-coherent preprecipitates in such a way that the boundary becomes incoherent, reducing the local elastic strains, and permitting the equilibrium precipitate to form. Also, the enhanced diffusion rate as a result of vacancies created by moving dislocations[80], and dislocations acting as diffusion pipes, are thought to accelerate the aging process. Clark and McEviley[86] were more specific about the phenomena and proposed that the deleterious softening depends upon the alloy and the relative rate of nucleation of the transition structure. The faster the nucleation of the transition structure, the greater the probability of overaging. This postulate was demonstrated using Al-4 weight per cent Cu and Al - 15 weight per cent Ag. The nucleation rate of γ' is greater than that of θ', thus overaging occurs in Al-Ag and reversion in Al-Cu.

Laird and Thomas[88] have concluded that reversion of pre-precipitates in high-purity 7XXX and 2XXX alloys does not occur, and they relate the softening to crack nucleation in the soft regions like precipitate free zones or quench bands. Fatigue cracks have often been preferentially observed to nucleate in the grain boundaries of high purity Al-Zn-Mg alloys.

Low Cycle Fatigue Testing

Low cycle fatigue is generally defined to be failure of a material under cyclic loading in less than 10^5 cycles. Plastic strain has been determined to be the controlling parameter in the instability of microstructures. The only significant difference between various ranges is the degree of cyclic plastic damage[89].

The cyclic stress-strain response can be expressed similarly to the monotonic stress-strain response with the total strain equal to the sum of the elastic and plastic portions of strain:

$$\frac{\Delta\varepsilon_t}{2} = \frac{\Delta\varepsilon_e}{2} + \frac{\Delta\varepsilon_p}{2} = \frac{\sigma_a}{E} + \varepsilon_f' \left(\frac{\sigma_a}{\sigma_f'}\right)^{1/n'} \qquad (3)$$

where,

$\Delta\varepsilon_t$ - is the total strain range,

$\Delta\varepsilon_e$ - is the elastic strain range,

$\Delta\varepsilon_p$ - is the plastic strain range,

ε_f' - is the fatigue ductility coefficient,

σ_a - is the stress amplitude,

σ_f' -is the fatigue strength coefficient,

E - is the elastic modulus,

and

n' - is the cyclic strain hardening exponent.

Figure 7 is a schematic representation of the quantities with respect to a generalized hysteresis loop.

Low cycle fatigue experiments can be carried out in the strain control mode. The independent variable, stress, is monitored and plotted as a function of the number of cycles. Figure 8 shows the cyclic-dependent material responses under constant strain control. An increase in stress amplitude indicates cyclic hardening; constant stress amplitude - saturation; and a reduction in stress amplitude, cyclic softening. By cycling several specimens to fracture, at a constant strain amplitude, the empirical Coffin-Manson relationship can be plotted. Mathematically, this relationship is of the form

$$\frac{\Delta \varepsilon_p}{2} = \varepsilon_f' \, (2N_f)^{-c} , \qquad (4)$$

and can be plotted

$$\log \frac{\Delta \varepsilon_p}{2} = \log (\varepsilon_f') - c \log(2N_f),$$

which results in a linear plot. Two relationships are plotted in Figure 9. The first has a slope of -1, which implies that the total plastic strain to fracture is a constant, regardless of the life. The second curve has a slope of -0.5. From these two plots a physical meaning for the fatigue ductility exponent can be appreciated. The smaller $|c|$, the greater will be the material's tolerance to cyclic

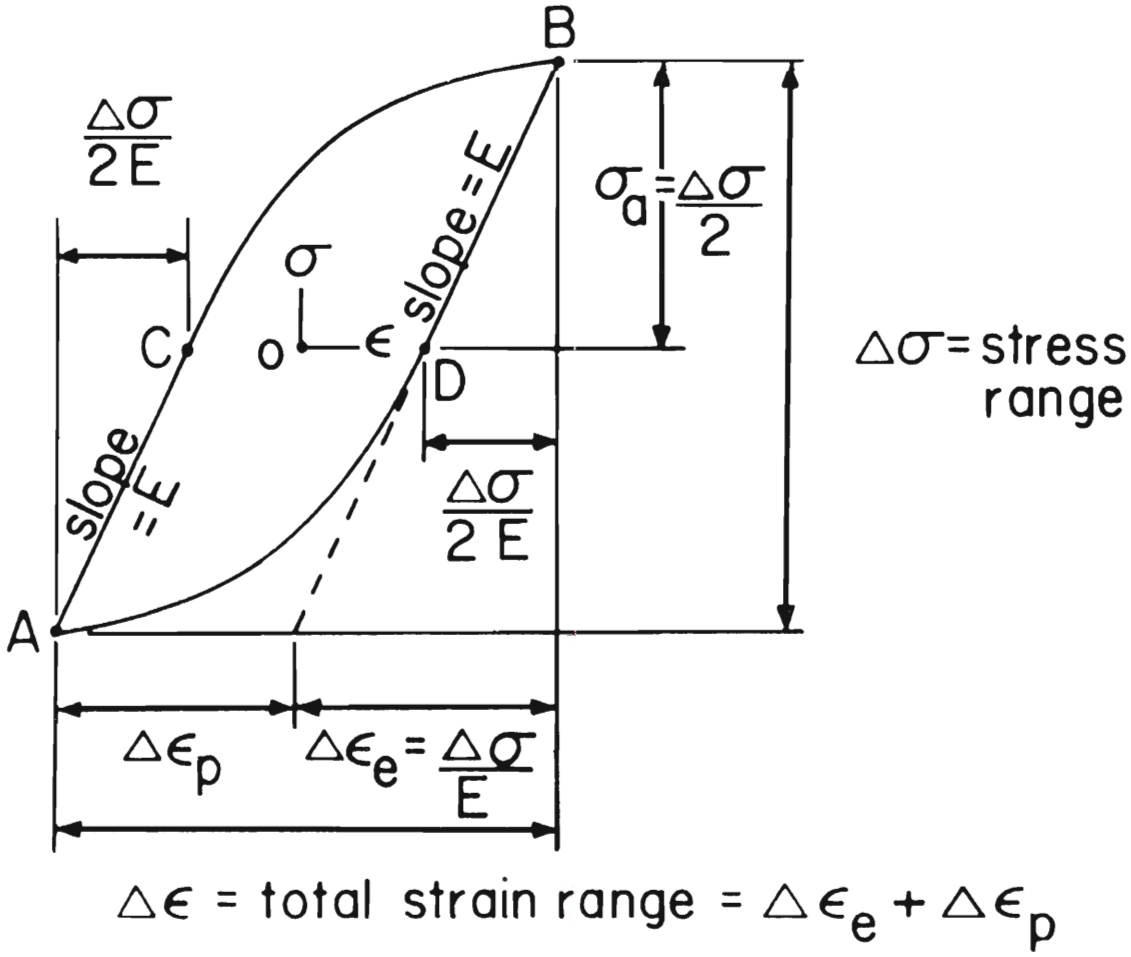

Figure 7. Schematic Representations of the Quantities Associated With the Hysteresis Loop[89].

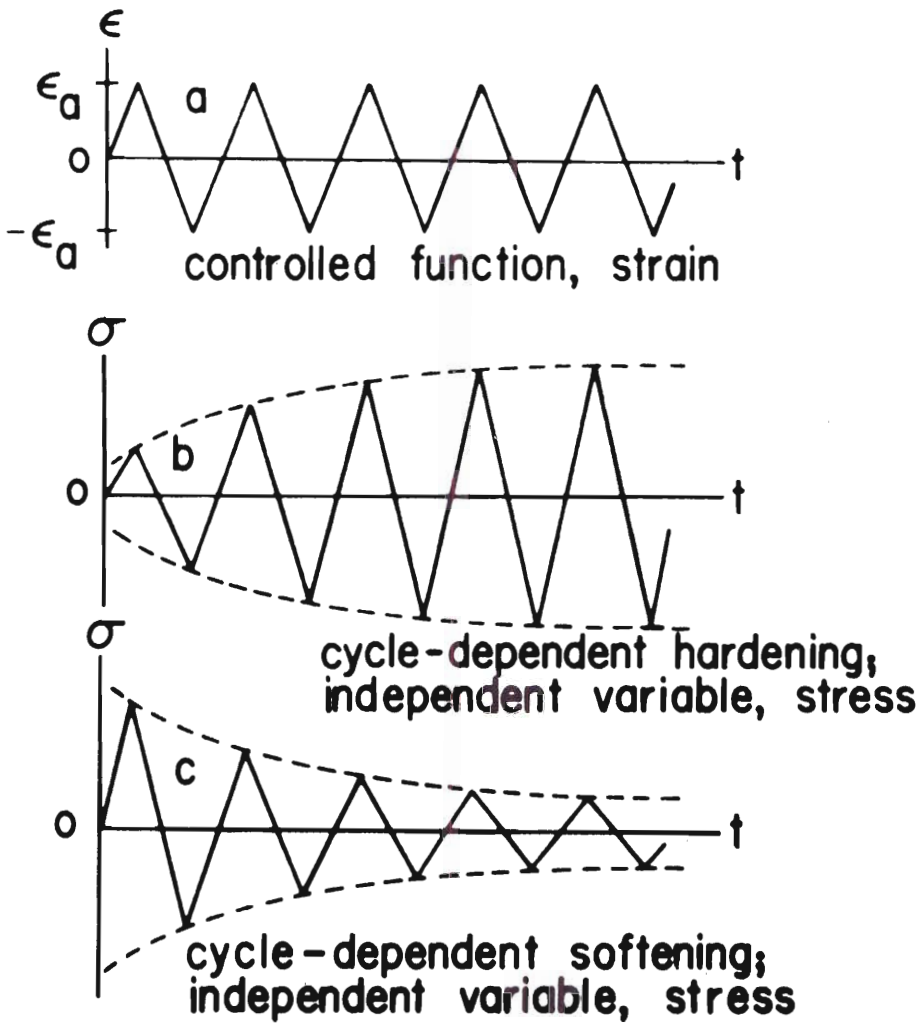

Figure 8. Cycle-Dependent Material Responses Under Strain Control[89].

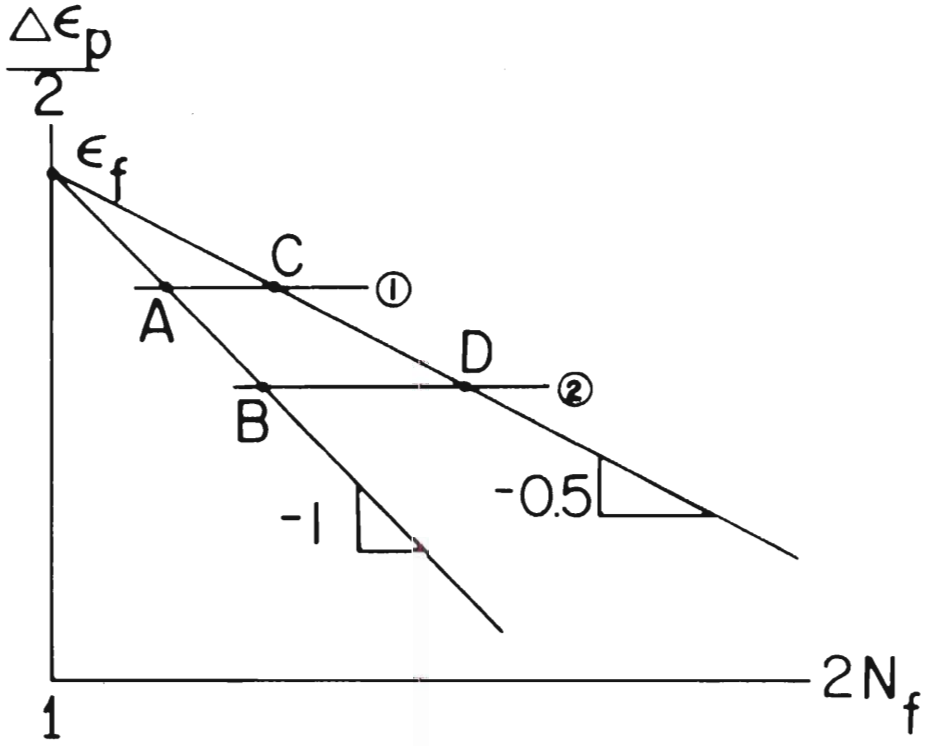

Figure 9. The Relationship Between the Plastic Strain Amplitude $\frac{\Delta\epsilon_p}{2}$, and the Number of Reversals to Failure, $2N_f$, at Two Different Values of Fatigue Ductility Exponent, C[89].

plastic straining.

A cyclic stress-strain curve can be obtained by plotting the values of stress amplitude versus the corresponding values of strain amplitude. The stress amplitude is determined at saturation; however, if saturation does not occur, the stress amplitude at half-life is generally used[89]. If the log (σ_a) versus log ($\frac{\Delta\varepsilon_p}{2}$) is plotted, the slope, n', may be determined. The slope is the cyclic strain hardening exponent and is similar to that obtained by plotting the monotonic stress-strain values.

CHAPTER III

EXPERIMENTAL PROCEDURES

The alloys used in the research were prepared at the ALCOA Technical Center, ALCOA Center, Pa.. The cast ingots were hot rolled at 750°F (398°C) to a nominal thickness of 0.17 inches for the Al-Zn-Mg alloy and 0.20 inches for the 7050 alloy. The 7050 plates were then annealed, solutionized, double aged at 250°F (121°C) for 12 hours and 325°F (163°C) for 24 hours. The chemical analysis for the alloys is given in Table 1.

Table 1.

Composition Of The Two Aluminum Alloys

	Si	Fe	Cu	Mn	Mg	Cr	Zn	Ti	Be	Zr
Al-Zn-Mg (Ternary Alloy)	0.00	0.00	0.00	0.00	2.20	0.00	6.17	0.00	0.00	0.00
7050	0.06	0.08	2.55	0.01	2.21	0.01	6.31	0.02	0.001	0.10

Samples of the as received plates, sectioned parallel and transverse to the rolling direction, were mounted in epoxy resin, mechanically polished, and etched with dilute Kellers' reagent, for metallographic examination.

Samples of the ternary alloy were solutionized at 480°C for one hour and quenched in agitated ice brine; this will hereafter be re-

ferred to as the standard method of heat treatment. The heat-treated samples where then mounted, polished and examined metallographically to determine the morphology and grain size distribution in the longitudinal and two transverse directions.

Samples for hardness measurements were cut from the plates and the rolled surfaces were carefully ground parallel. The samples were then heat-treated by the standard method and immediately transferred to a constant temperature bath, to be aged. Isothermal aging was done at 120°C and at 150°C $\pm$ 0.1 C°. Vickers diamond pyramid hardness (10 kg load) was determined from the arithemetic mean of the diagonals of five indentations on each of the two parallel ground surfaces.

Transmission electron microscopy was performed on samples which had been aged corresponding to salient points on the hardness curves for isothermal aging. Thin foils were prepared by a dimpling technique. A solution of 75 per cent methanol and 25 percent nitric acid, by volume, was used for dimpling and electropolishing. The polishing solution was cooled to -35°C $\pm$ 2°C. Microscopy was done using a Siemens Elmiskop IA equipped with a metallurgical stage and a precision darkfield attachment. The operating voltage was 125Kv.

Pole figure data was collected on a General Electric XRD-5 modified with an oscillation stage. The intensity was fixed time counted at equal increments of Φ (the rotation axis of Φ was perpendicular to the plate surface) at fixed angles of inclination from 0° to 70°. The axis of rotation of the inclination angle, χ, was perpendicular to the axis of rotation of Φ. To completely describe the

texture, (111), (200), and (220) pole figure data was collected.

Samples of the as-received plates were reduced by cold rolling with intermediate anneals, to a thickness of 0.35mm, which is approximately $1/\mu$ where μ, is the x-ray absorption coefficient for copper radiation. The strips were degreased first with acetone and then with methanol, clamped between two 1.6mm aluminum plates, heat-treated, and immediately transferred to the constant temperature baths.

After aging, the foils were degreased and mounted on a Kratky camera. A high intensity, finely focused copper source was used. The tube was operated at 50 KV and 20 ma. A mechanical pump was used to evacuate the beam path, to reduce air scattering. A 1:2 ratio of entrance to exit slit heights was employed (80 and 160μ respectively). The incident beam was nickel filtered and a scintillation counter with a pulse height discriminator received the scattered radiation.

The data was corrected for air scattering by comparison with data from a standard aluminum foil of 99.99 per cent purity, the same thickness as the samples, and placed on a relative scale using a lupolen standard scatterer. The corrected data was then smoothed and desmeared using a computer program described by Hendricks[89]. The particle radius of gyration was determined using the Guinier approximation[90].

Fatigue and tensile samples were machined from the as-received plates in the longitudinal and long transverse directions. The specimens were of the smooth, cylindrical gage section type. The gage section of the tensile samples was approximately 18mm long by 3mm diameter, and the gage section of the fatigue samples was

approximately 6mm long by 3mm diameter. The machined specimens were hand polished first with 600 grit emory paper, then with a billard cloth impregnated with 6μ diamond paste. The samples were then heat-treated and aged to correspond to salient points along the hardness curves, and electropolished.

Tensile tests were conducted on an Instron testing machine, with a 10mm Instron extensometer positioned directly on the gage section of the specimen. The specimens were deformed to fracture under uniaxial tension at a strain rate of 10^{-3}/second.

Push-pull low cycle fatigue tests were performed on the two aluminum alloys. The fatigue tests were conducted on an Instron testing machine, using strain control and cycling about zero mean stress. The strain was measured with a 10mm Instron extensometer clamped to struts rigidly fixed to the grips. A self aligning Woods' metal reservior was used to insure the coincidence of the machine axis with the specimen axis. All tests were carried out in a dry gaseous argon atmosphere and at a total strain rate of 0.5×10^{-2}/second.

Fractography was performed on a Cambridge Stereoscan equipped with a non-dispersive x-ray detector.

CHAPTER IV

EXPERIMENTAL RESULTS

A deformed dendritic structure was observed in the Al-Zn-Mg alloy by metallographic examination of specimens of the as-received plate. There was a notable lack of intermetallic inclusions and casting defects, and heat treating for one hour at 480°C produced large, equiaxed grains with a mean grain diameter of 0.5 mm. The alloy 7050 had been solutionized and aged 12 hours at 121.0°C (250°F) and 24 hours at 152.8°C (325°F) prior to delivery. Optical metallographic examination revealed a fine grained microstructure with mean grain dimensions: 0.05 mm x 0.04 mm x 0.02 mm, Figure 10. This "plate-like" morphology gives rise to the poor fracture properties in the short transverse direction. Solutionizing 7050 for one hour at 480°C had no measurable effect on the grain size.

Upon careful examination of Figure 10, uniformly distributed particles can be seen. These particles have been identified by electron microprobe as containing copper, aluminum and magnesium[92], Figure 11. Other investigators[93] have observed these types of particles in a similar alloy, and identified them as $CuMgAl_2$.

The texture of the Al-Zn-Mg and 7050 alloys was determined from pole density data taken from the (111), (200) and (220) reflections, Figures 12 and 13. The texture was predominantly cube, (001) [100], with the [100] direction parallel to the rolling direction.

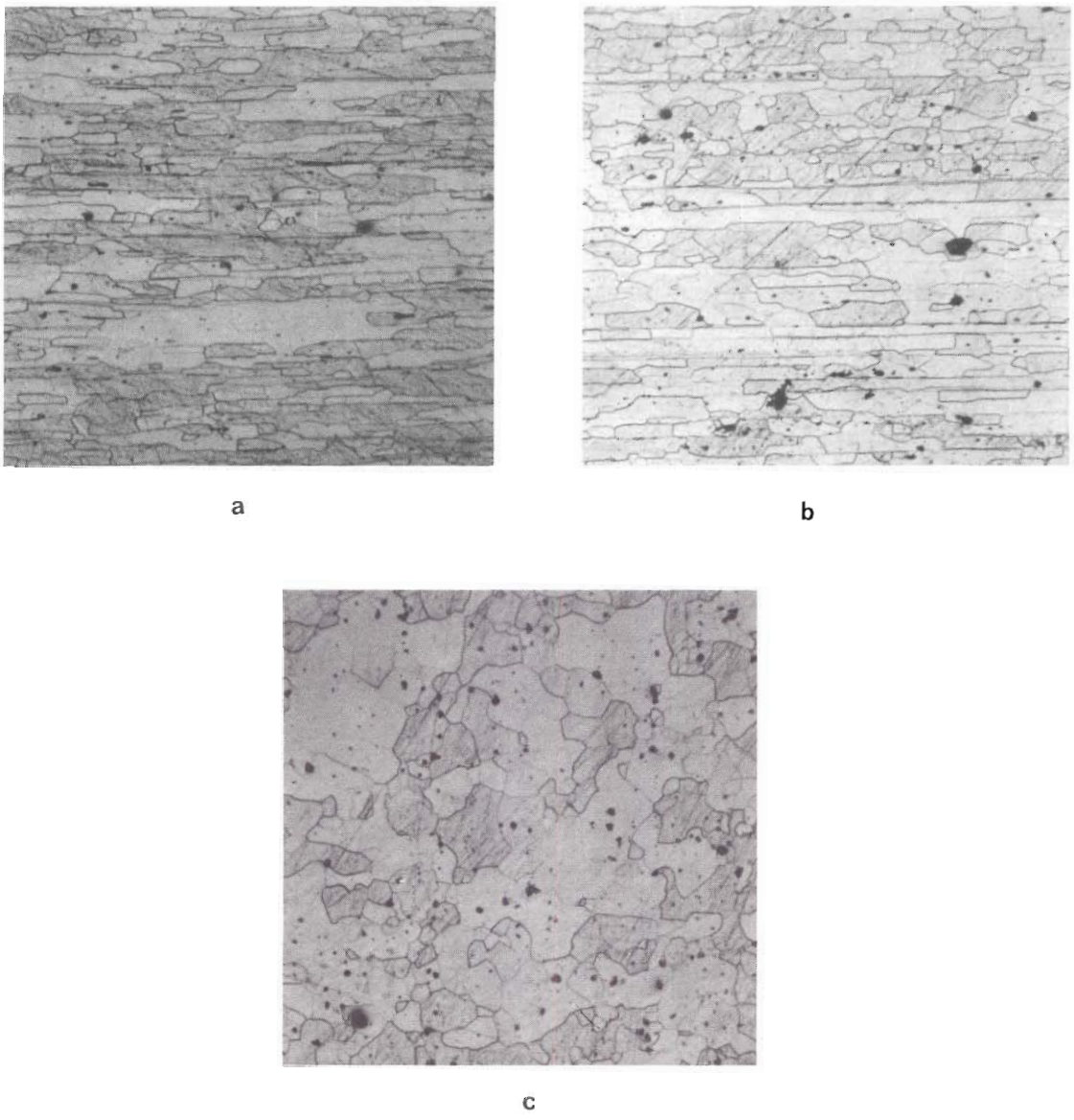

Figure 10. Microstructure of As Received 7050, Showing Size and Morphology of Grains and Copper Rich Intermetallics; (a) Short Transverse, (b) Long Transverse and (c) Longitudinal Sections. Magnification: 100X

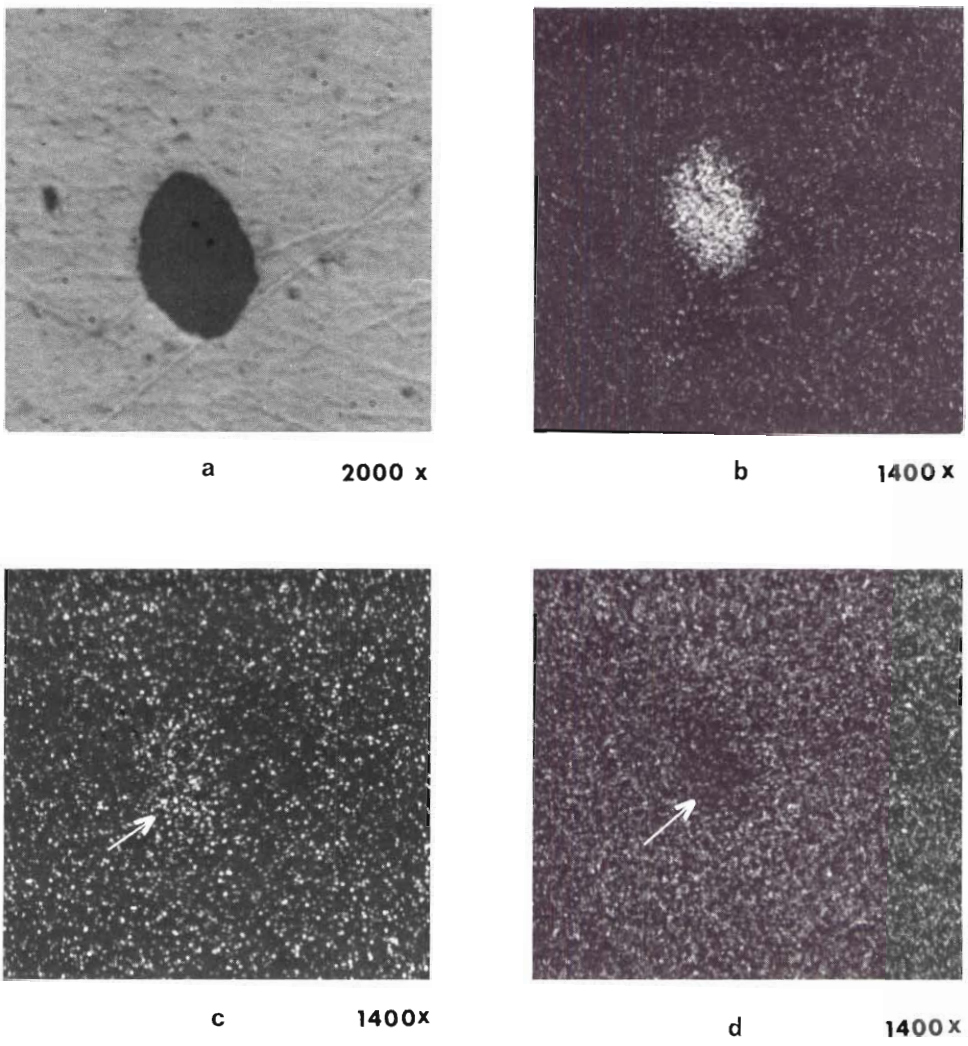

Figure 11. (a) Large Intermetallic Particle in a Section of 7050 Solutionized at 480°C for 1 Hour and Quenched. Microprobe Results showing: (b) High Density of Copper at the Particle, (c) Slightly Higher Density of Magnesium at the Particle, and (d) Low Density of Zinc at the Particle[91].

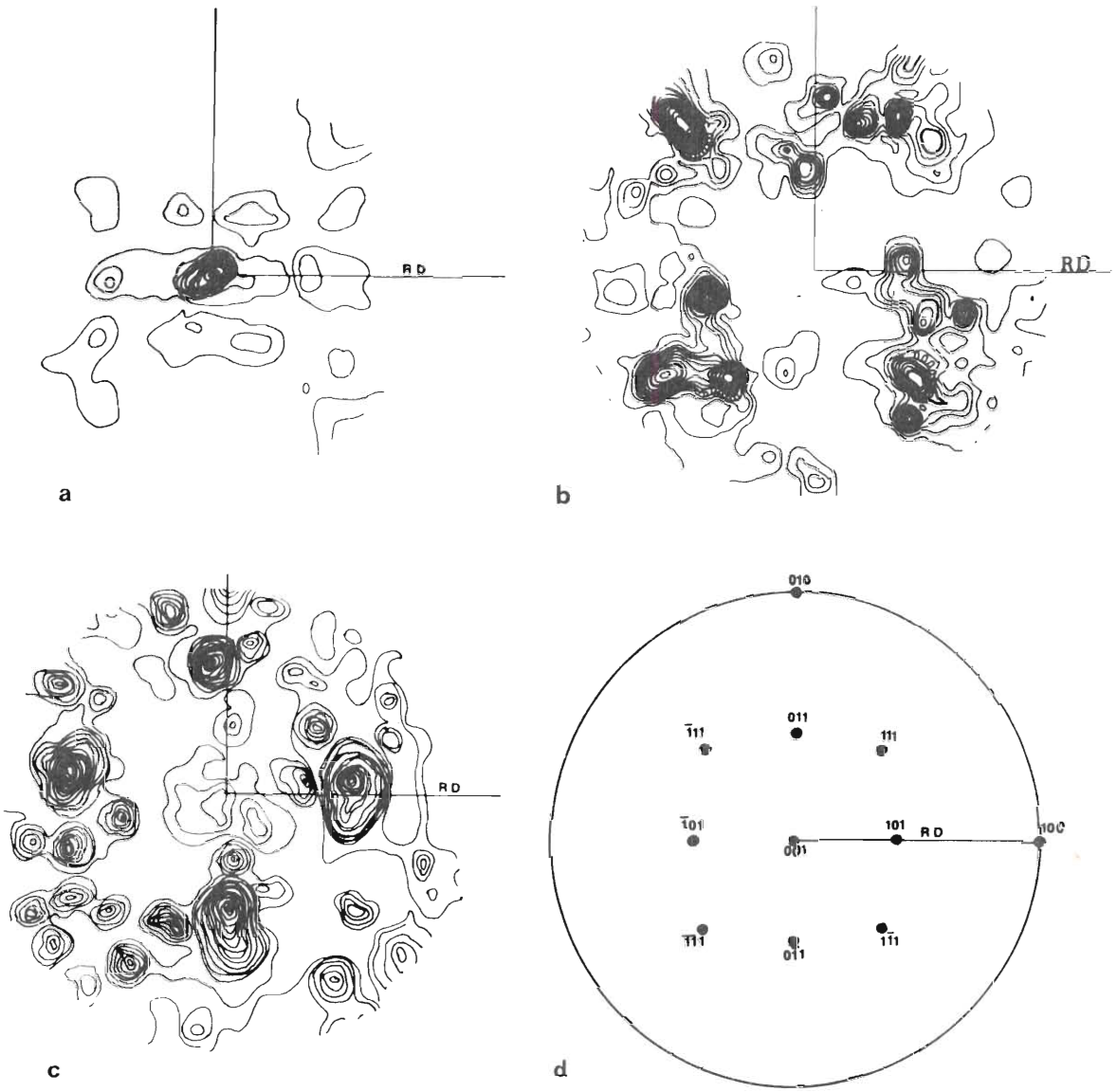

Figure 12. Pole Figure Data for the Ternary Al-Zn-Mg Alloy Showing: (a) (200), (b) (111), (c) (220) Reflections and (d) the (001) Stereographic Projection Indicating the Predominant (001) [100] Texture.

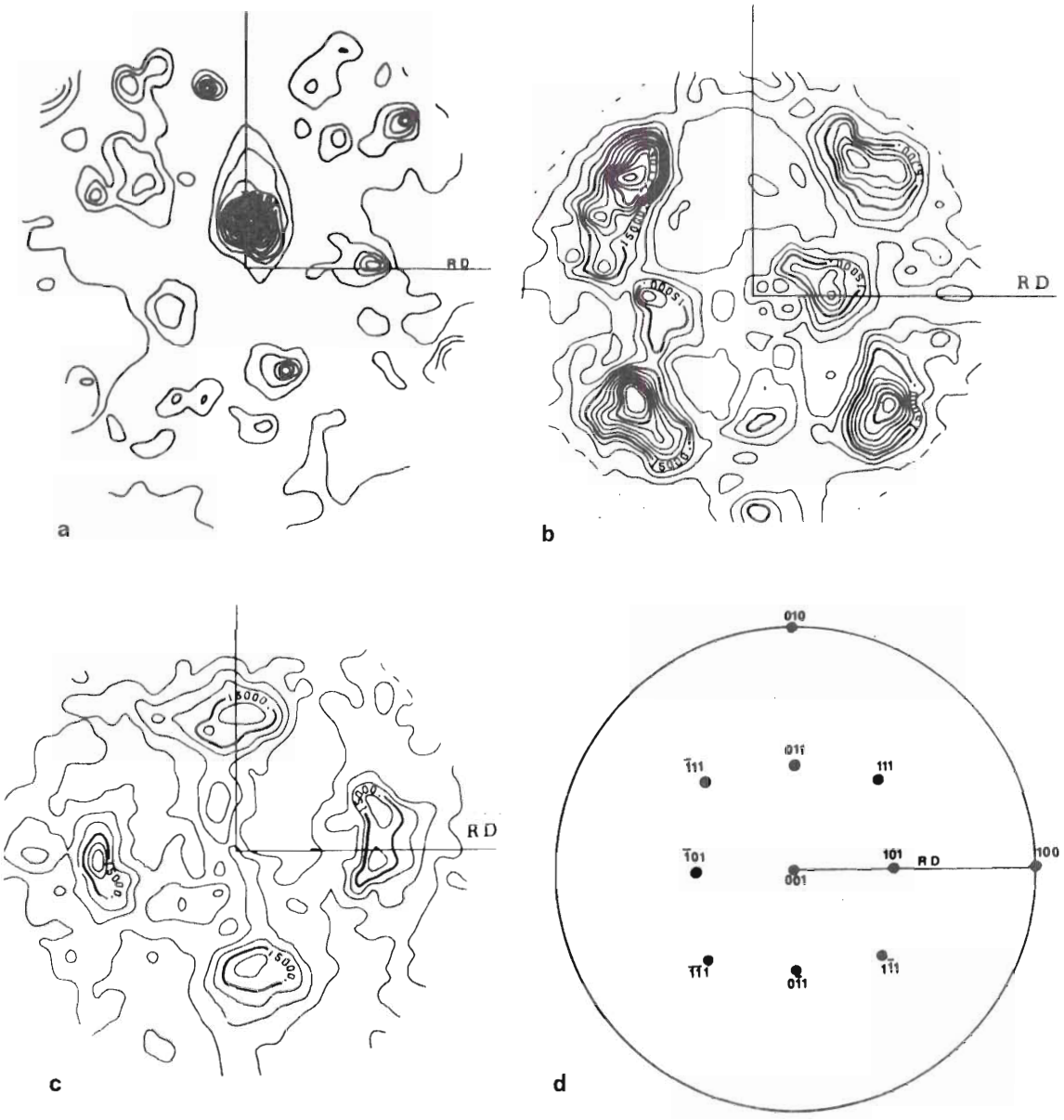

Figure 13. Pole Figure Data for the 7050 Alloy: (a) (200), (b) (111), (c) (220) Reflections and (d) the (001) Stereographic Projection Indicating the Predominant (001) [100] Texture.

The kinetics of the precipitation process was initially characterized by hardness measurements, Figure 14. The relative behavior of the two alloys was similar. Differences between the two alloys were a matter of absolute values, rather than relative rates of change. The growth of the precipitates was measured by x-ray small angle scattering (XSAS). Figure 15 shows that the rate of growth at 150°C was considerably more rapid than at 120°C. Also, aging at 120°C produced the characteristic interparticle interference hump generally associated with closely spaced particles. A discontinuous change in the Guinier radius was observed when both alloys were aged at 120°C. This type of change has been observed by other investigators[94] and has been attributed to the formation of η' from G.P. zones. It was observed that this transition occurs earlier in the 7050 alloys. The x-ray small angle scattering (XSAS) results for double aging of the two alloys for four hours at 120°C followed by continued aging at 150°C and 24 hours at 120°C followed by continued aging at 150°C are given in Figure 16.

TEM studies revealed that preferential precipitation occurred on dislocations and at grain boundaries. The precipitates at the grain boundaries were η, while those on the dislocations were η'[3]. Also, in the 7050 alloy, Al_3Zr particles were observed to be uniformly distributed throughout the grains, Figure 17. Precipitate free zones (PFZ's) were observed in both alloys. In general, the zones were narrower in 7050 than in the ternary Al-Zn-Mg alloy, with comparable heat treatment, and the PFZ width was smaller at 120°C than at 150°C. Figure 18 shows typical electron micrographs of the two alloys aged at both temperatures.

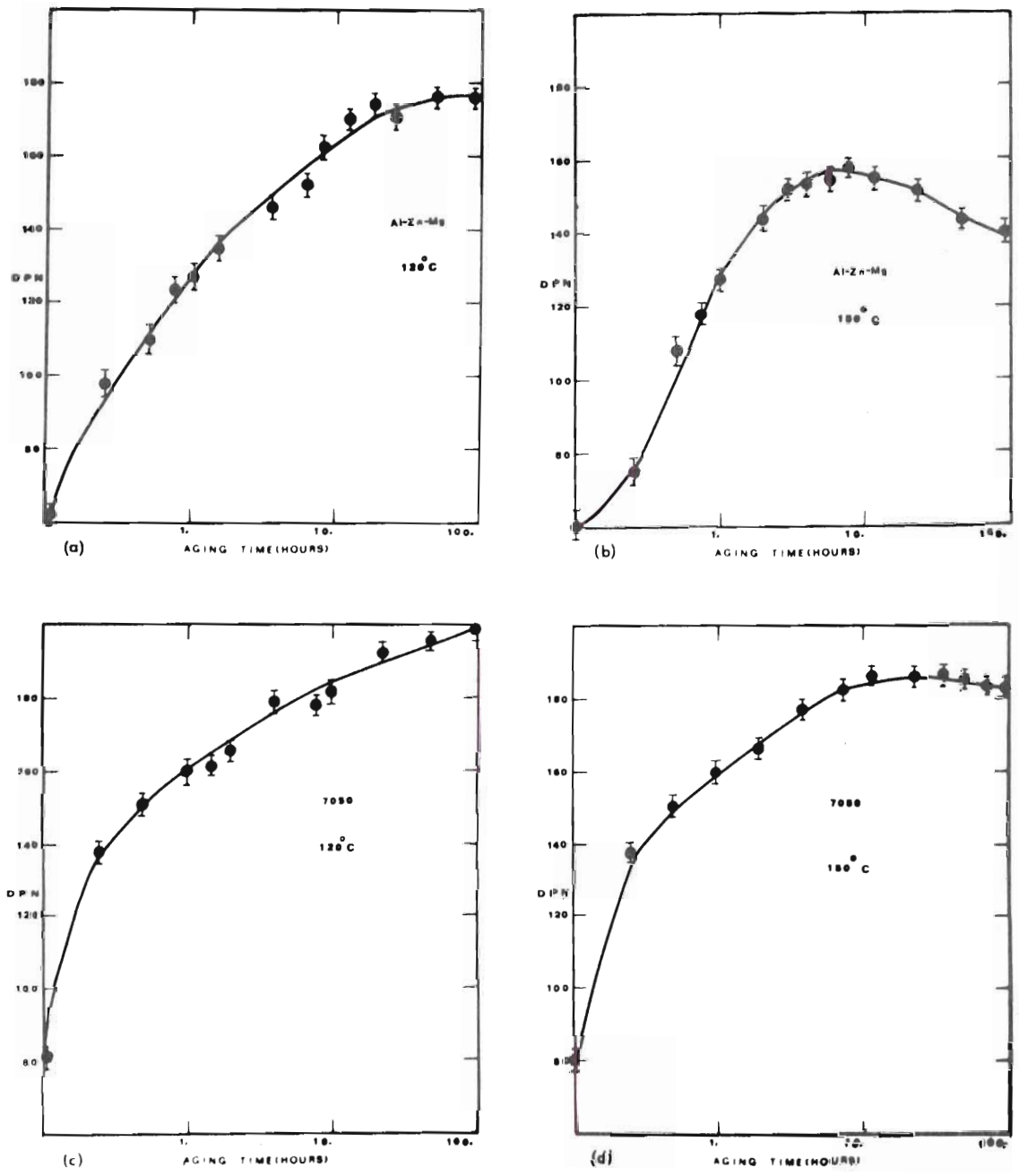

Figure 14. The Effect of Aging on the Hardness (D.P.H., 10 Kg Load) of (a) Al-Zn-Mg at 120°C, (b) Al-Zn-Mg at 150°C, (c) 7050 at 120°C, and (d) 7050 at 150°C.

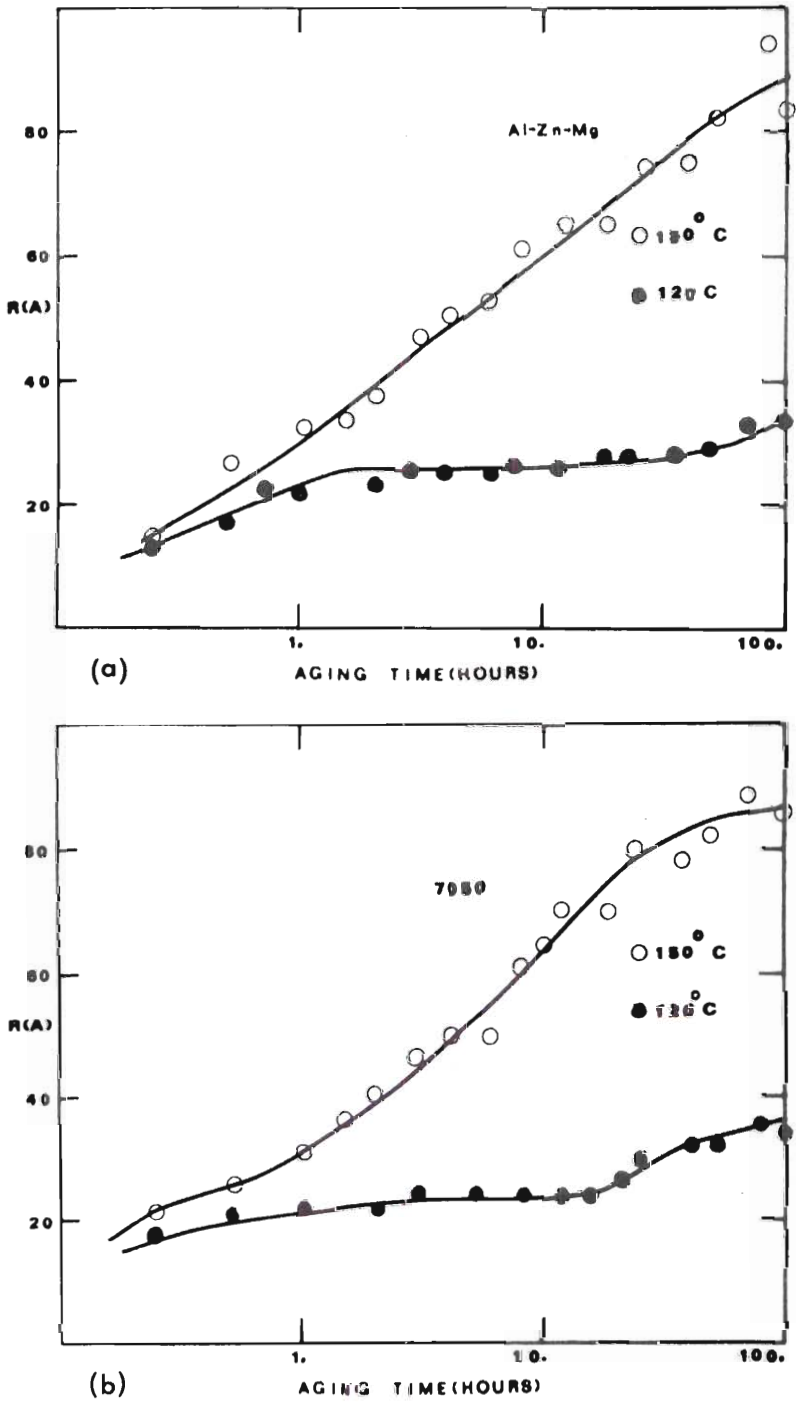

Figure 15. Variation of Guinier Radius with Aging Time; (a) Al-Zn-Mg, (b) 7050.

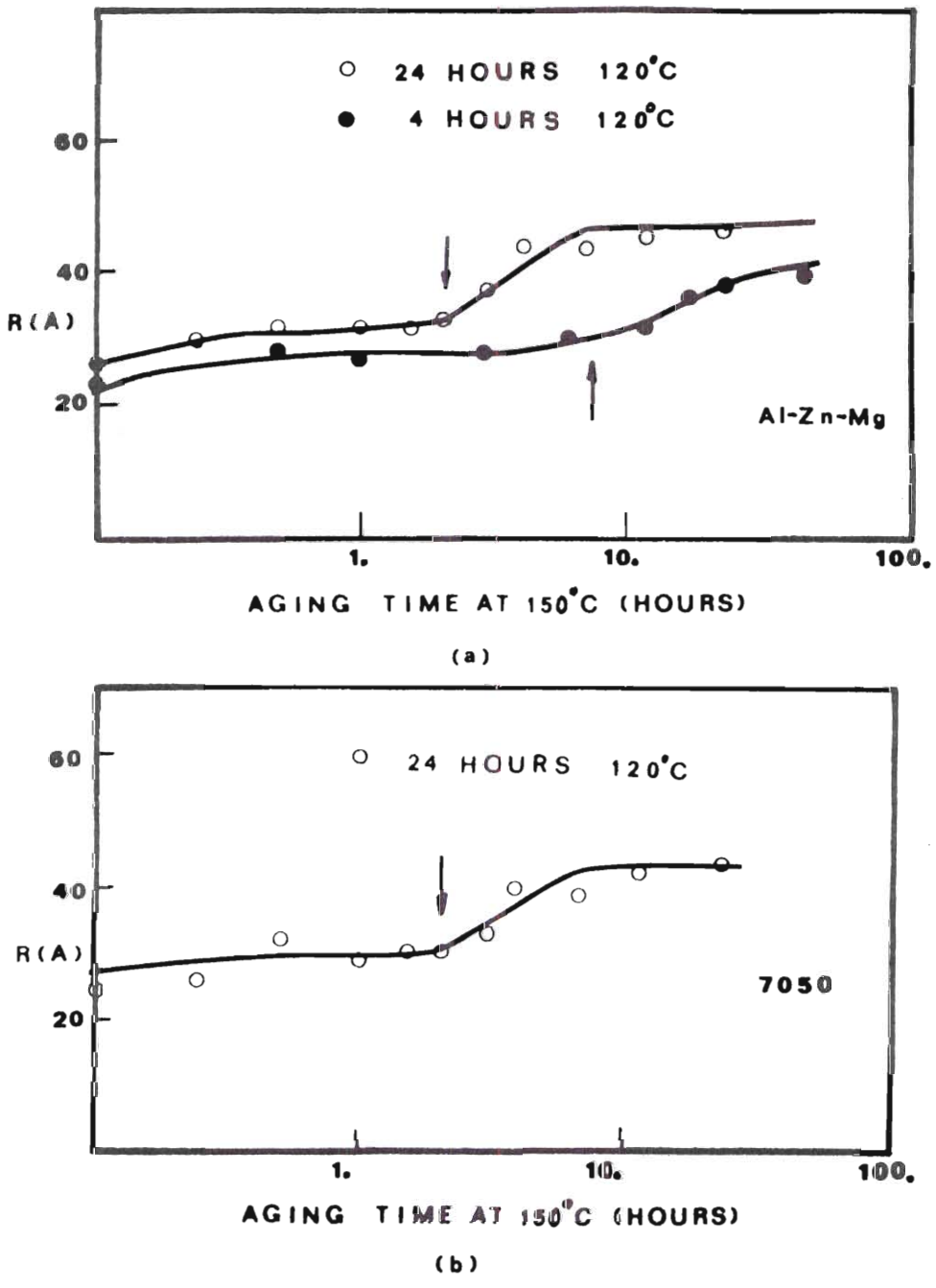

Figure 16. The Effect of Double Aging on the Guinier Radius of (a) Al-Zn-Mg, (b) 7050.

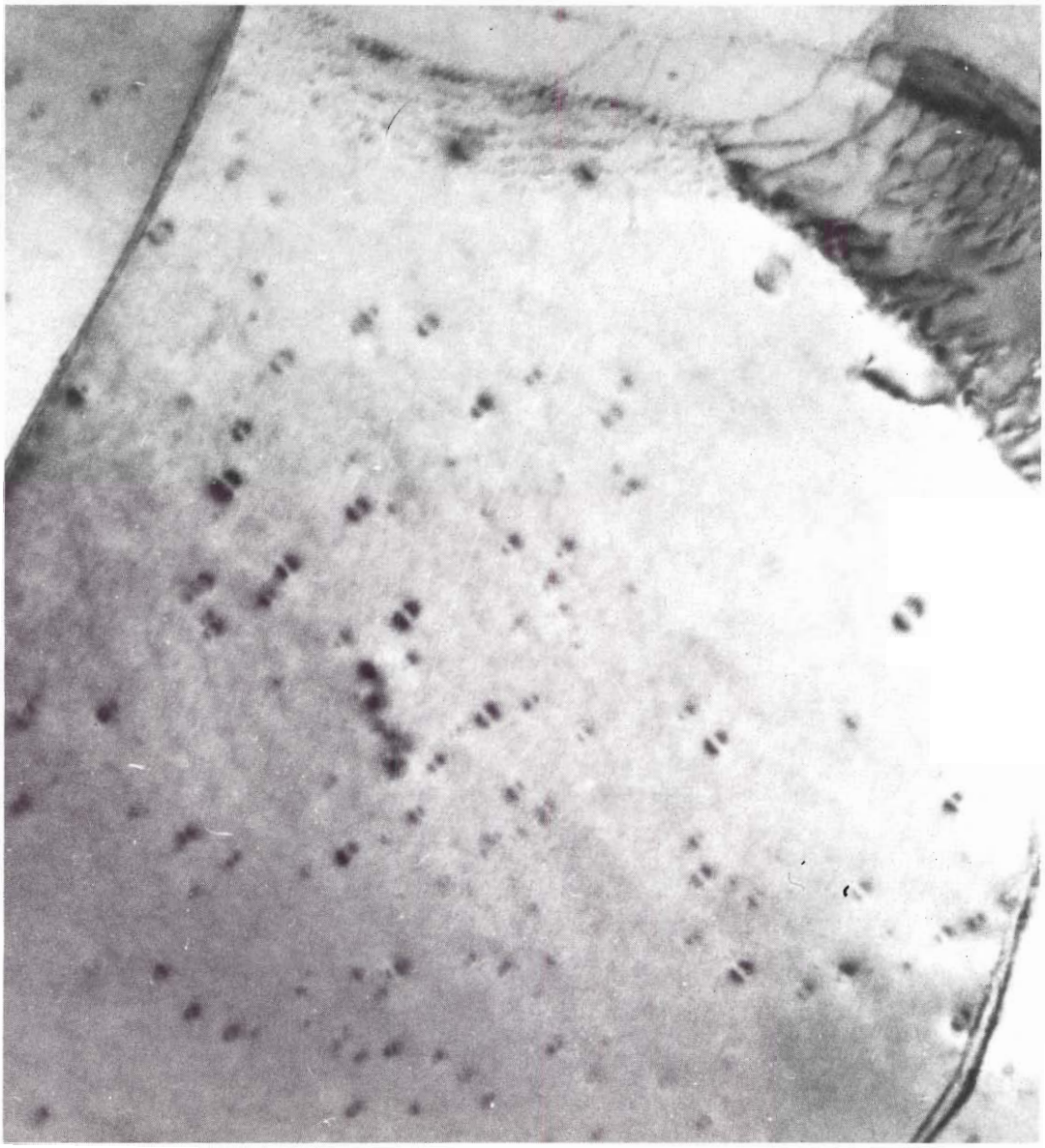

Figure 17. Fine $ZrAl_3$ Particles Distributed throughout 7050, with the Line of No Contrast in Each Particle Perpendicular to the Operating Reflection.

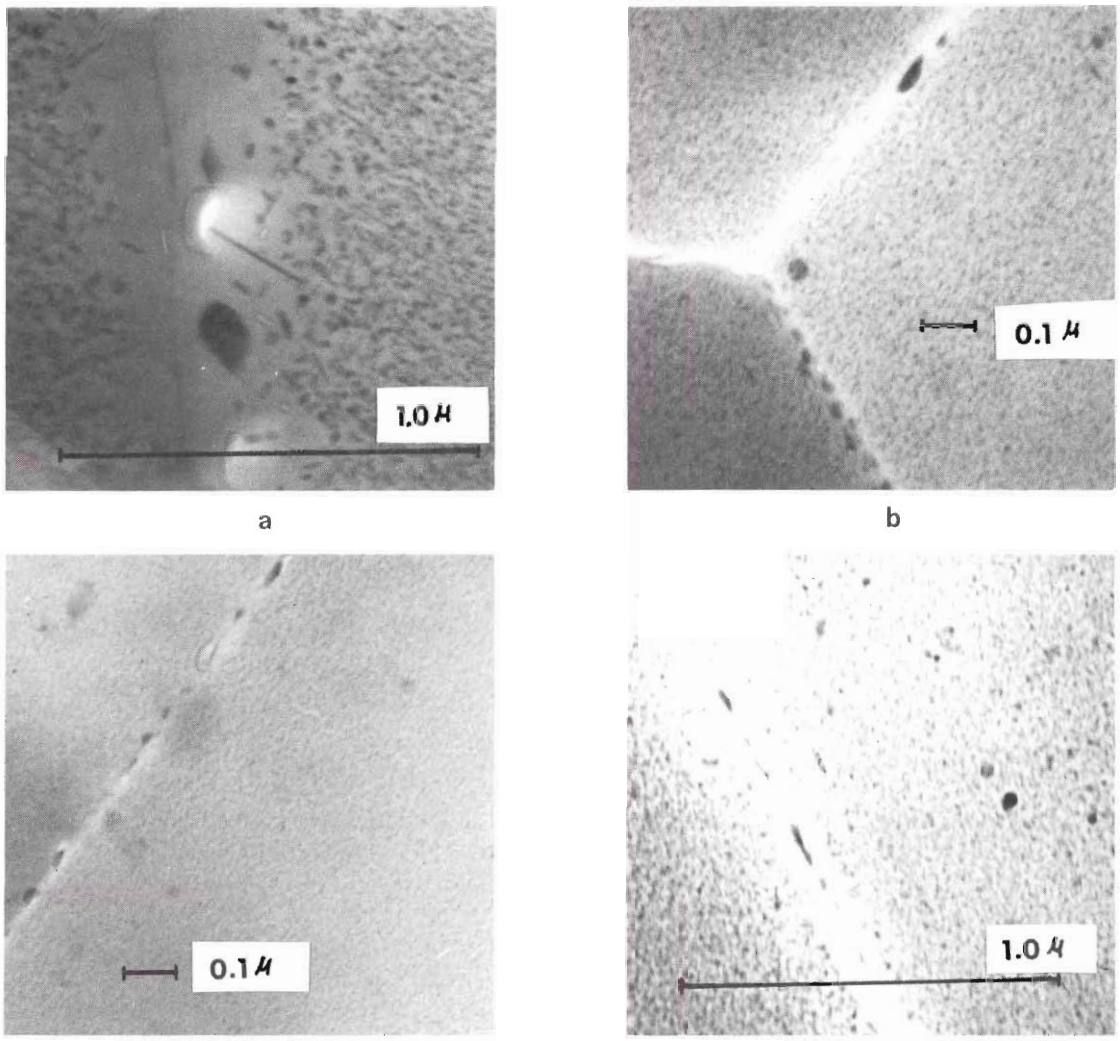

Figure 18. The Effect of Aging Temperature and Copper Content on the Width of the PFZ. (a) Wide PFZ of Al-Zn-Mg Aged 8 Hours at 150°C. (b) Narrow PFZ of 7050 Aged 8 Hours at 150°C. (c) Narrow PFZ of Al-Zn-Mg Aged 8 Hours at 120°C. (d) Narrow PFZ of 7050 Aged 8 Hours at 120°C.

Tensile samples of the two alloys aged at 120°C and 150°C exhibited a uniform increase in proof stress (0.2 per cent offset) and a decrease in the strain to fracture and strain hardening exponent. The variations of these parameters are summarized in Table 2. The change of fracture behavior of the Al-Zn-Mg alloy with aging was a gradual change from ductile, dimple rupture, in the as-quenched and under aged samples, to a brittle intergranular fracture in overaged samples. The transition of the fracture mode was significantly more rapid when the samples were aged at 120°C than at 150°C. Tensile samples of this alloy aged beyond 24 hours at 120°C fractured before any measurable yielding had occured. Figure 19, shows typical scanning electron fractographs, which clearly illustrate the transition from transgranular dimple rupture to intergranular separation.

The dislocation structure produced after small amounts of deformation, $\varepsilon_p < 2.0$ per cent, was similar to that reported by other workers[3]. Briefly, as-quenched and under aged samples deformed homogeneously and had a uniform dislocation distribution which contained a large number of long dislocation segments, with numerous dislocation dipoles and debris. Samples in the vicinity of maximum hardness exhibited inhomogeneous deformation. Slip was confined to narrow bands parallel to {111} planes containing short dislocation segments with much loop debris.

Tensile samples pulled to fracture of as-quenched and quenched and aged for 0.25 hours at 120°C are shown in Figure 20a and b. The deformation structure was characterized by uniformly distributed short

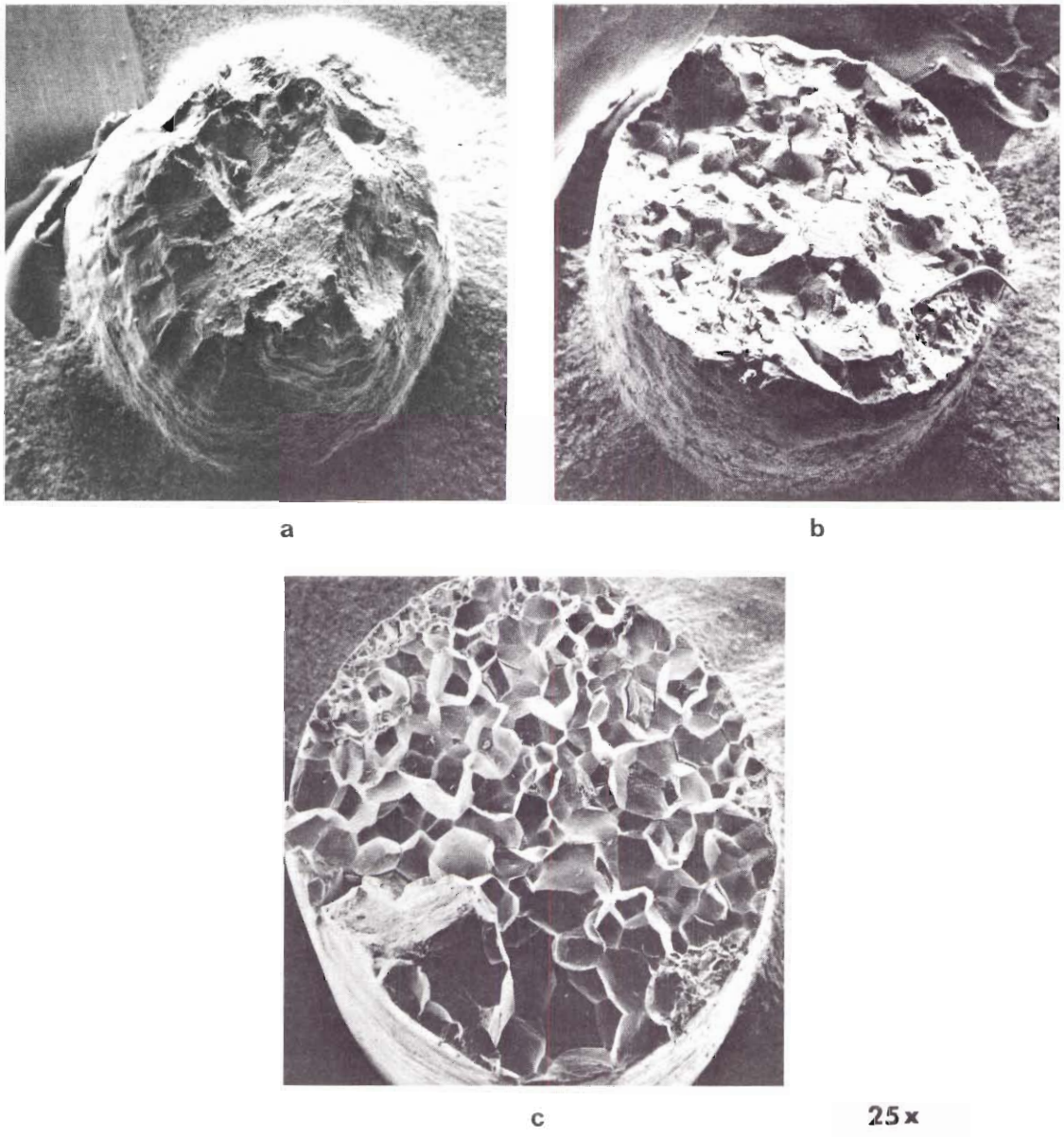

Figure 19. Effect of Aging on the Fracture Behavior of Al-Zn-Mg; (a) As Quenched, Ductile Transgranular Fracture; (b) 1 Hour at 120°C, Mixed Mode; (c) 12 Hours at 120°C, Low Energy, Intergranular Separation.

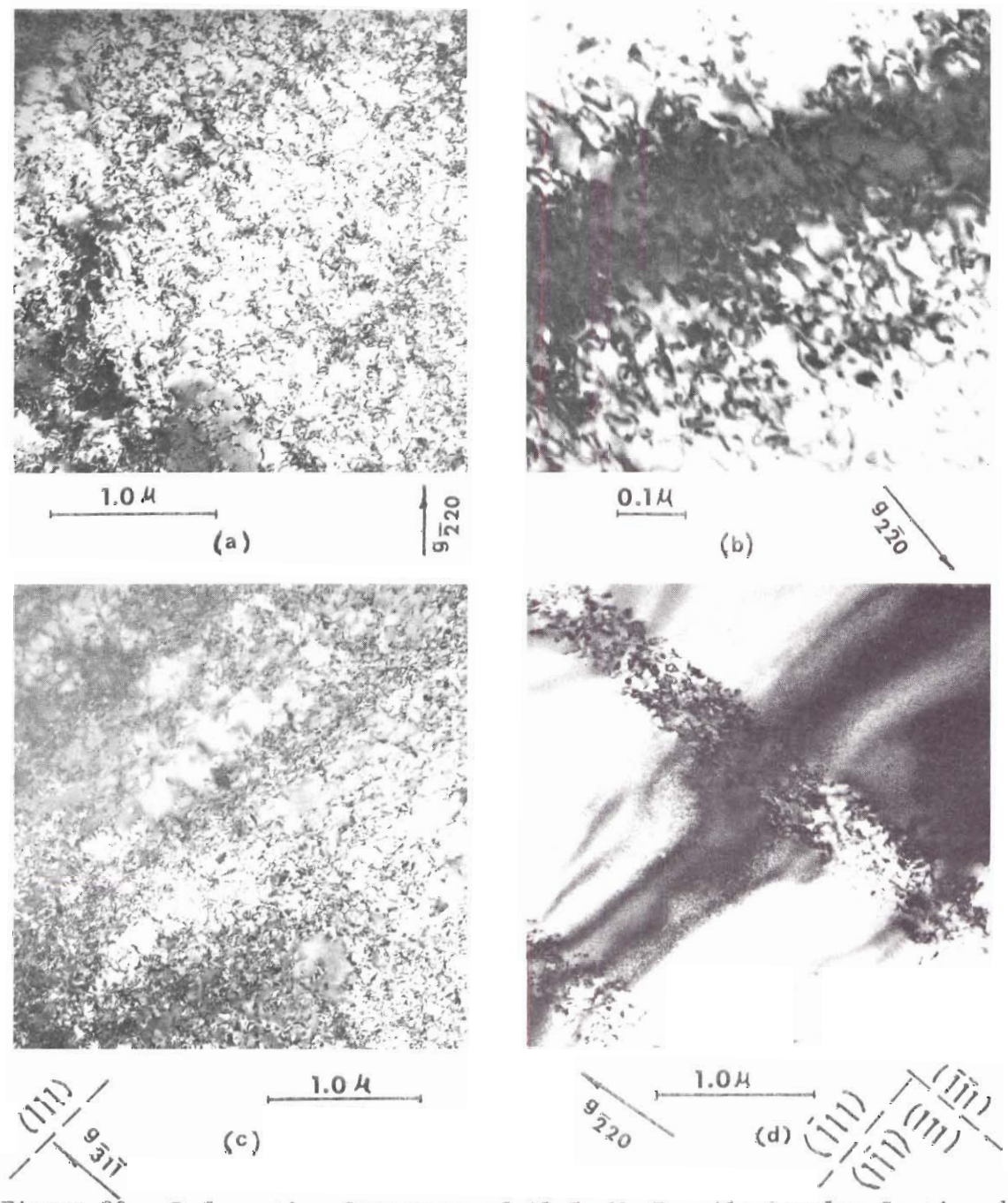

Figure 20. Deformation Structure of Al-Zn-Mg Tensile Samples Sectioned Below the Fracture Surface. (a) As-quenched, (b) 0.25 Hours, (c) and (d) 12 Hours at 120°C.

dislocation segments. Samples aged 4 hours at 120°C showed the onset of dislocation bands, Figure 20c. In samples aged 12 hours at 120°C, fracture occured before significant yielding, ε_p < 2 per cent, and the deformation structure was characterized by narrow, widely spaced dislocation bands, Figure 20. The region between the bands was observed to be free of dislocation debris.

Comparison of deformation structure in tensile samples aged at 150°C and pulled to fracture showed the uniform dislocation structure at the early stages of aging, 0.25 hours, Figure 21a, and a tendency toward wide, overlapping dislocation bands at the later stages of aging, Figure 21b and c. Wide dislocation bands were still observed after 96 hours, Figure 22. The wide overlapping bands were associated with the large plastic strain accommodated before fracture, ε_p > 5.0 per cent. Cross sections of fracture surfaces at various stages of aging were mounted, mechanically polished and etched, Figure 23. The traces of the slip lines, parallel to {111}, were found in samples in which nonhomogeneous deformation had been shown to exist by TEM. In the as-quenched and under-aged samples, slip traces were not found.

Aging the tensile samples of the 7050 alloy produced a uniform increase in the proof stress, a decrease in the strain hardening exponent, and a reduction in the elongation at fracture. These trends in the data are summarized in Table 2. Examination of the fracture surface of 7050 tensile samples revealed transgranular fracture for all aging times tested. Typical fracture behavior of 7050 can be seen in the scanning electron fractographs of samples as-quenched and aged

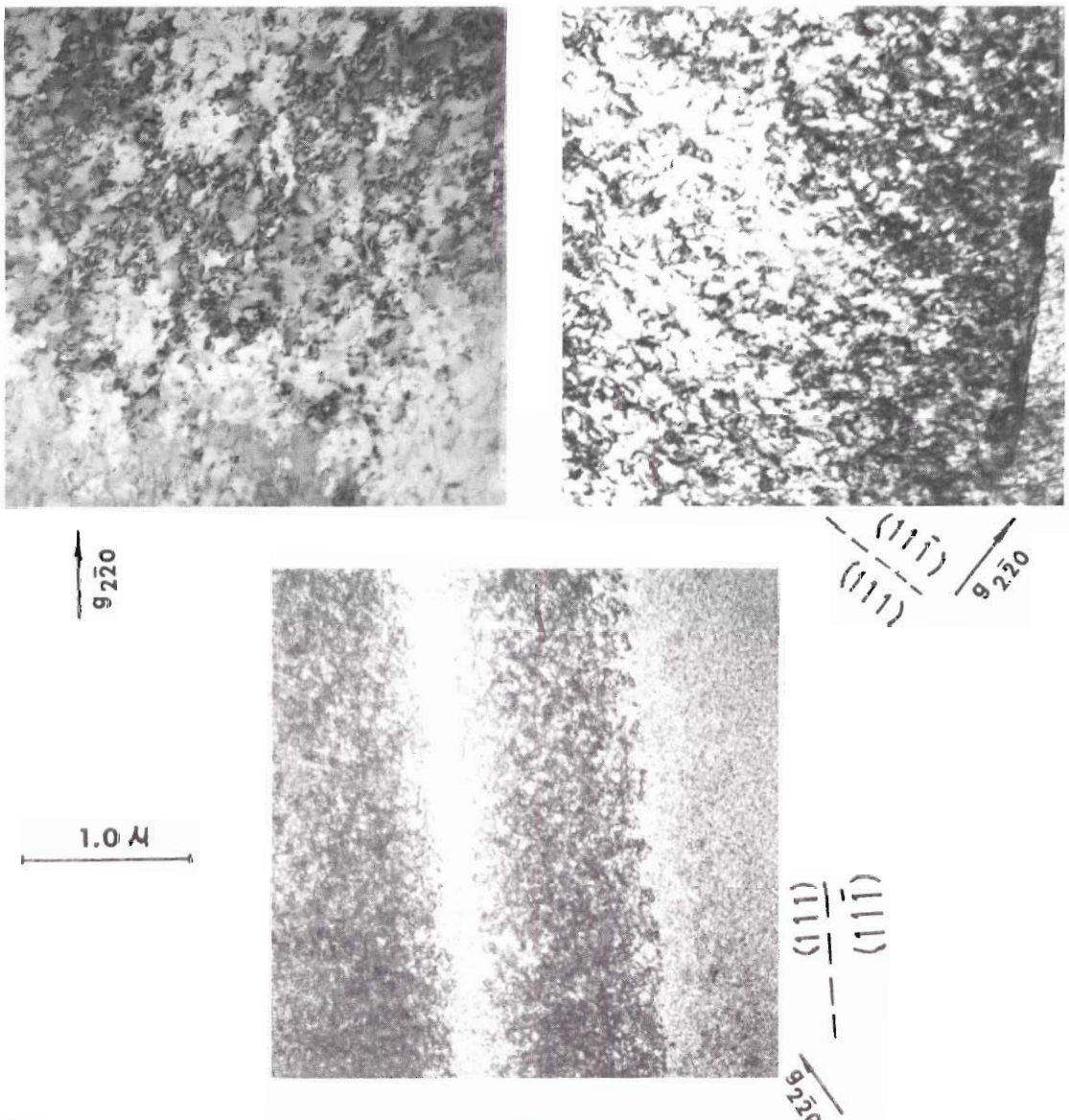

Figure 21. Deformation Structure of Al-Zn-Mg Tensile Samples Sectioned Below Fracture Surfaces. (a) 0.25 Hours, (b) 4 Hours, and (c) 12 Hours Aged at 150°C.

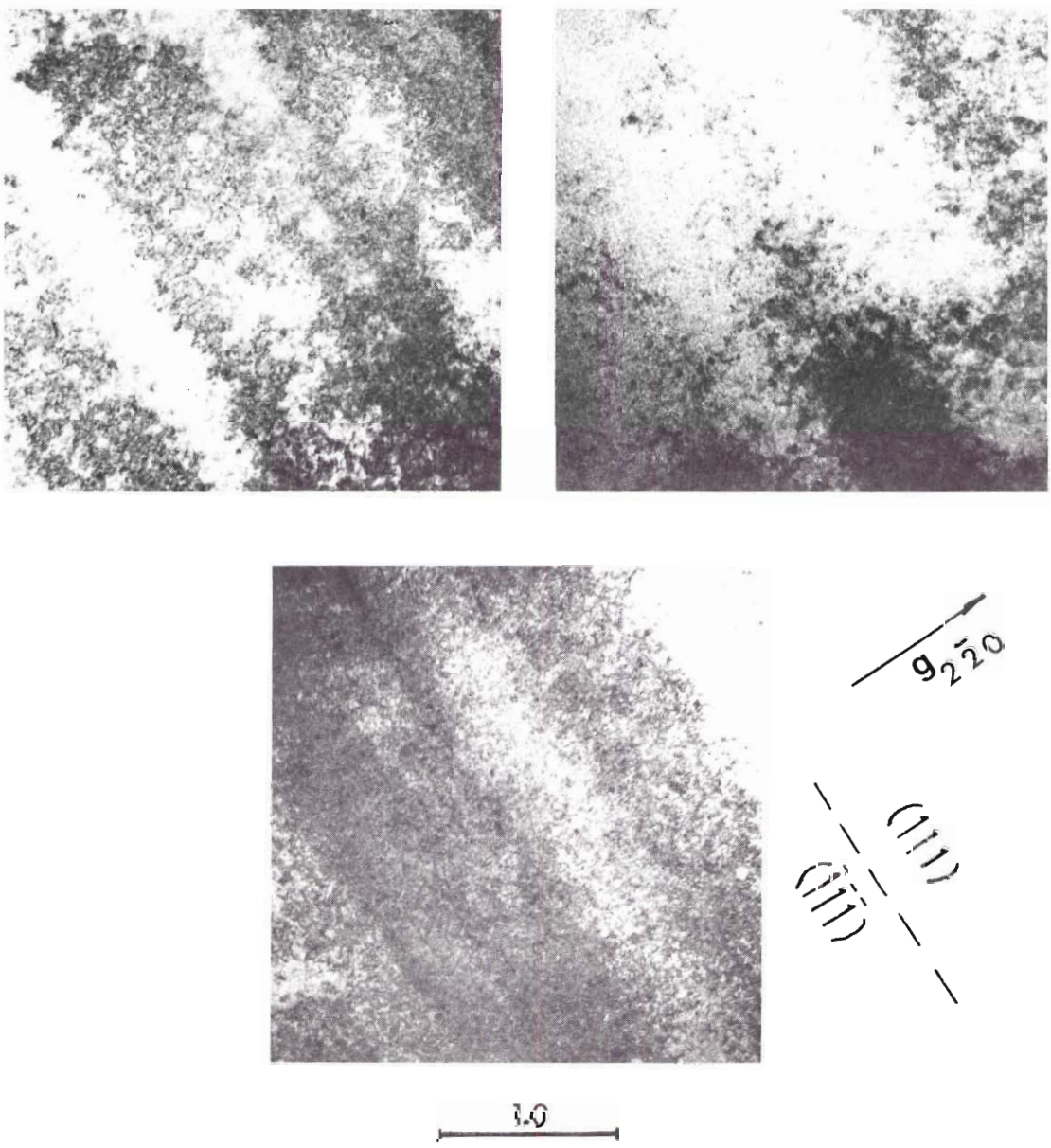

Figure 22. Variation of Dislocation Contrast with Foil Tilt, in a Tensile Specimen Aged 96 Hours at 150°C, Sectioned Directly Below Fracture Surface.

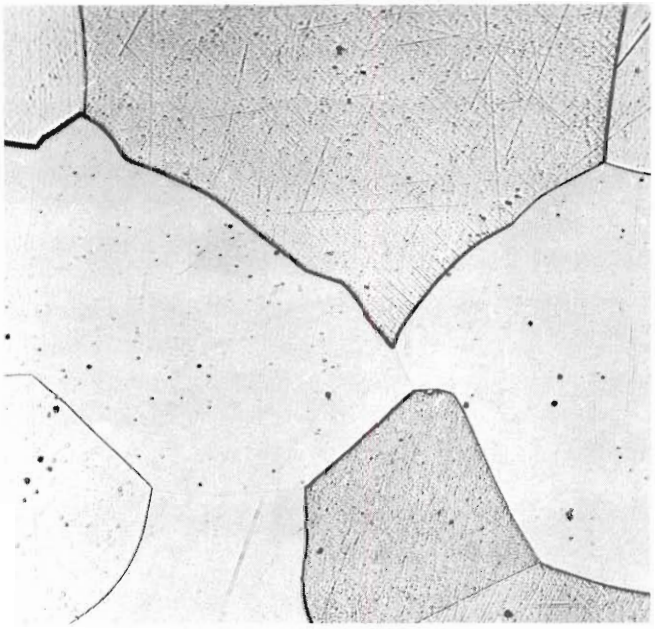

a

100 x

b

Figure 23. Effect of Aging on Slip Band Formation in Al-Zn-Mg: (a) Under-aged Sample, Showing no Slip Traces, (b) Aged Sample Showing Slip Bands.

Table 2. Summary of Tensile and Fatigue Data

Treatment	σ_o (0.2% Off-Set) Kg/mm^2	ε_f%	n	n'	-c	ε'_f%
		Al-Zn-Mg				
0.25 hr. @ 120°C	15	33	0.150	0.160	0.59	30
4 hr. @ 120°C	33	11	0.055	0.045	0.50	10
0.25 hr. @ 150°C	15	38	0.110	0.130	0.66	35
4 hr. @ 150°C	30	22	0.070	0.095	0.64	30
9 hr. @ 150°C	36	12	0.080	0.080	0.50	13
24 hr. @ 150°C	37	6	0.050	0.050	0.46	10
96 hr. @ 150°C	36	8	0.050	0.050	0.50	11
4 hr. @ 120°C + 24 hr. @ 150°C	36	5	0.050	0.050	0.50	4
		7050				
4 hr. @ 120°C	50	20	0.065	0.115	0.610	19
24 hr. @ 120°C	54	12	0.075	0.130	0.590	22
0.25 hr. @ 150°C	43	19	0.090	0.130	0.609	19
4 hr. @ 150°C	51	13	0.050	0.105	0.840 0.450	125 17
24 hr. @ 150°C	53	13	0.080	0.110	0.780 0.450	100 17
96 hr. @ 150°C	50	15	0.040	0.040	0.780 0.450	100 17
24 hr. @ 120°C + 24 hr. @ 150°C	58	11	0.015	0.015	0.670	26

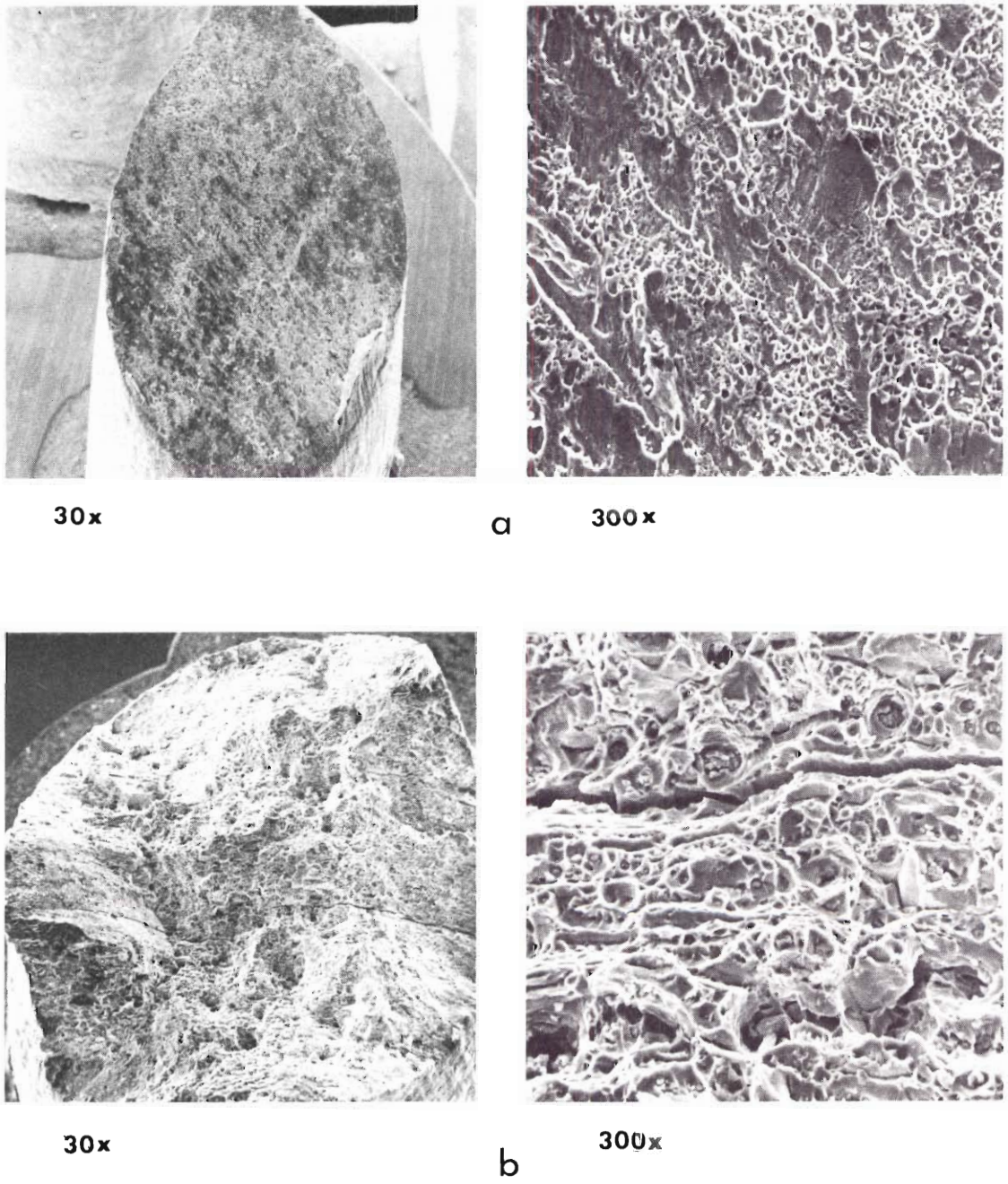

Figure 24. Fracture Behavior of 7050: (a) As Quenched, (b) Aged 96 Hours at 120°C.

for 96 hours at 120°C, Figure 24.

Detailed TEM of 7050 samples pulled to fracture revealed, generally, the same type of dislocation behavior as indicated earlier for the ternary Al-Zn-Mg alloy. However, it was noted upon optical examination that the tensile sample surfaces did not exhibit the coarse slip lines that had been seen in the large grained ternary Al-Zn-Mg alloy. In some cases regions of small, non-uniform grains or subgrains were observed prior to the deformation, Figure 25(a) and (b). Subgrains or cells were also observed, in a few instances, after deformation, Figure 25(c) and (d). This type of structure was never observed in the ternary alloy.

Low cycle fatigue behavior for most materials has been shown to fit the Coffin-Manson[89] relationship in the form:

$$\frac{\Delta\varepsilon_p}{2} = \varepsilon_f' \, (2N_f)^{-c} \qquad (5)$$

where,

$\Delta\varepsilon_p$ - is the plastic strain range,

ε_f' - is the fatigue ductility coefficient,

$2N_f$ - is the number of reversals to failure, and

c - is the fatigue ductility exponent.

This general relationship was found to describe the low cycle fatigue behavior of the Al-Zn-Mg alloy aged at 120°C and 150°C for various times. Two complete data sets that demonstrate the typical response to various levels of cyclic straining are given in Figures 24 and 25. The complete set of data for all aging temperatures and times is given in Appendix A.

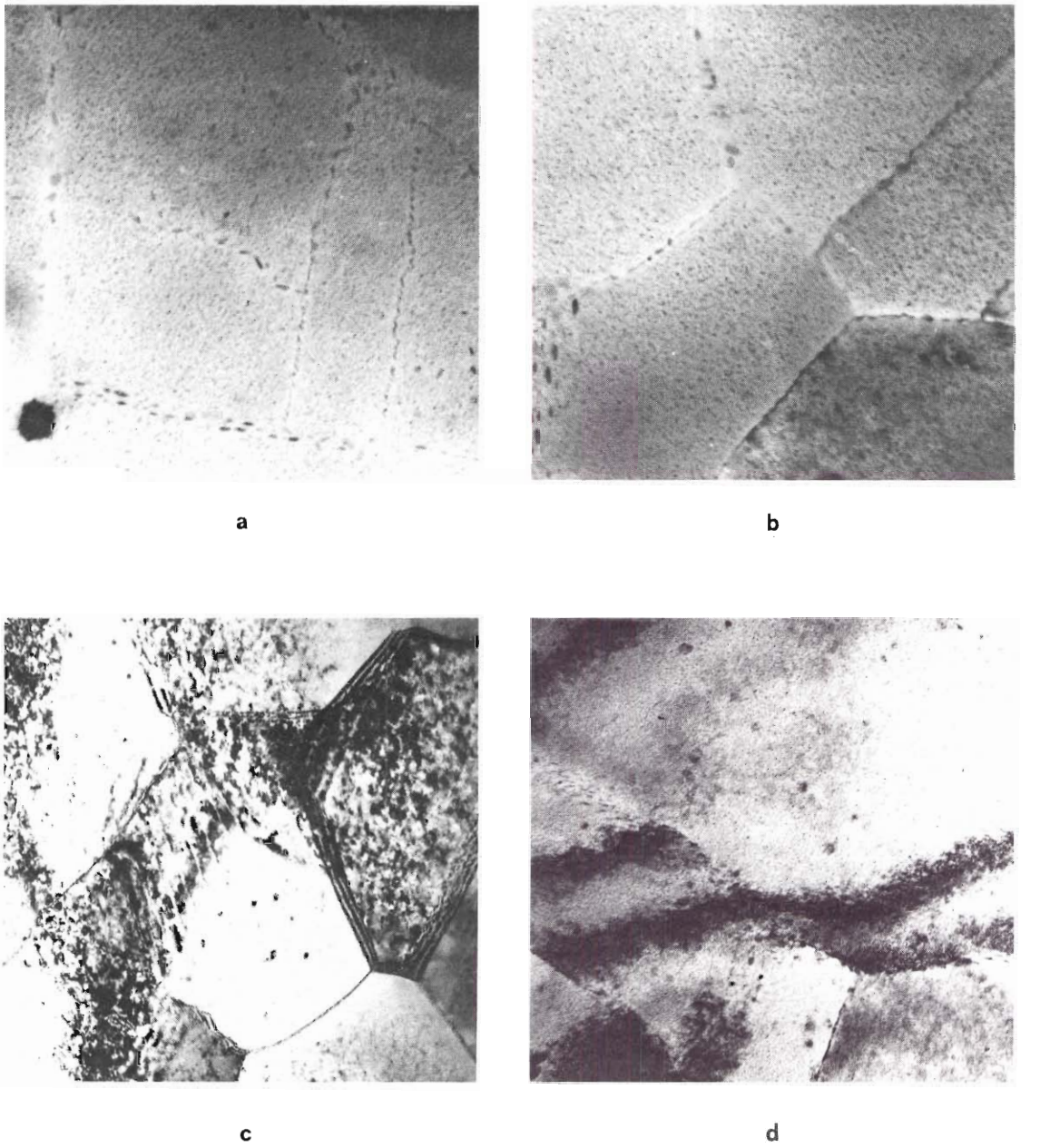

Figure 25. Example of Non-uniform Grain Size and Shape: (a) and (b) Underformed Sample Aged 8 Hours at 120°C, (c) and (d) Deformed Samples at 0.25 Hours at 150°C and 24 Hours at 150°C, Respectively, Containing Small Sub-Grains.

There are essentially three methods of plotting the cyclic data. First, the variation of mean stress with cycles; second, the plastic strain amplitude versus cycles to failure, which is called the Coffin-Manson plot; and third, a cyclic stress-strain curve giving the cyclic hardening exponent, n', which can be expressed mathematically as

$$\sigma_a = \sigma_f' \left(\frac{\Delta\varepsilon_p}{2}\right)^{n'} \qquad (6)$$

where

σ_a - is the stress amplitude and

σ_f' - is the fatigue strength coefficient

The Coffin-Manson relationship was found to describe the low cycle fatigue behavior of the Al-Zn-Mg alloy aged at 120°C and 150°C for the times tested. However, extrapolating $2N_f = 1$ for samples aged at 150°C for four hours or longer gave a value $\varepsilon_f' > \varepsilon_f$, where ε_f is the fracture elongation determined from monotonic tension tests. It was also found that as aging time increased, there was a corresponding decrease in c, the slope of the Coffin-Manson plot, thus indicating a low cycle fatigue dependence on the microstructure. Representative fatigue curves are given in Figures 26 and 27. All the fatigue data are summarized in Table 2 along with the monotonic properties. The complete set of fatigue date is given in Appendix A.

Optical examination of the fractured fatigue specimens showed the same general variation of fracture features exhibited by the uniaxial tensile samples. Coarse slip lines were only observed in aged fatigue samples; metallographic examination of polished and etched

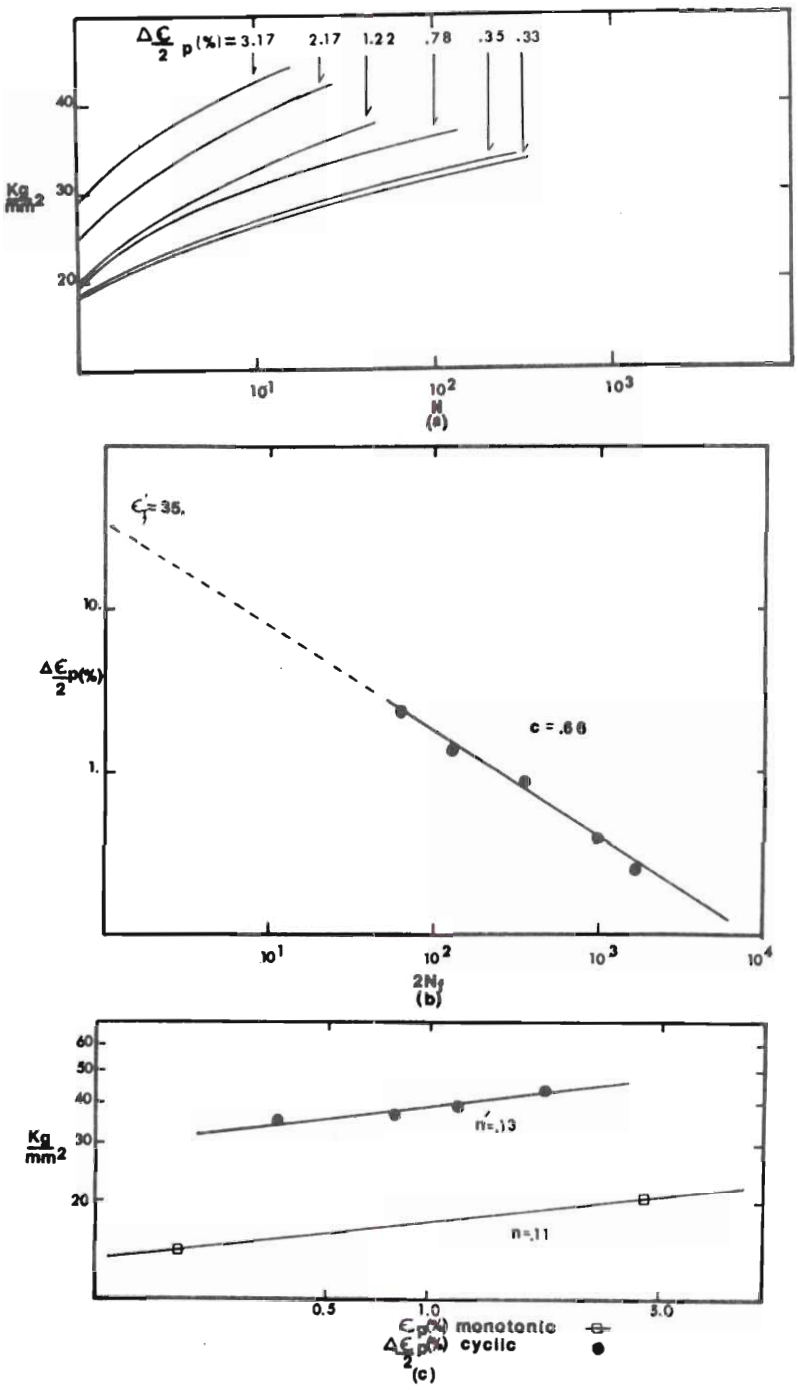

Figure 26. Low Cycle Fatigue Behavior of Al-Zn-Mg Aged at 150°C for 0.25 Hours: (a) Stress Amplitude versus cycles, (b) Coffin-Manson Plot, and (c) Cyclic and Monotonic Stress-Strain.

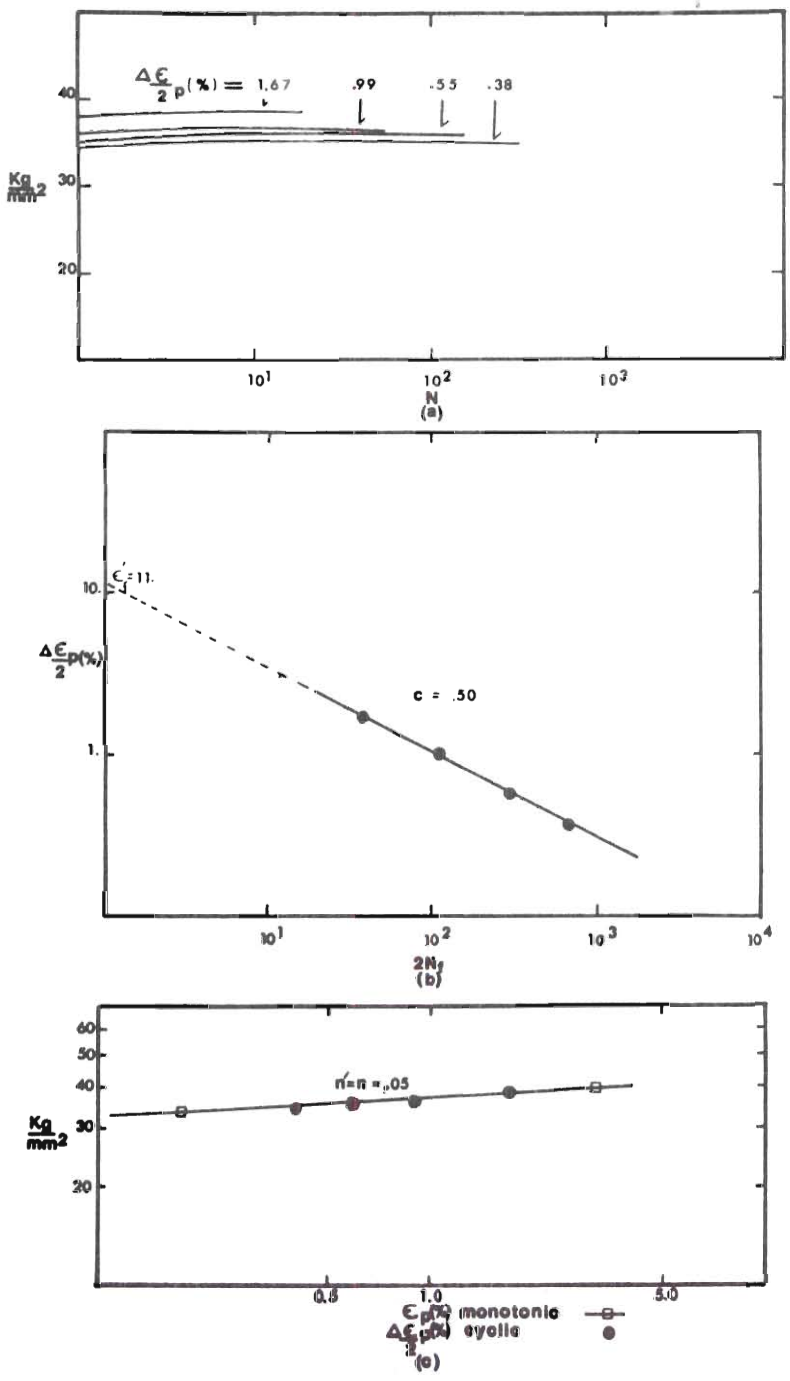

Figure 27. Low Cycle Fatigue Behavior of Al-Zn-Mg Aged at 150°C for 96 Hours: (a) Stress Amplitude versus cycles, (b) Coffin-Manson Plot, and (c) Cyclic and Monotonic Stress-Strain.

fracture cross sections showed non-uniformly distributed coarse slip in the aged samples. Figure 28 shows slip lines on a specimen aged at 120°C for four hours and fatigued at $\Delta\varepsilon_p/2 = 0.3$ per cent to failure, $N_f = 666$ cycles. A high density of slip lines was observed around a secondary crack that appeared below the main crack. Scanning electron fractography illustrated the tendency toward transgranular fracture. In Figures 29 a and b, and 30 a and b, a ring of transgranular fracture can be seen. The fatigue crack initiated at the surface and a circumfrential crack front propagated radially toward the center. The fatigue damage was characterized by beach marks and can be seen in Figures 29b and 30b. The overload failure, characterized by intergranular fracture for this heat treatment, is located in the central portion of Figures 29a and 30 a. High magnification micrographs for the overload failure are shown in Figures 29 c and d, and 30 c and d.

TEM on thin foils from under aged fatigue specimens sectioned directly below the fracture surfaces, generally showed dense, uniform dislocation tangles, indicative of homogeneous slip. Slip bands were observed in foils prepared from directly below the fracture surfaces on samples aged to maximum strength or overaged samples. Aging had simila effects on the resultant deformation microstructure,as was observed during uniaxial tension tests. Figures 31 and 32 show the deformation structure for Al-Zn-Mg aged at 150°C and double agedfor 4 hours at 120°C followed by 24 hours at 150°C.

Low cycle fatigue behavior of the 7050 alloy aged 4 hours at 120°C and 0.25 hours at 150°C was found to comply with the Coffin-

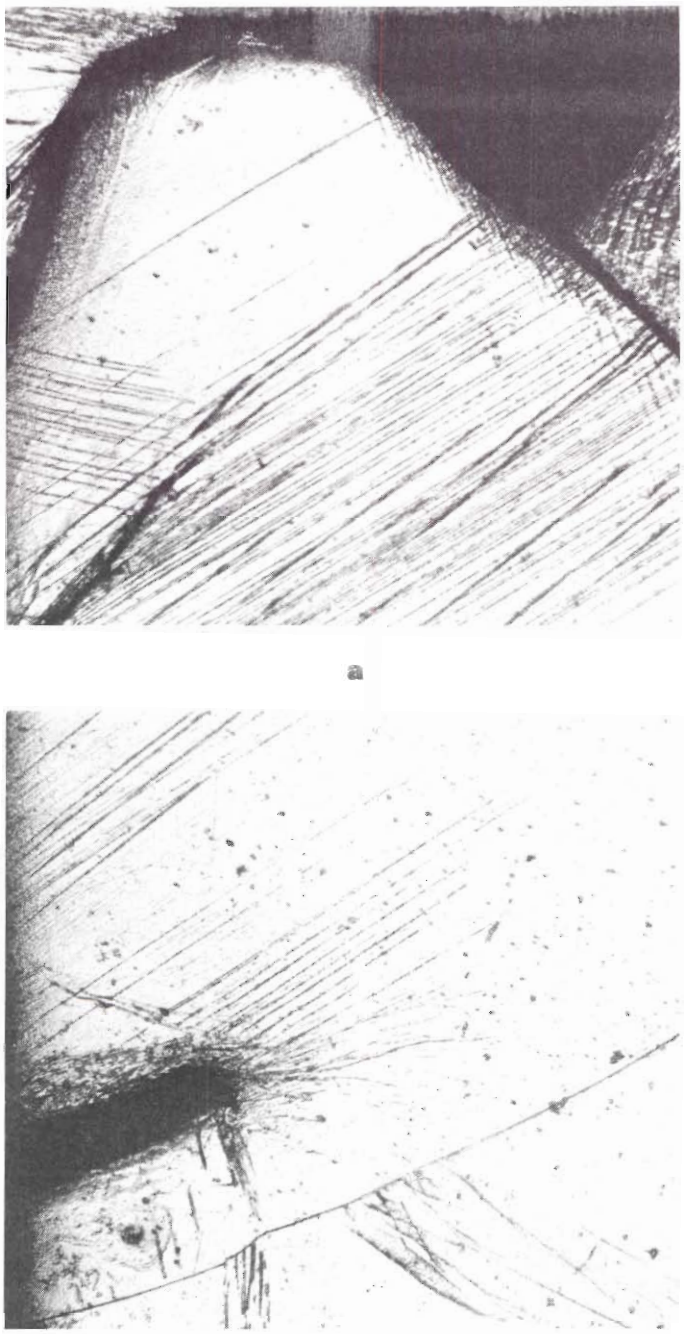

Figure 28. Al-Zn-Mg Aged 4 Hours at 120°C, Fatigued to Failure, $\Delta\varepsilon_p/2 = 0.3\%$ and $N_f = 666$. The Specimen was Sectioned Perpendicular to the Fracture Surface. (a) Slip Traces in a Grain at the Fracture Surface, (b) Secondary Crack Elsewhere in the Gage Section.

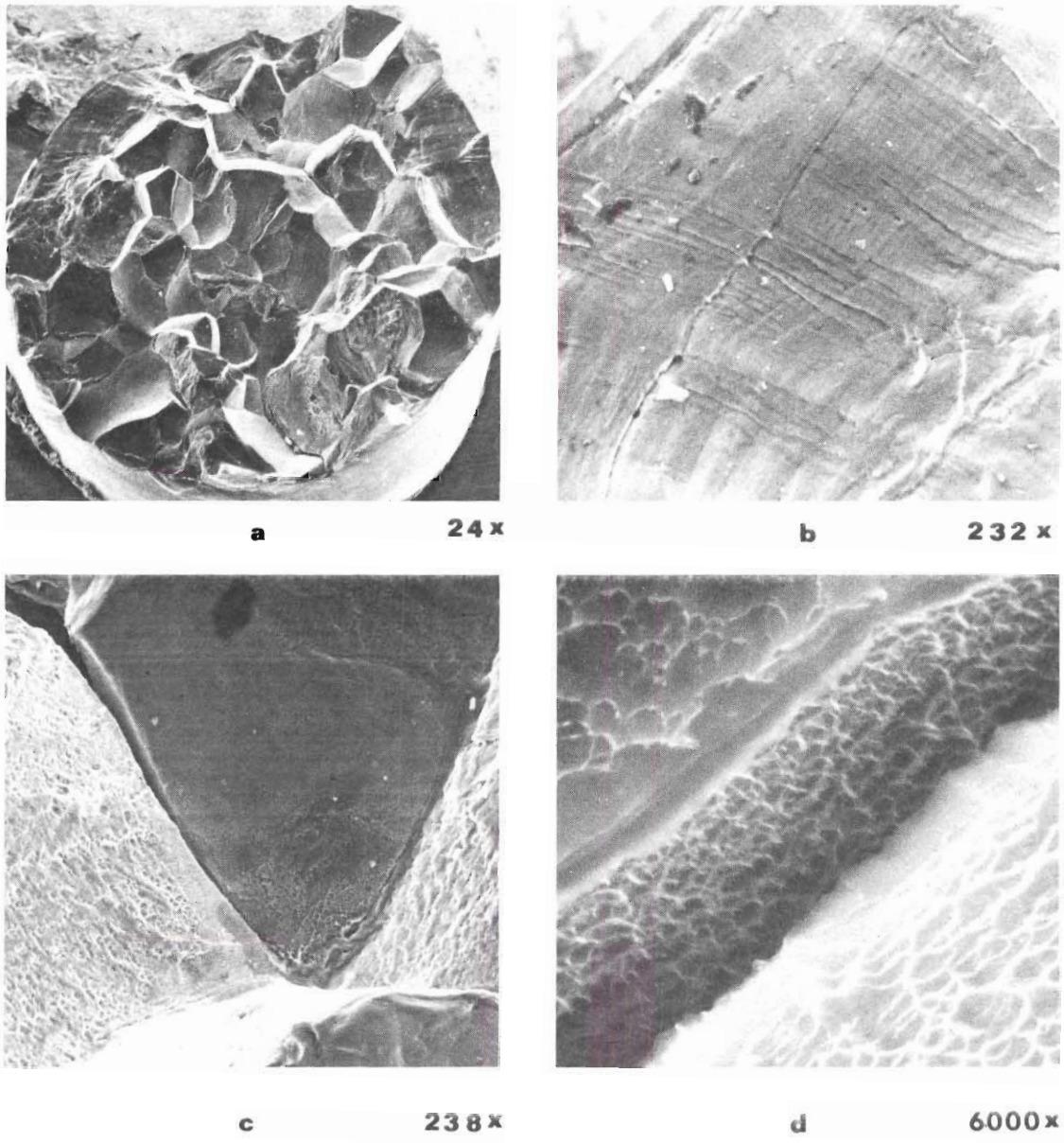

Figure 29. Fractographs of Al-Zn-Mg. Aged 24 Hours at 150 °C and Fatigue to Fracture: $\Delta\varepsilon_p/2$ = 1.10 per cent, and N_f = 49 Cycles: (a) Overall view of the Fracture Surface, (b) Expanded View Showing the Presence of the Characteristic "Beach Marks" Associated with Fatigue Damage, (c) Overload Failure, Characterized by the Intergranular Fracture for this Aging Condition, and (d) High Magnification Micrograph Showing Dimple Features on the Overload Fracture Surface.

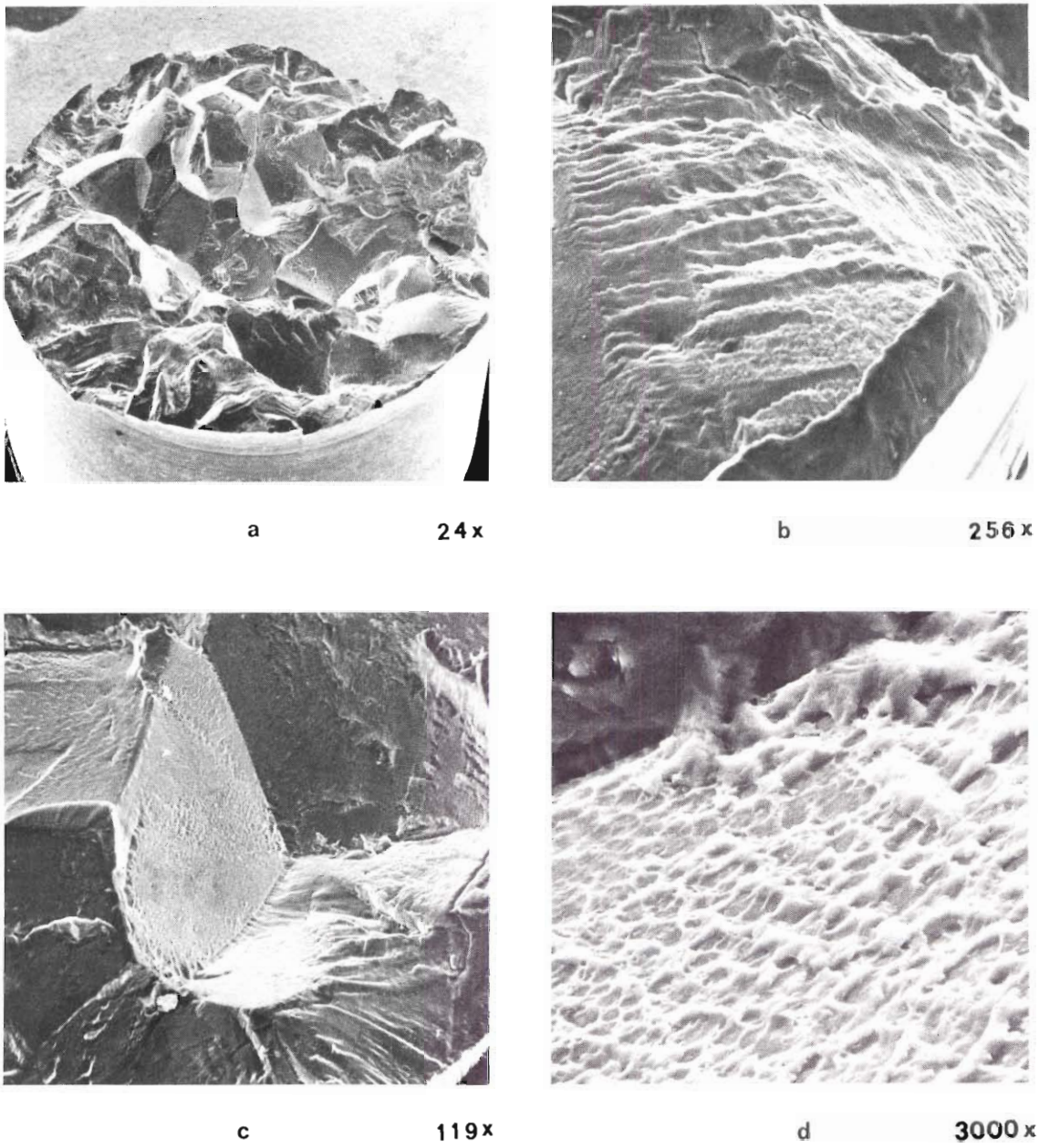

Figure 30. Fractographs of Al-Zn-Mg, Aged 24 Hours at 150°C, Fatigued to Fracture: $\Delta\varepsilon_p/2$=0.12 Percent, N_f = 3000 Cycles: (a) Overall View of the Fracture Surface, (b) Expanded View Showing the Presence of the Characteristic "Beach Marks" Associated with Fatigue Damage, (c) Over-load Failure, Characterized by the Intergranular Fracture for this Aging Condition, and (d) High Magnification Micrograph Showing Dimple Features on the Overload Fracture Surface.

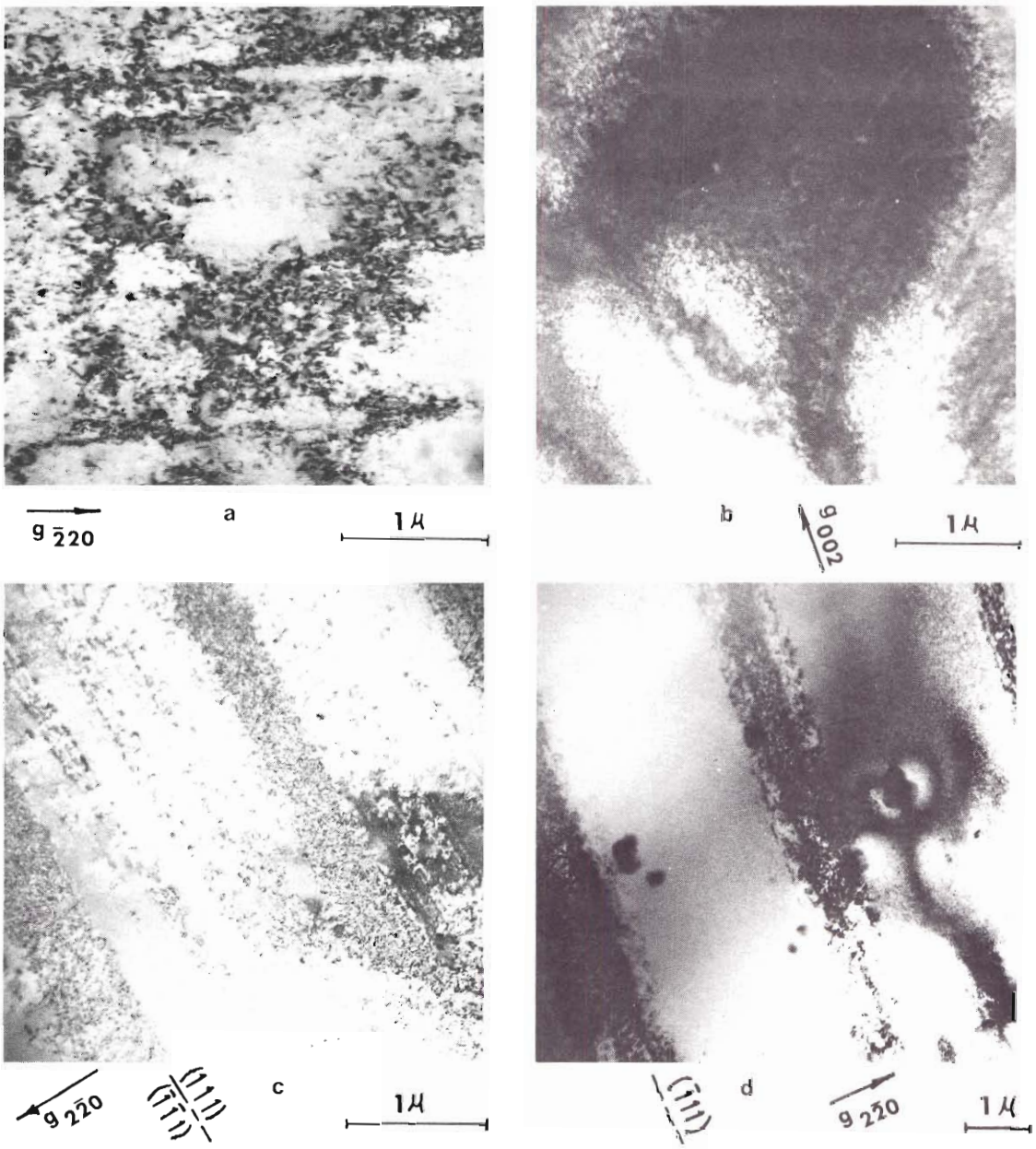

Figure 31. Deformation Structure of Al-Zn-Mg Aged at 150°C for Different Times and Fatigued to Failure: (a) 0.25 Hours $\Delta\varepsilon_p/2$ = 0.35 per cent, N_f = 4000 Cycles, (b) 4 Hours $\Delta\varepsilon_p/2$ = 0.31 per cent, N_f = 520 Cycles, (c) 9 Hours $\Delta\varepsilon_p/2$ = 0.26 per cent, N_f = 380 Cycles, and (d) 24 Hours, $\Delta\varepsilon_p/2$ = 0.35 per cent, N_f = 1000 Cycles.

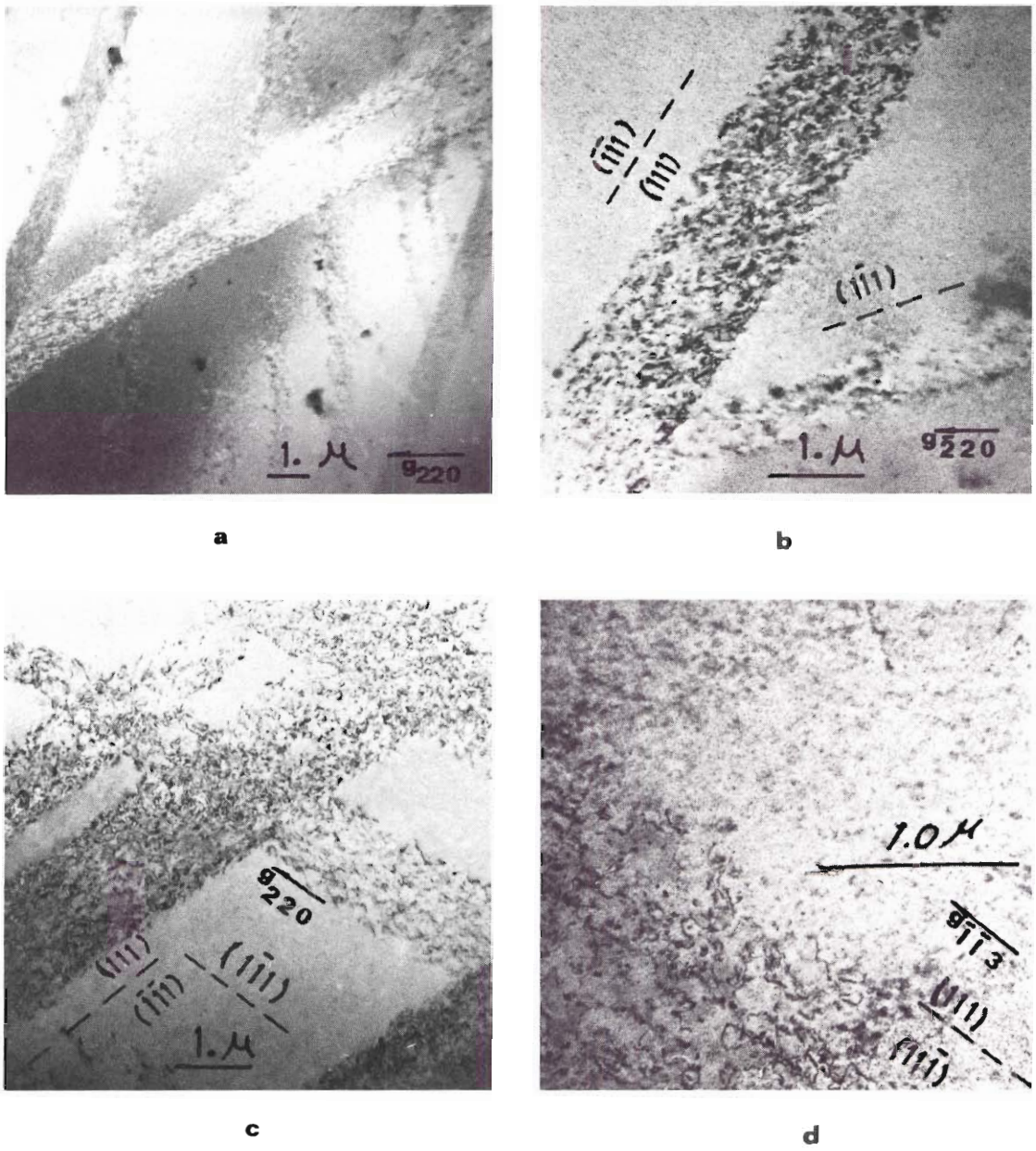

Figure 32. Al-Zn-Mg Double Aged 4 Hours at 120°C and 24 Hours at 150°C, and Fatigued to Failure: (a) and (b) $\Delta\varepsilon_p/2$ = 2.1 per cent, N_f = 42 Cycles, and (c) and (d) $\Delta\varepsilon_p/2$ = 0.6 per cent, N_f = 476 Cycles.

Manson relation. The extrapolated values for the monotonic elongation at fracture were in good agreement with the tensile data. The low cycle fatigue data of the 7050, aged for 24 hours at 120°C or double aged for 24 hours at 120°C followed by 24 hours at 150°C, were found to fall on a straight line, but the extrapolated fracture values were higher than those obtained in the monotonic tests. However, the low cycle fatigue data for 7050 aged for4 hours or longer (at least up to 96 hours) at 150°C resulted in a data set which had a distinct break at $\Delta\varepsilon_p/2 \simeq 1.0$ per cent. Representative data are given in Figures 33-37, and the cyclic and monotonic properties are summarized in Table 2.

Optical and scanning microscopic examination of the fractured fatigue specimens showed a transverse fracture propagating from the surface of the fatigue specimen toward the center, Figure 38a and c. The fatigue damage can be seen in Figure 38b, and the overload region in Figure 38d. Metallographic examination did not reveal coarse surface slip lines like those observed for the large grained ternary Al-Zn-Mg alloy. TEM on thin foils from below the fracture surface revealed dislocation structure similar to the tensile deformation. Microscopy on samples cycled on either side of the break in the fatigue life curve showed a tendency for cell like structure to form on the high plastic strain amplitude side of the break, and dislocation bands at the low plastic strain amplitude side, Figures 39 and 40.

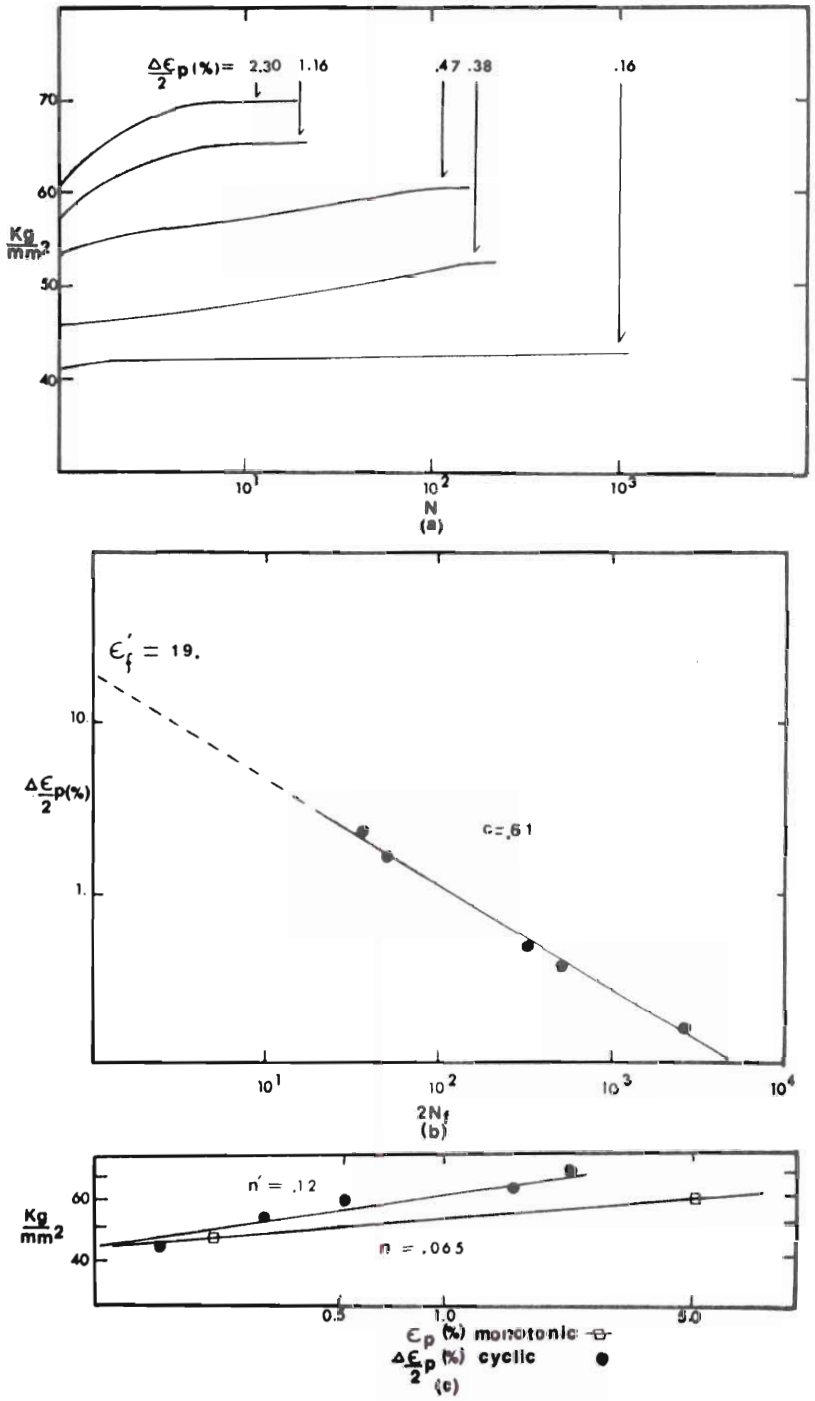

Figure 33. Low Cycle Fatigue Behavior of 7050 Aged 4 Hours at 120°C (a) Stress Amplitude versus N, (b) Coffin-Manson Plot, and (c) Cyclic and Monotonic Stress-Strain.

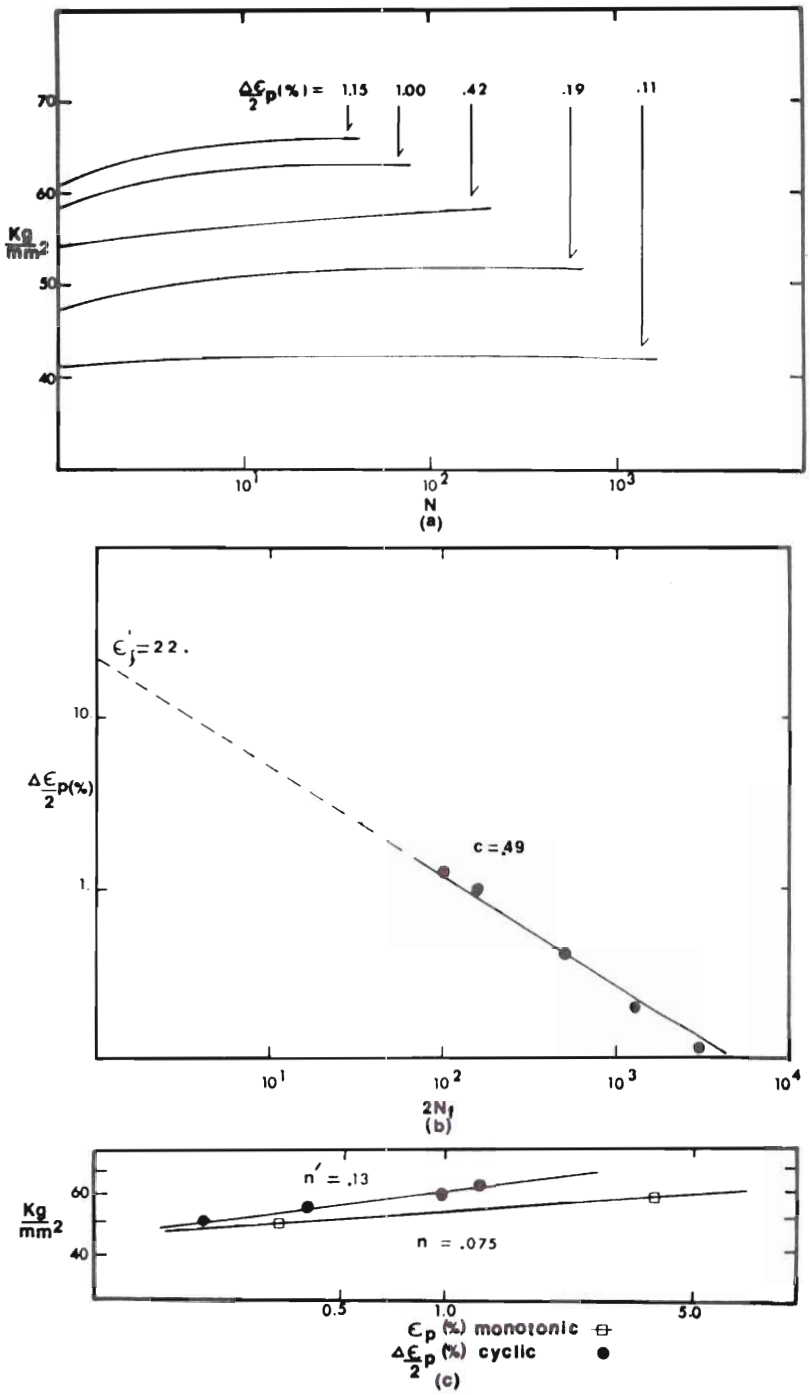

Figure 34. Low Cycle Fatigue Behavior of 7050 Aged 24 Hours at 120°C: (a) Stress Amplitude versus N, (b) Coffin-Manson Plot, and (c) Cyclic and Monotonic Stress-Strain.

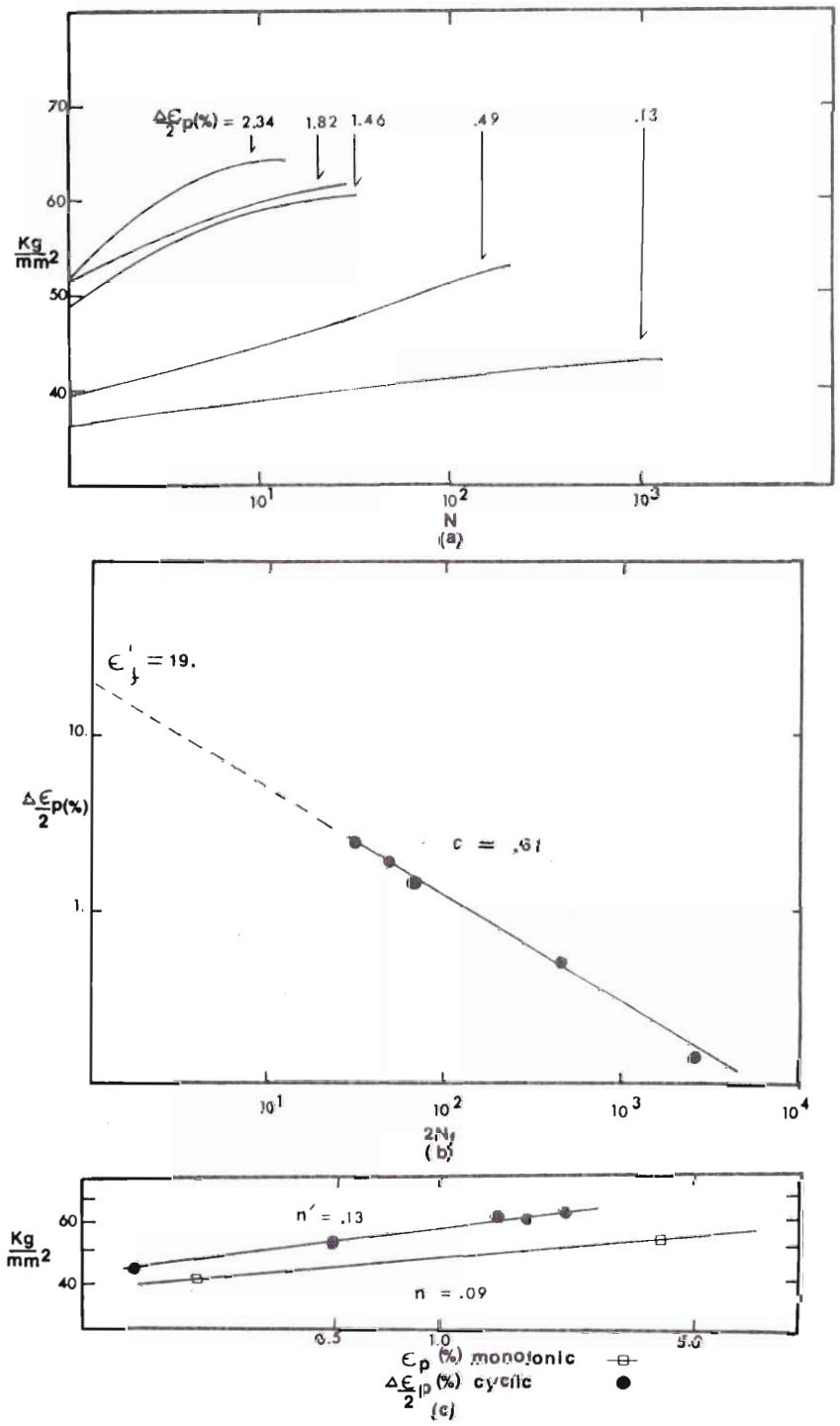

Figure 35. Low Cycle Fatigue Behavior of 7050 Aged 0.25 Hours at 150°C: (a) Stress Amplitude versus N, (b) Coffin-Manson Plot, and (c) Cyclic and Monotonic Stress-Strain,

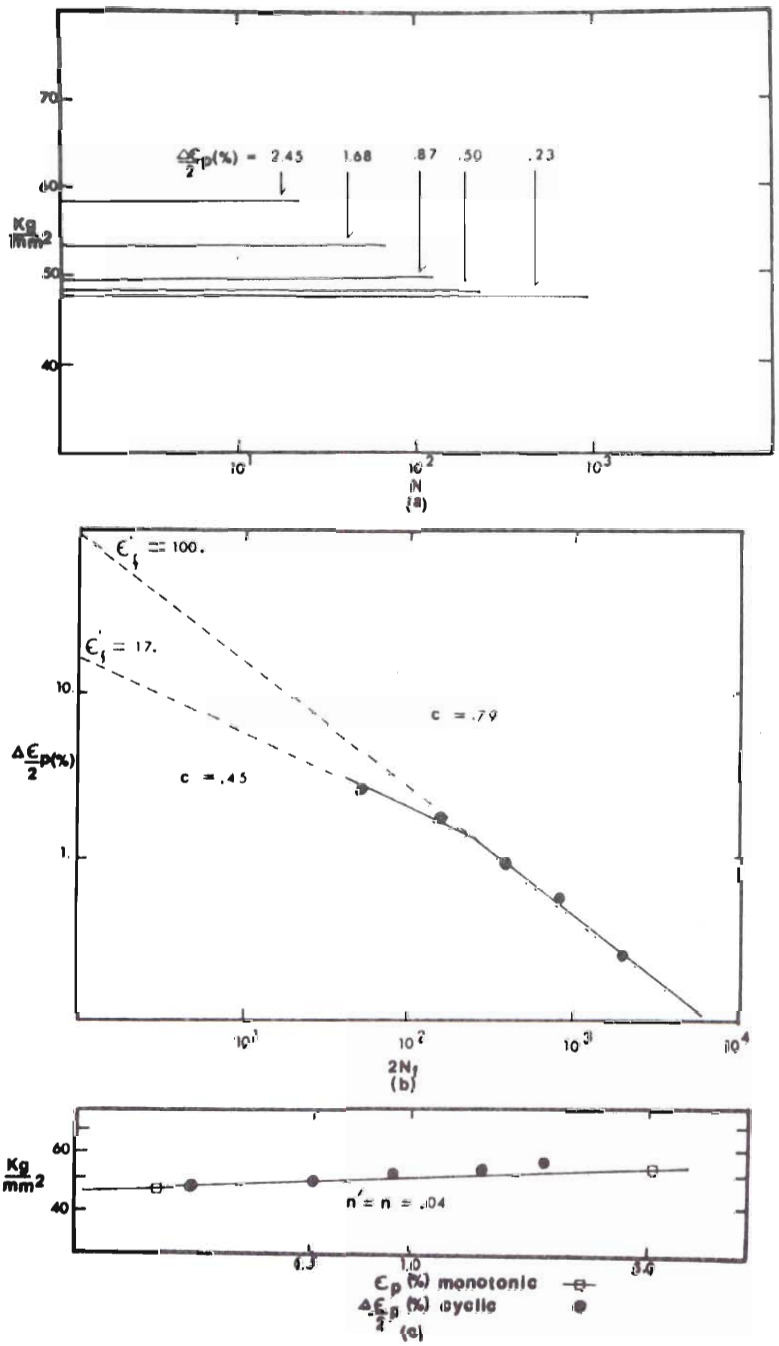

Figure 36. Low Cycle Fatigue Behavior of 7050 Aged 96 Hours at 150°C: (a) Stress Amplitude versus N, (b) Coffin-Manson Plot, and (c) Cyclic and Monotonic Stress-Strain.

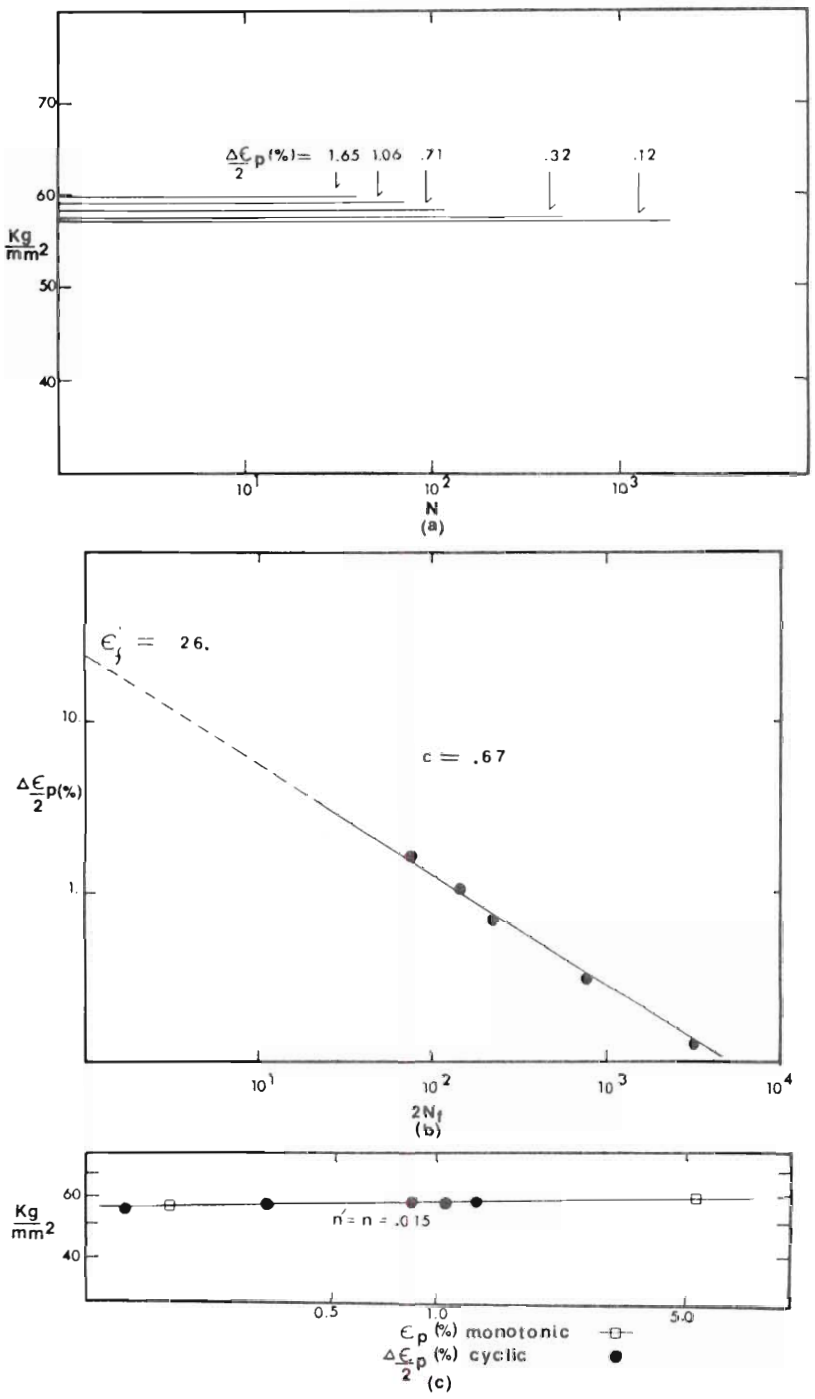

Figure 37. Low Cycle Fatigue Behavior of 7050 Double Aged 24 Hours at 120°C Followed By 24 Hours at 150°C: (a) Stress Amplitude Versus N, (b) Coffin-Manson Plot, and (c) Cyclic and Monotonic Stress-Strain.

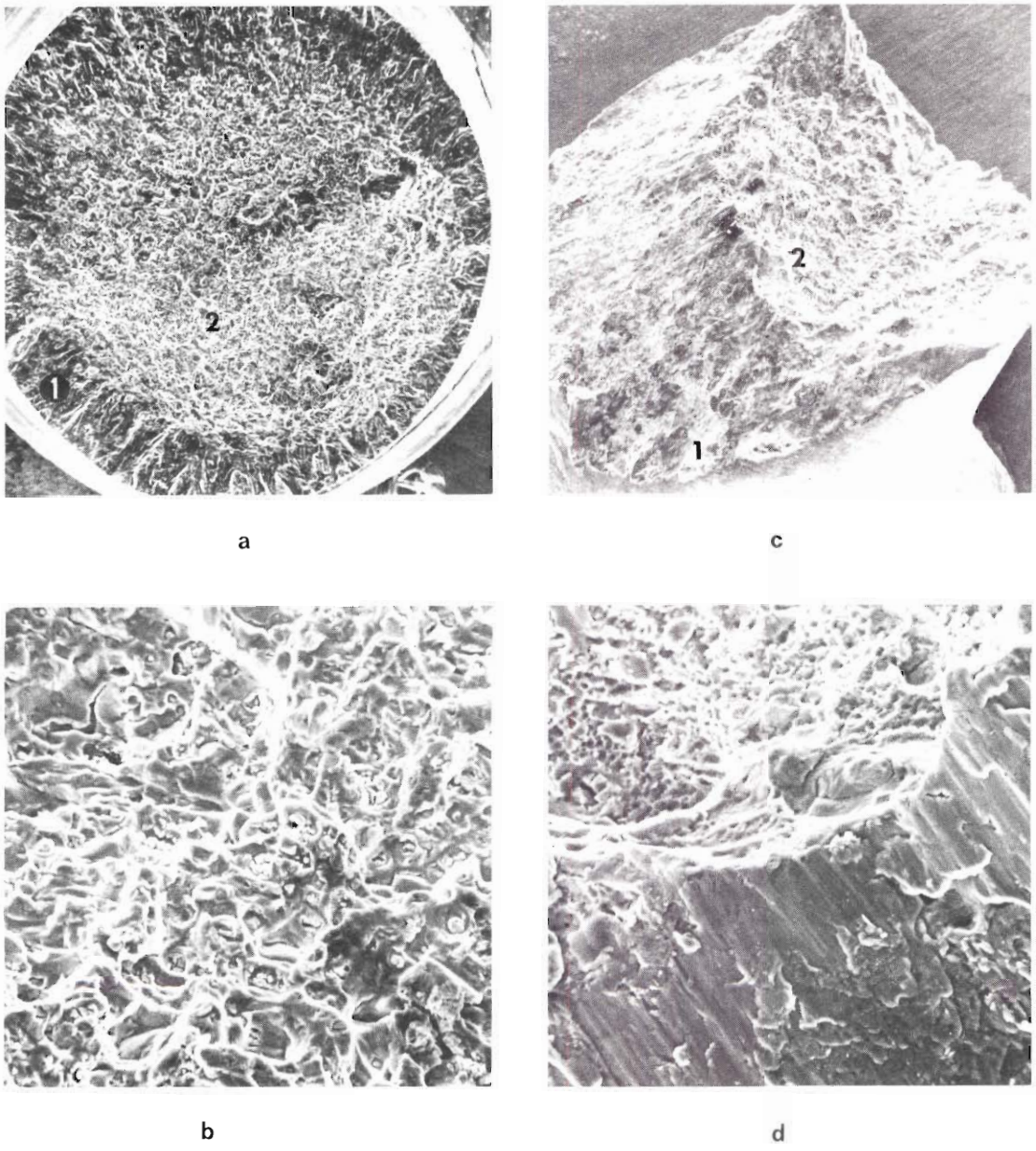

Figure 38. Fractographs of 7050, Aged 24 Hours at 150°C and Fatigued to Failure: (a) and (b), $\Delta\varepsilon_p/2$ = 3.8 per cent, N_f = 9 Cycles, and (c) and (d), $\Delta\varepsilon_p/2$ = 0.17 per cent, N_f = 1680 Cycles; (a) Region 1 Shows the Transverse Fatigue Fracture Initiated at the Surface, Region 2 is the Overload Fracture Surface; (b) Expanded View of (a); (c) Region 1 Shows the Ring of Fatigue Damage that Initiated at the Surface and Propagated Radially Toward the Center, Region 2 Shows the Transverse Overload Fracture Surface, and (d) Expanded View of Region 2 Showing the Overload Fracture Surface.

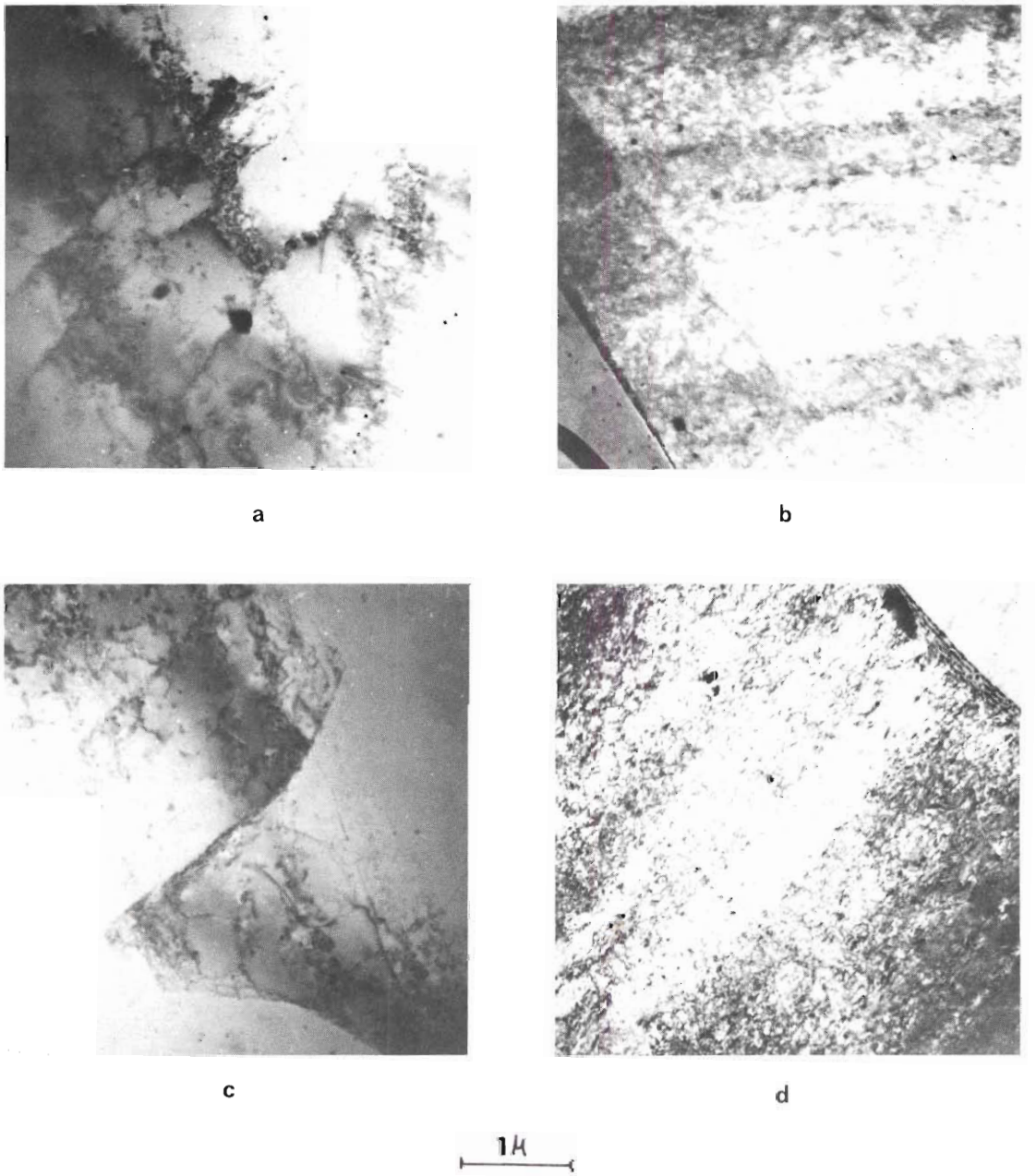

Figure 39. Deforamtion Structure in 7050, Aged 4 Hours at 150°C and Fatigue to Failure (a) and (c) Cell Formation at High Plastic Strain Amplitudes and (b) and (d) Dislocation Bands at Low Plastic Strain Amplitudes.

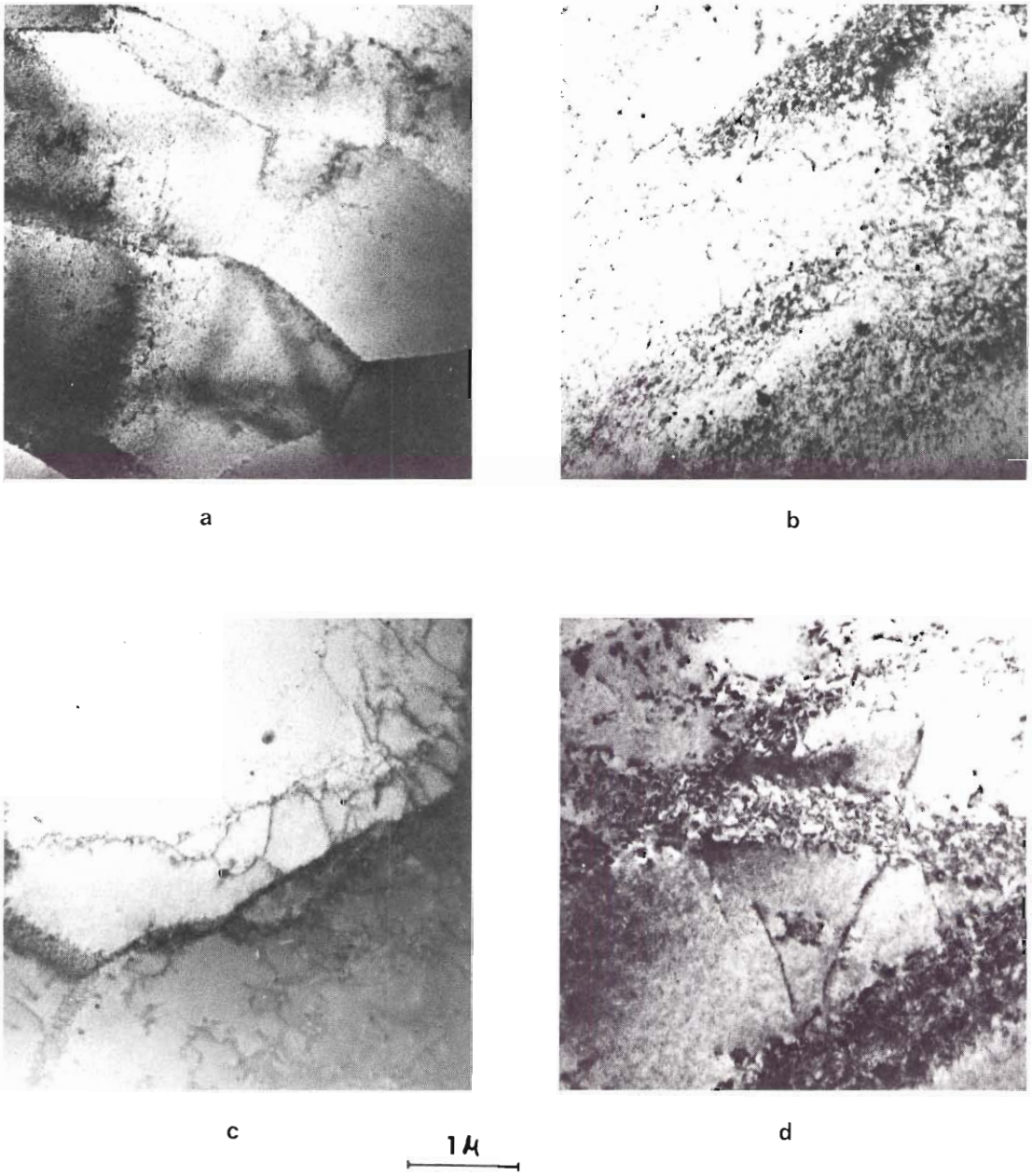

Figure 40. Deformation Structure in 7050, Aged 24 Hours at 150°C and Fatigued to Failure. (a) and (c) Cell Formation at High Plastic Strain Amplitude, and (b) and (d) Dislocation Bands at Low Plastic Strain Amplitude.

CHAPTER V

DISCUSSION OF RESULTS

The intermetallic compounds Al_2CuMg and Al_2Cu were distributed throughout the 7050 alloy. Extensive cold work followed by solutionizing at 480°C for as long as 24 hours did not cause these particles to dissolve. This fact indicates that the solid solution temperature for this alloy is greater than 480°C. The extent of solubility of copper in this system depends upon the zinc:magnesium ratio; increasing this ratio increases the amount of copper that can be taken into solution at a given temperature.

The chemical composition of the two quarternary alloy that are being concurrently investigated is shown in Table III.

Table III. Chemical Analysis of the Two Alloys Concurrently Being Investigated

Alloy Number	Si	Fe	Cu	Mn	Mg	Cr	Ni	Zn	Ti	Be
77	.01	.00	1.55	.00	2.23	.00	.00	6.16	.00	.00
78	.01	.00	2.53	.00	2.40	.00	.00	6.29	.00	.00

The alloy containing less copper had a grain size and morphology similar to the ternary Al-Zn-Mg alloy[95]; however, the alloy with the higher copper content was found to be similar to the 7050 alloy in grain size and morphology and in distribution of the copper rich

intermetallics, as well. From these results it may be deduced that at least 1.5 per cent copper can be dissolved at 480°C. Copper in excess of this quantity forms the copper rich intermetallics, which can act as a grain refiner.

The presence of at least 1.5 per cent copper that does not participate in the formation of the Al_2Cu intermetallics, for the heat treatments used in this investigation, must be considered. There are essentially three possibilities concerning the function of copper. It may:

1. precipitate as θ (Al_2Cu),
2. precipitate as S (Al_2CuMg),

   or

3. enter into η ($MgZn_2$) precipitation sequence.

Polmear[51] proposed that the rapid hardness increase in the initial stage of aging was associated with the S(Al_2MgCu) sequence. However, analysis of hardness data by Silcock[96] on the Al-Cu-Mg system could not account for the initially high hardness values.

Given the orientation relationship for the S phase:

$[100]_S \parallel [100]_{Al}$, $[010]_S \parallel [0\bar{2}1]_{Al}$ and

$[001]_S \parallel [012]_{Al}$

along with the orthorhombic cell:

a = 4.0, b = 9.23 and c = 7.14 A,

generated diffraction patterns did not produce a distribution of diffraction spots similar to that observed in the SAD patterns, Appendix B. Diffuse streaking in the Al-Cu-Mg and Al-Cu systems (in

both x-ray and electron diffraction patterns) has been reported in the $\langle 100 \rangle_{Al}$ [96] direction. No diffuse streaks in the SAD patterns in $\langle 100 \rangle_{Al}$ were ever observed in the present study, therefore, the θ precipitation sequence was ruled out.

Thomas and Nutting[97] investigated two Al-Zn-Mg alloys, one of which contained copper additions. They concluded that the three stage aging sequence remained essentially the same, i.e.,

$$\text{G.P.} \rightarrow \eta' \rightarrow \eta, \tag{7}$$

and that copper entered directly into the G.P. zones. However, this explanation was not complete because the electron:atom ratio range for which the $MgZn_2$ type structure is stable was not taken into consideration.

The type of Friauf-Laves structure that will form has been found to be sensitive to the electron:atom ratio. (See the Literature Review for a discussion on this point.) The addition of copper to $MgZn_2$ would cause the structure to become the $MgCu_2$ type, which would require a change in space group from $P6_3/mmc$ to Fd3m. To compensate for the presence of copper, aluminum may go into the zones, allowing the $MgZn_2$ structure to be maintained. In support of this argument, it has been shown[98] that the structure series from $MgZn_2$ to MgAlCu is isomorphous. It would therefore seem logical to assume that copper does enter into the precipitation process along with aluminum.

The most profound effect that copper had on the precipitation process was observed when Al-Zn-Mg and 7050 samples, aged at 150°C, were examined by TEM. In 7050 the precipitates were uniformly dis-

tributed up to the grain boundaries, which is in marked contrast to the PFZ formation seen in the ternary Al-Zn-Mg alloy. Figure 38 is a representation of the surface for homogeneous nucleation as a function of zinc and magnesium additions. Figure 41 predicts that the ternary alloy used in this research, Al-6.2%Zn-2.2%Mg, should have a homogeneous nucleation temperature in the vicinity of 150°C[99]. The presence of the large PFZ in the ternary alloy aged at 150°C, Figure 18a, demonstrated that the homogeneous nucleation temperature was below 150°C[100]. However, the narrow PFZ observed for 7050 alloy indicated that 150°C is below the G.P. solvus for this copper containing alloy[100]; This also gives credence to the idea that copper is participating in the G.P. zone formation.

The apparent increase in the critical temperature and the large, initial increase in hardness and proof stress observed in this research may be considered to be a result of a reduction of the barrier to nucleation by the presence of copper. This may be due to a reduction in the interfacial energy, or changes in the volume free energy or strain energy, or all three[100]. From the type data gathered in this research, it was not possible to determine which change (if not all) is occurring. However, regardless of the reason, a decrease in the nucleation barrier will cause a higher frequency of nucleation. Since it has been shown that copper has directly entered into the precipitation process, there is also an increase in the amount of solute available to form nuclei, resulting in a higher volume fraction of G.P. zones for the copper containing alloy. The differences in

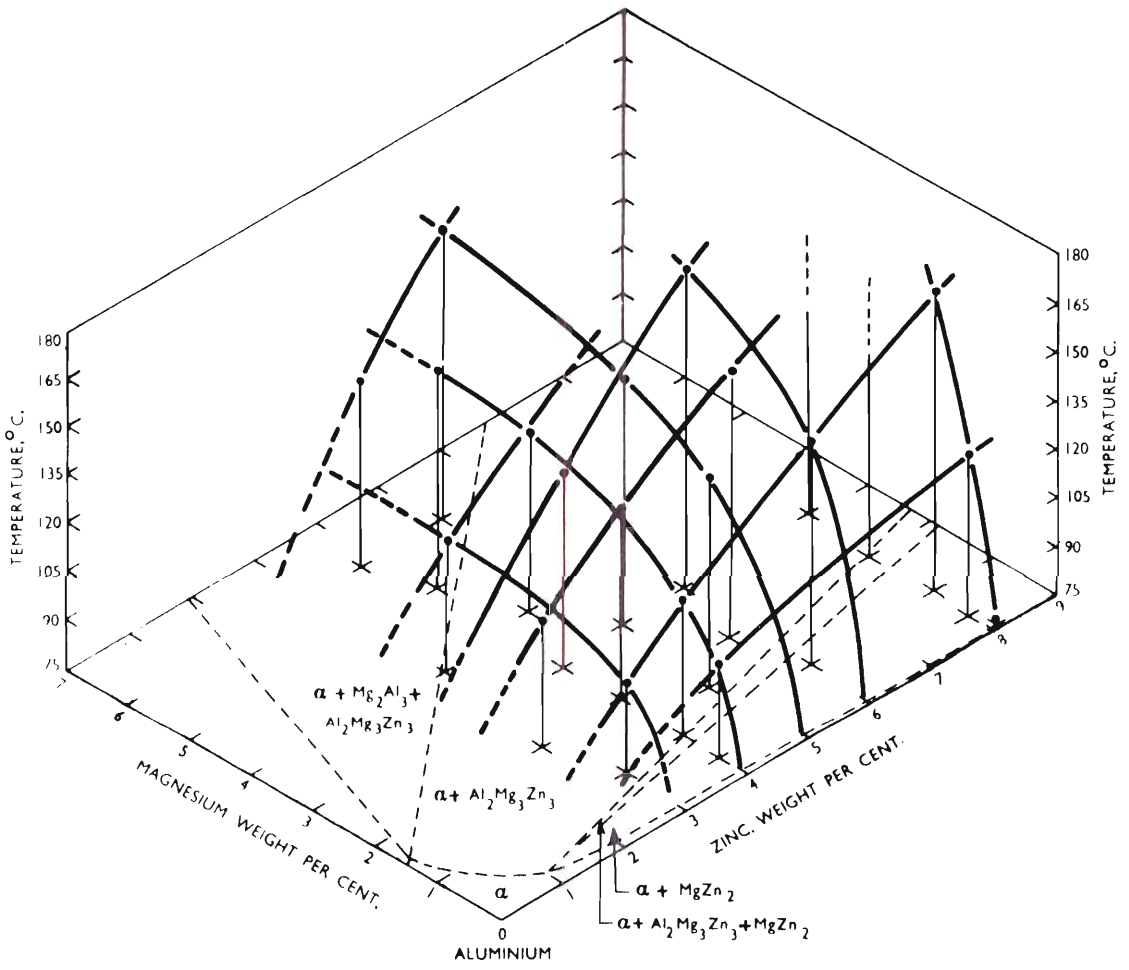

Figure 41. A Representation of the Upper Temperature Limit of Stability of G.P. Zones in Aluminum - rich, Aluminum - Zinc - Magnesium Alloys[99].

mechanical properties of the two alloys may be partly attributed to this difference in volume fraction. The increase in proof stress with aging time for both alloys is proportional to the increase in the size of the precipitates, as predicted by the shearing mechanism, Equation 2.

The growth rate at 120°C was low due to slow diffusion, and a maximum of R/b = 14 was reached in the time interval investigated. The high strength obtained was a result of the large volume fraction of pre-precipitates associated with aging at 120°C. In both the Al-Zn-Mg and 7050 alloys, an interparticle interference hump associated with closely spaced particles, was observed. The brittle nature of the ternary Al-Zn-Mg alloy did not permit a complete assessment of the variation of proof stress with aging; however, in the 7050 alloy, it was found that the proof stress increased and leveled off after 9 hours at 120°C. This behavior was associated with the slow particle growth shown in the XSAS measurements, Figure 15, and with a shearing mechanism operating for all aging times investigated.

Aging at 150°C produced similar effects; the increase in proof stress was shown to be the result of the growth of the particles. The initial increase was related to the shearing of the particles; however, at approximately R/b = 27 for Al-Zn-Mg and R/b = 23 for 7050 a progressive drop in proof stress began. This reduction in proof stress is predicted when the dislocations begin to loop the second phase particles, and is in good agreement with the predictions of Figure 6.

The highest proof stress was attained when the 7050 alloy was double aged. Table 4 is a summary of the effect of double aging on the

Table 4. Summary of the Effect of Double Aging on the Monotonic Properties of 7050

Treatment	σ_o (0.2 per cent off-set) K_g/mm^2	ε_f (per cent)	n
4 hr. @ 120°C + 12 hr. @ 150°C	56.	16.5	0.038
4 hr. @ 120°C + 24 hr. @ 150°C	59.	14.0	0.030
4 hr. @ 120°C + 48 hr. @ 150°C	56.	12.0	0.032
24 hr. @ 120°C + 12 hr. @ 150°C	58.	12.0	0.031
24 hr. @ 120°C + 24 hr. @ 150°C	58.	11.0	0.015
24 hr. @ 120°C + 48 hr. @ 150°C	51.	13.5	0.020
24 hr. @ 120°C + 96 hr. @ 150°C	46.	16.0	0.029

tensile properties. Within the statistical significance of the data, 4 hours at 120°C followed by 24 hours at 150°C produced the greatest proof stress while maintaining adequate ductility, i.e., 12 per cent elongation at fracture. The static strength is directly related to the density of small particles that resulted from the initial aging at 120°C and the size increase obtained from step aging to 150°C, Figure 16b, as predicted by the shearing mechanism. The Guinier radius after aging at 150°C for 24 hours was still less than the critical size for a transition from shearing to looping.

The variation of the deformation process as a function of aging was followed by observation of sectioned tensile samples in the electron microscope. In both alloys, at both aging temperatures, homogeneous deformation was observed in the early stages of aging (less than four hours). This fact has generally been attributed to the small resistance to dislocation motion offered by the pre-precipitates in the early stages [101,102]. However, samples aged for four hours or more exhibited localized deformation on narrow bands parallel to {111}. (The Guinier radii obtained after 4 hours at 120°C was approximately 24A and after 4 hours at 150°C it was 50A, for both alloys.) This localized deformation has been observed by other investigators and has generally been considered to be either an inherent weakness due to inhomogeneities in quenching[101,102] or localized weakening due to dislocations shearing the zones[101]. In the first case dislocations are initially generated in 'soft' regions which resulted from the quenching inhomogeneities. Wide quench bands have been observed by some authors[103]

to be completely free of precipitates. Lynch[104], however, has pointed out that these weaker areas need only have a slightly lower precipitate density than adjacent areas, and they would thus be difficult to detect. In the alternative explanation, bands form because the initial dislocations shear the coherent and semi-coherent pre-precipitates thereby reducing the effectiveness of these particles in retarding slip. Examination of numerous TEM foils did not reveal the type of quench bands found by Embury and Nicholson[103]. However, the large volume fraction of precipitates and the high degree of particle overlap would prevent the observation of lower precipitate density suggested by Lynch. It is possible that a combination of both mechanisms was operative. Dense dislocation tangles and much loop debris were observed within the deformation bands, but the high particle density and overlapping strain fields of the dislocations prevented direct observation of the interactions between dislocations and precipitates. A change in mechanism from shearing to looping was inferred from the reduction of flow stress with increased particle radius, for samples of the two alloys aged at 150°C.

Differences in elongation at fracture and the appearance of the fracture surfaces were the primary evidence of significant variations in the mechanical behavior of the ternary Al-Zn-Mg alloy and 7050 alloy, with aging. In the ternary alloy the fracture process gradually changed from ductile, micro-void coalesence, in the as-quenched condition, to brittle, low energy, intergranular separation upon aging. In contrast, 7050 exhibited ductile transgranular fracture for all aging conditions investigated.

There have been numerous attempts to correlate fracture behavior with material parameters. The most general parameters that have been considered for similar alloys are:

1. grain size,

2. the area fraction and size of the grain boundary precipitates, and

3. width of the PFZ.

Lynch[104] investigated the fracture behavior of two high strength Al-Zn-Mg alloys. One alloy was a large-grained, high pruity ternary and the other a fine-grained commercial alloy containing 1.3 per cent copper. He observed a lower ductility and a tendency toward low energy inter-granular separation in the ternary alloy, and since it had a larger grain size than the alloy containing copper, he concluded that grain size was a controlling factor. Variation of the width of the PFZ has been cited as the controlling factor in the ductility of the alloy by other investigators[105]. Their general conclusion was: the larger the PFZ, the greater the ductility. Cornish and Day[106] varied the size and number of grain boundary precipitates by step quenching from 465 to 200°C using different holding times at 200°C. They concluded that the size and spacing of the grain boundary precipitates, rather than the width of the PFZ, controlled the ductility. They found that larger particles lowered the ductility and that within the range of 600-2000A, the PFZ width was found to have little effect. Similar results were also reported by Unwin and Smith[107].

In the alloy 7050, narrow PFZ's were observed, Figure 18b and d

however, fractures were transgranular and there was at least 12 per cent elongation; this supports the idea of Cornish and Day[106] and Unwin and Smith[107] that the PFZ has little effect on ductility.

It was shown earlier that copper directly participated in the precipitation process by reducing the nucleation barrier. Therefore, more solute would be participating in the

$$G.P. \rightarrow \eta' \rightarrow \eta \qquad (7)$$

sequence, rather than diffusing to the grain boundaries and forming large η particles. However, measurements of the area fraction of grain boundary precipitates were not made, and so the influence of grain boundary precipitates on the fracture process can not be quantitatively established.

Optical examination of tensile samples showed the presence of coarse slip bands on the surfaces of monotonically deformed Al-Zn-Mg alloys aged for greater than 4 hours. As pointed out earlier, slip bands were not optically visible in 7050. Depending on the size and spacing of the slip bands, high stress concentrations can exist across grain boundaries, leading to premature grain boundary fracture. If the amount of plastic strain in each grain of a deformed polycrystal can be considered to be the same[108] and the grain size proportional to l, then the amount of plastic strain can be written as:

$$\Delta\varepsilon_p = \frac{\Delta\ell}{\ell} \qquad (8)$$

where, $\Delta\ell$ is the off-set. For a given amount of plastic strain, increasing ℓ will require a proportionate increase in $\Delta\ell$. A large $\Delta\ell$

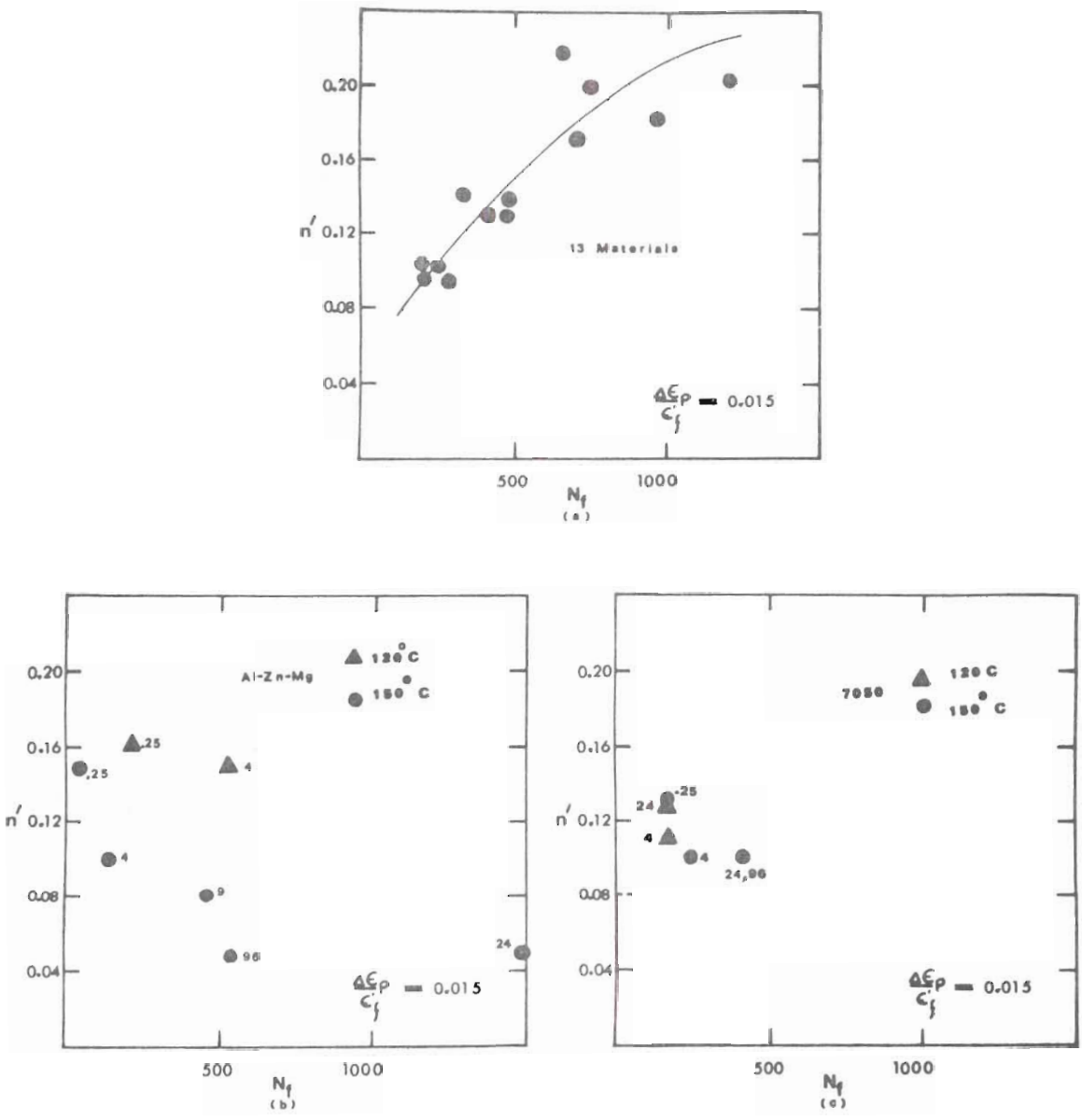

Figure 42. Variation of n' With Fatigue Life: (a) Comparison of Data by Feltner and Beardmore, (b) Al-Zn-Mg aged 150°C and 120°C and (c) 7050 Aged at 150°C and 120°C.

will result in a large stress concentration across the boundary. Consequently, the presence or absence of intergranular fracture is associated with both the stress concentration across the boundary and the strength of the boundary; the former being influenced by the grain size and matrix precipitates, and the latter by the size and spacing of the grain boundary precipitates.

The fatigue crack propagation model[109] relates the rate of crack growth with n', the cyclic strain hardening exponent, in the following manner:

$$\frac{da}{dN} = a \cdot \frac{\pi}{32} \cdot \frac{\sigma_f^2}{(\varepsilon_f)_{n'}} \cdot \frac{1}{(\sigma_y')2} \cdot \Delta\varepsilon_p^{2n'+1} \quad . \qquad (9)$$

where

$\frac{da}{dN}$ - is the crack growth cycle,

a - is the crack length,

σ_f, ε_f - are monotonic stress and elongation at fracture, respectively

σ_y' - is the fatigue fracture stress, and

n' - is the cyclic strain hardening exponent

The above equation predicts that as n' is increased N_f increases. Using this as a basis, Feltner and Beardmore[108] plotted the n' values for 13 materials, the results of which are given in Figure 42a. The values of N_f obtained in this study has been plotted as a function of n', Figure 42b and c. As n' decreases, N_f generally increases, opposite to the trend presented by Feltner and Beardmore[108]. It must, however, be pointed out that the validity of plotting n' for different materials

is questionable and their analysis might be fortuitous.

The discrepancy with Equation (9) is not surprising. Fatigue is the sum of both initiation and propagation, hence, the deviation from the equation does not violate either the crack propagation model or does the model dispute the data.

Examination of the fracture surfaces of fatigued-to-failure ternary Al-Zn-Mg and 7050 showed that a circumferential crack front initiated on the surface and propagated radially toward the center. The fatigue cracks appeared to propagate transgranularly, Figures 29 and 30, with fatigue surface damage characterized by beach marks. As the fatigue crack propagated toward center, a point was reached where the fracture strength was exceeded during the tension cycle, and the remaining fracture was monotonic. This was more evident in the aged Al-Zn-Mg alloy where there was a change in fracture mode from transgranular fatigue to intergranular monotonic.

The response of the stress amplitude during a strain controlled low cycle fatigue test reveals much useful information concerning the mechanical nature of the material. The stress amplitude curves for Al-Zn-Mg and 7050 are given in Appendix A. Briefly, in the early stages of aging, when the particles are small and represent little resistance to the motion of mobile dislocations, the mechanical behavior is similar to the initial response of an annealed solid solution alloy. There is an increase in the stress amplitude with the number of cycles. This increase is a result of dislocation multiplication during cyclic straining. The stress amplitude increases in both alloys until a macro-

scopic crack begins to propagate and the specimen becomes unstable in tension.

Aging the two alloys produces a high density of G.P. zones and η' particles, which causes the deformation to become less homogeneous. This relationship is illustrated by the onset of dislocation banding observed in TEM foils, Figures 31, 32. Stabilization of the stress amplitude has been attributed to the development of a stable dislocation structure[110]. In the case of the ternary Al-Zn-Mg, the deformation structure at a stabilized stress amplitude is composed of dislocation slip bands. For 7050, aged to produce coherent or partially coherent particles, the stable dislocation structure was also dislocation slip bands. However, when 7050 was aged to produce large particles, a cell structure was observed, Figures 39, 40, at plastic strain amplitudes greater than 1.0 per cent, where cross slip was energetically possible. Plastic strain amplitudes less than 1.0 per cent produced only dislocation slip bands.

The notion of cyclic softening has generally been associated with the poor fatigue ratio (fatigue strength:ultimate tensile strength $\leq$ 0.3). In a recent paper by Kralik and Schneiderhan[112], it was reported that the cyclic softening was found to occur in single crystals of an Al-Zn-Mg alloy. These authors suggested that the drop in stress amplitude was a result of the to and fro motion of dislocations, whereby softening in narrow slip bands was caused by the repeated cutting of the particles by the dislocations. However, the reduction in stress amplitude was not observed in either alloy in-

vestigated.

The fact that this process was not observed in the polycrystalline samples might be explained by the presence of grain boundaries. As the number of boundaries increases, the back stresses on the disloctions increase. This increased back stress would reduce the number of dislocations that follow earlier dislocations on the same glide plane. This process would also tend to explain the increased homogeneity of deformation when the grain size is reduced. Furthermore, observation of numerous electron micrographs failed to reveal regions of lower than average precipitate density or regions of large incoherent η in specimens sectioned after fracture. The poor fatigue properties have generally been attributed to either a reversion[70-77] or overaging[79-87] which would alter the precipitate distribution in the slip bands.

The Coffin-Manson[94] Relationship predicts that:

$$\frac{\Delta\varepsilon_p}{2} = \varepsilon_f' \ (2N_f)^{-c} \qquad (10)$$

This emperical relationship was developed for the low cycle fatigue regime, $N_f < 10^4$ cycles. When plotted in the form

$$\log\left(\frac{\Delta\varepsilon_p}{2}\right) = \log\ (\varepsilon_f') - c \log\ (2N_f), \qquad (11)$$

the extrapolated value of plastic strain amplitude when $2N_f = 1$ should be approximately equal to the monotonic fracture elongation. However, numerous investigators[112-116] have observed a break in the slope, such that extrapolated values of ε_f' from the low plastic strain amplitude regime, gives values an order of magnitude greater than

measured in a monotonic tensile test.

Attempts have been made to relate this non-ideal behavior with a change in fatigue crack propagation mode as a function of plastic strain amplitude[112]. Investigations by Fine, et al.[113] indicated that the break in the curve was related to the crack initiation process, rather than the propagation process. These authors plotted the numberof cycles to crack initiation, rather than the cycles to failure, versus plastic strain amplitude. They also found a break in the curve when this data was plotted, and they concluded that the change in slope is related to the crack initiation process.

The effect of stacking fault energy, SFE, on the fatigue deformationprocess in the Cu-Al system was recently studied by Saxena and Antolovich[114]. They found that at high SFE the fatigue life plot was linear, with little scatter in the data. However, with low SFE a distinct break in the fatigue life curve was observed. The authors also plotted the plastic work per cycle, and these results are shown in Figure 43. They interpreted the break in the curve to be the result of inability of the dislocations to cross-slip, in the case of low SFE. The non-linear behavior in the plastic work per cycle demonstrated that crack initiation must be the critical process and indicated that the plastic work process changes with the plastic strain amplitude. As the plastic strain amplitude increases (lower N_f) less work is required than that which would be predicted by extrapolation from the low plastic strain amplitude regime (high N_f). The same type of argument can be used to interpret the data in this research.

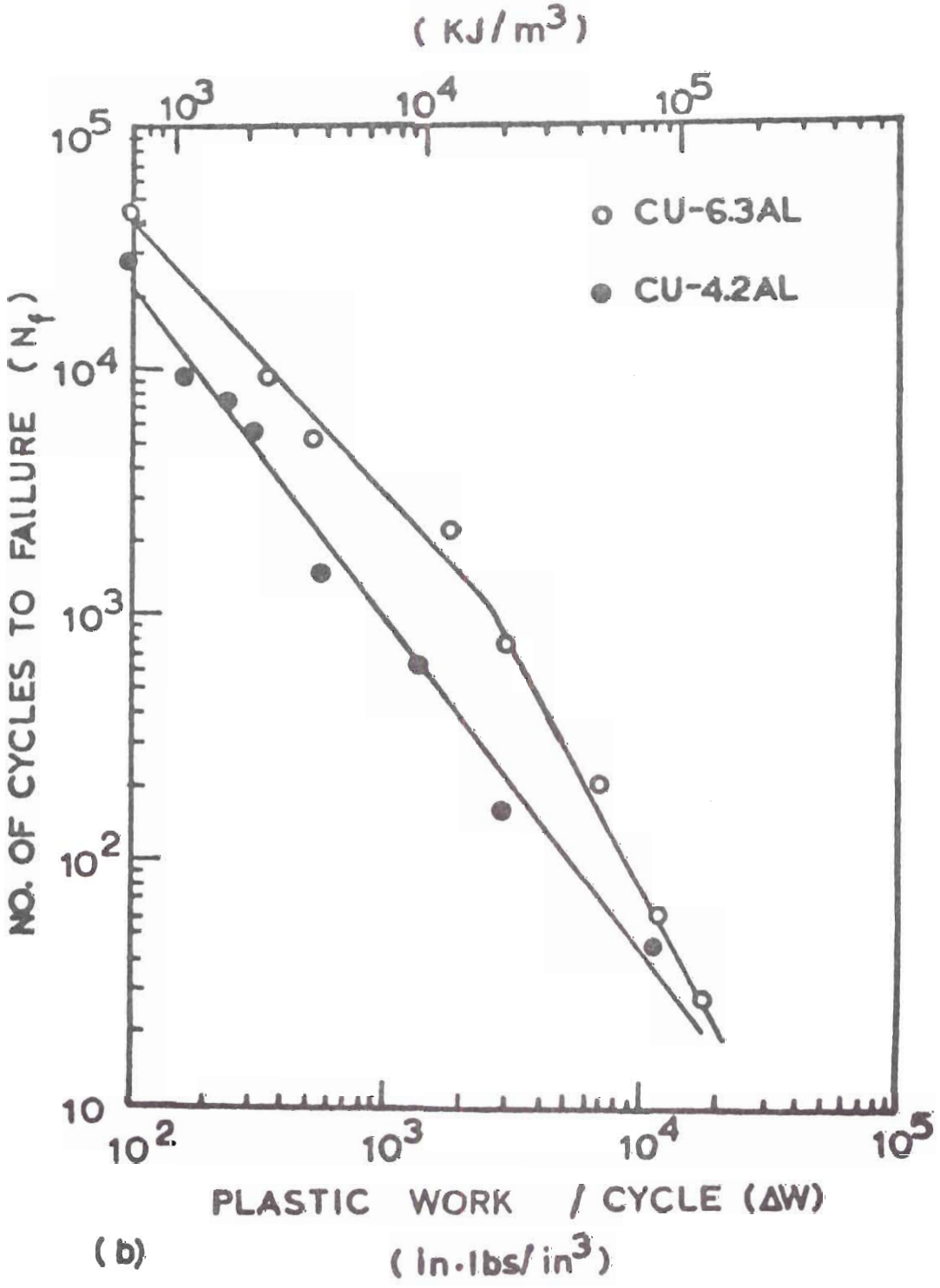

Figure 43. Plastic Work Per Cycle Plot Showing the Break in the Curve for Low Stacking Fault Energy[114].

In the 7050 alloy aged four hours or longer at 150°C, there are numerous precipitate particles large enough to represent obstacles to dislocation flow. At high plastic strain amplitudes there is sufficient energy for the dislocations to by-pass the obstacles by a cross-slip mechanism. Dislocation cell structures were observed in TEM samples from tensile specimens aged greater than four hours at 150°C and deformed in excess of 3 per cent plastic strain. Examples of this type of microstructure are shown in Figures 44 and 45. In the lower plastic strain regime this process was not energetically feasible. When the 7050 alloy was aged for 0.25 hours at 150°C (or for any time $\leq$ 24 hours at 120°C), the particles were small and partially coherent and could be sheared by the dislocations.

The non-linearity in the fatigue life plot for the ternary Al-Zn-Mg alloy was small and could only be observed by comparing the extrapolated value, ε_f', to the measured ε_f from the uniaxial tensile tests; ε_f' was found to be larger. The smaller effect of particles in the ternary Al-Zn-Mg alloy may have been the result of a lower particle density than that of 7050. Such a difference in particle density could be explained by the greater effective solute and the proposed lower barrier to nucleation in 7050.

A model for fatigue crack initiation in Al-Zn-Mg alloys has been proposed by Duquette and Swann[117]. These authors proposed that when dislocations are inhibited from remaining in the slip plane by particle interaction, portions of these dislocations are observed to cross slip out of the primary slip plane. This action results in the

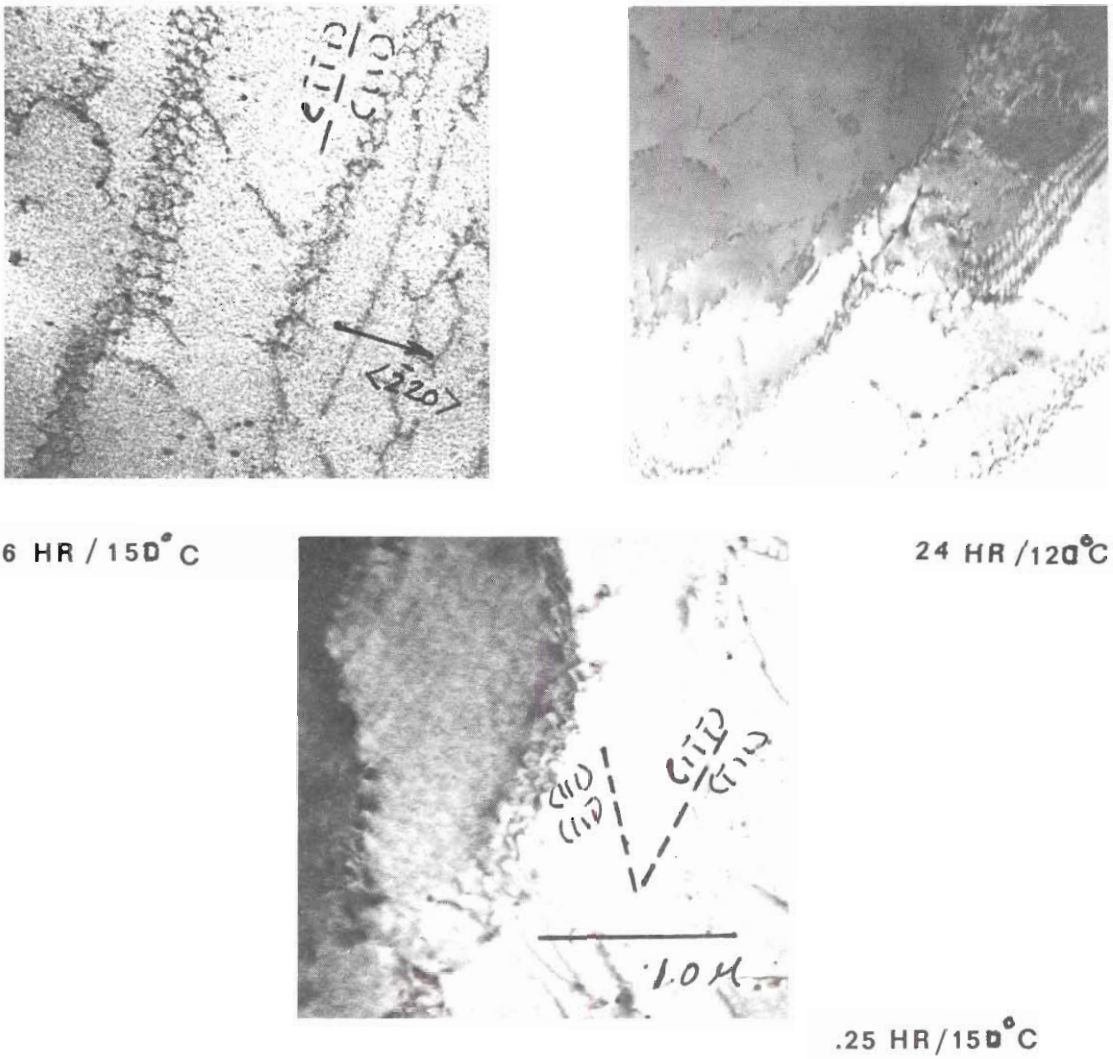

Figure 44. Cell Type Formations in 7050 Alloy Pulled to 3 per cent Plastic Strain.

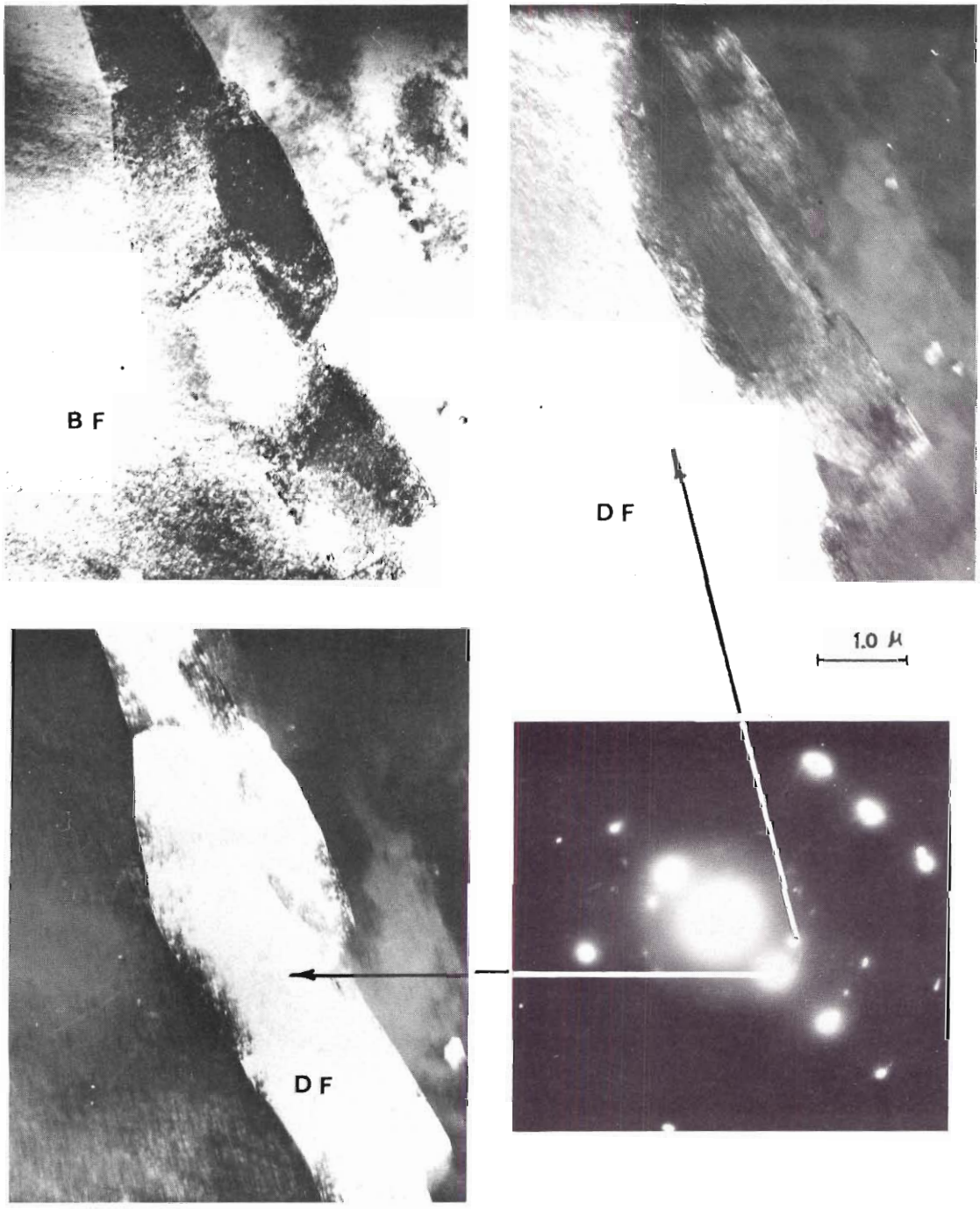

Figure 45. Bright Field, Dark Field Comparison Showing Slight Misorientation; 7050 Aged at 150°C, Pulled to Fracture.

generation of sessile dipolar edge dislocation jogs. Upon further cycling, the interaction of point defects generated by fatigue, pinch off the jogs to form dipolar dislocation loops across the primary slip plane. Crack initiation presumably occurs when a critical number of these loops are present across the primary slip plane, with the loops creating internal stress across the plane, which add to the externally applied stresses. The larger particle density in the 7050 would produce a greater number of dislocation loops and thus initiate fracture sooner than in the lower particle density ternary Al-Zn-Mg alloy, for the condition when looping is observed.

Single aging of 7050 at 150°C produces large, incoherent precipitates which cannot be sheared by dislocations, but must be bypassed. At high plastic strain amplitudes, the precipitates can be bypassed by a cross slip mechanism, as demonstrated by the formation of cells, shown in Figures 39(a) and (c) and 40(a) and (c). However, at low plastic strain amplitudes, the precipitates are looped, resulting in a high density of loops, which leads to premature failure. Aging at 120°C produced a high density of small precipitates which can be sheared at all plastic strain amplitudes, resulting in a single slope relationship for the Coffin-Manson plot. Double aging at 120°C and 150°C produces a microstructure which has a high density of precipitates, and, depending upon the length of time at 150°C, the precipitates can be sheared at all plastic strain amplitudes.

Based upon the observations made in this research and the general conclusions of otherworkers[114], it may be generally postulated that the deviation from linear behavior in the fatigue life plot can be associated with a change in deformation process as a function of the plastic strain amplitude and microstructural changes.

CHAPTER VI

CONCLUSIONS

1. The large, dispersed, second phase particles observed in the 7050 alloy are insoluble copper-rich particles which can act as grain refiners.

2. The solubility limit in the Al-6Zn-2Mg system is at least 1.5 per cent Cu at 480°C.

3. The copper that is in solid solution at 480°C directly enters into the precipitation process along with an equal atomic amount of aluminum.

4. The critical temperature for homogeneous precipitates for Al-6Zn-2Mg is less than 150°C and the presence of copper increases it to above 150°C.

5. The rolling texture for both the ternary Al-Zn-Mg alloy and 7050 alloy is predominantely cube, (001) [100].

6. The increase in proof stress with aging for both alloys is associated with a particle shearing mechanism and the progressive reduction in proof stress with aging at 150°C is considered to be the result of the change from shearing to looping.

7. The best combination of static strength and ductility for the ternary alloy obtained in this study occured when the alloy was aged at 150°C to produce the partially coherent η' precipitates with a Guinier radius of approximately 65A. The best monotonic properties

for the 7050 was obtained when aged to produce the maximum density of η' particles having a Guinier radius of approximately 45A. This type of microstructure resulted when 7050 was double aged for 4 hours at 120°C followed by 24 hours at 150°C.

8. The fracture mode of the ternary Al-Zn-Mg alloy changes progressively with aging from ductile, microvoid coalesence to low energy, intergranular seperation.

This contrasted to the ductile transgranular fracture behavior of the 7050 alloy at all aging conditions investigated. The variation in fracture behavior between the two alloys was related to the development of coarse slip bands in the large grained ternary alloy. The coarse slip bands produced large stress concentrations across the grain boundaries resulting in intergranular fracture.

9. Fatigue life increases with aging time at both 120°C and 150°C for both alloys. The best fatigue performance in the ternary alloy was found when the greatest density of η' occurs. Aging 7050 for 24 hours at 120°C, produces a high density of small particles, giving the best fatigue life, strength and ductility over the range of low cycle fatigue investigated.

10. Aging 7050 at 150°C produces large, closely spaced precipitates that are looped in the low plastic strain regime, $\Delta\varepsilon_p/2 < 1.0$ per cent leading to premature fracture. The premature fracture behavior may be associated with the high density of loops formed during low plastic strain cycling, as suggested by Swann and Duquette. At plastic strain amplitudes >1.0 per cent, the particles may be avoided by cross slip resulting in a lower concentration of loops and lower fatigue

ductility exponent.

11. The emperical Coffin-Manson relationship may be applied only when the deformation process is not dependent on the cyclic strain amplitude.

APPENDICES

APPENDIX A

LOW CYCLE FATIGUE DATA FOR THE TERNARY Al-Zn-Mg ALLOY AND 7050

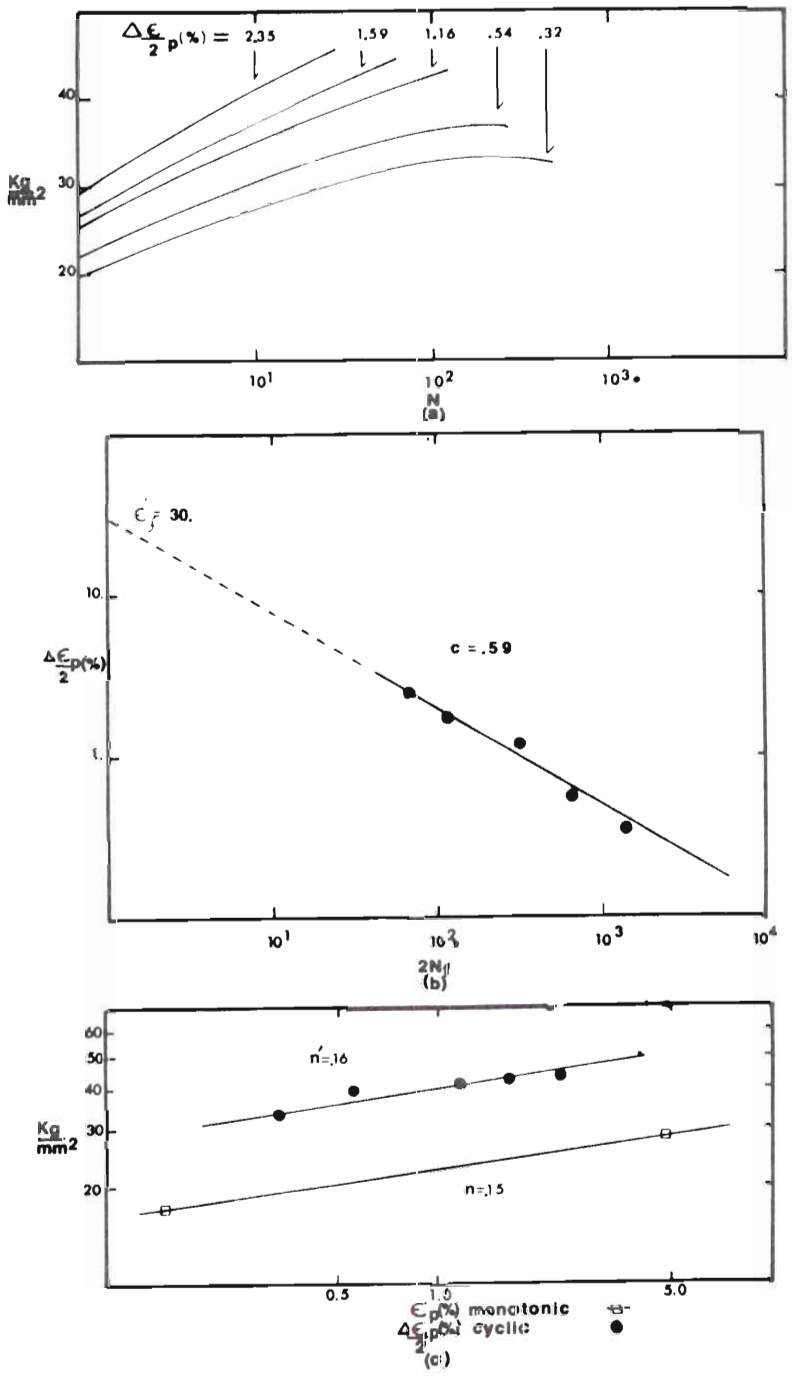

Figure 46. Low Cycle Fatigue Behavior of Al-Zn-Mg Aged at 120°C for 0.25 Hours: (a) Stress Amplitude Versus Cycles, (b) Coffin-Manson Plot, and (c) Cyclic and Monotonic Stress-Strain.

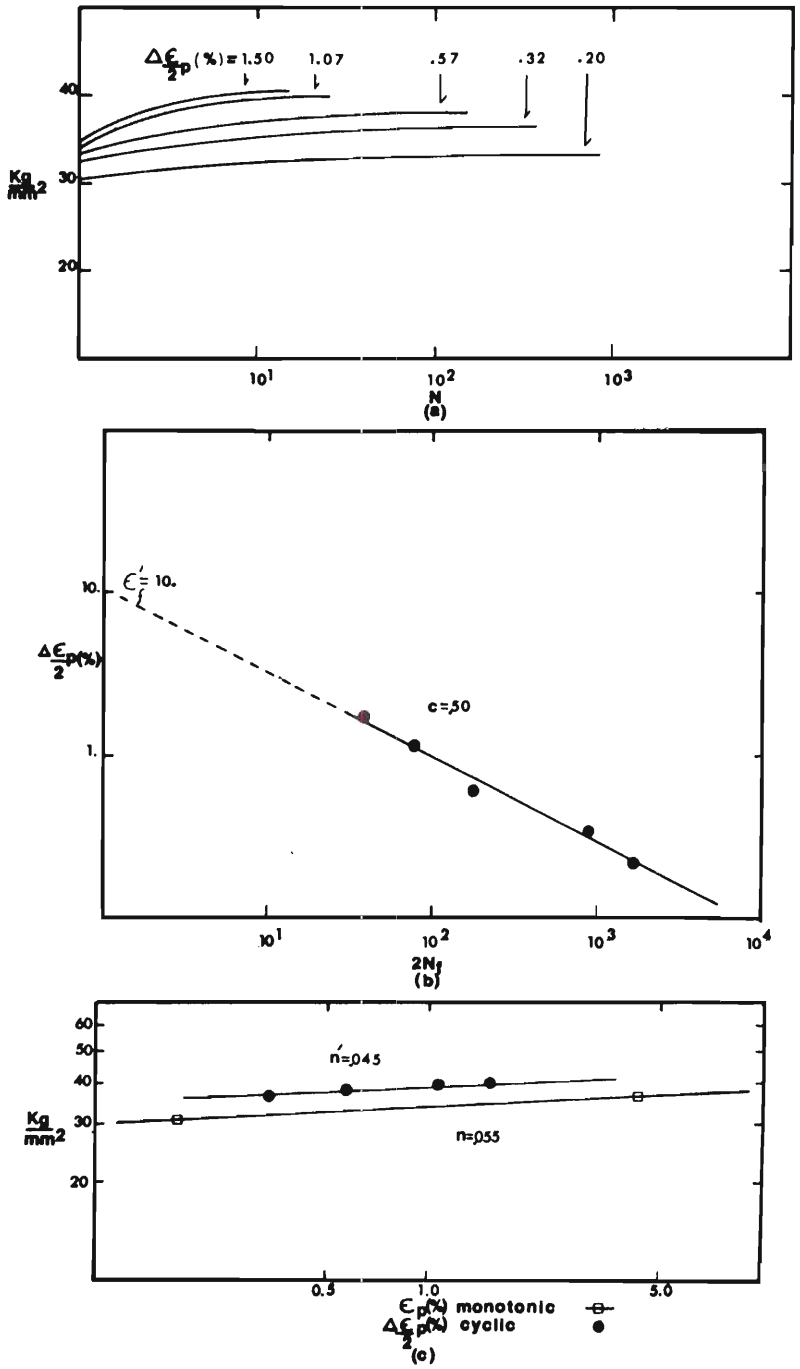

Figure 47. Low Cycle Fatigue Behavior of Al-Zn-Mg Aged at 120°C for 4.0 Hours: (a) Stress Amplitude Versus Cycles, (b) Coffin-Manson Plot, and (c) Cyclic and Monotonic Stress-Strain.

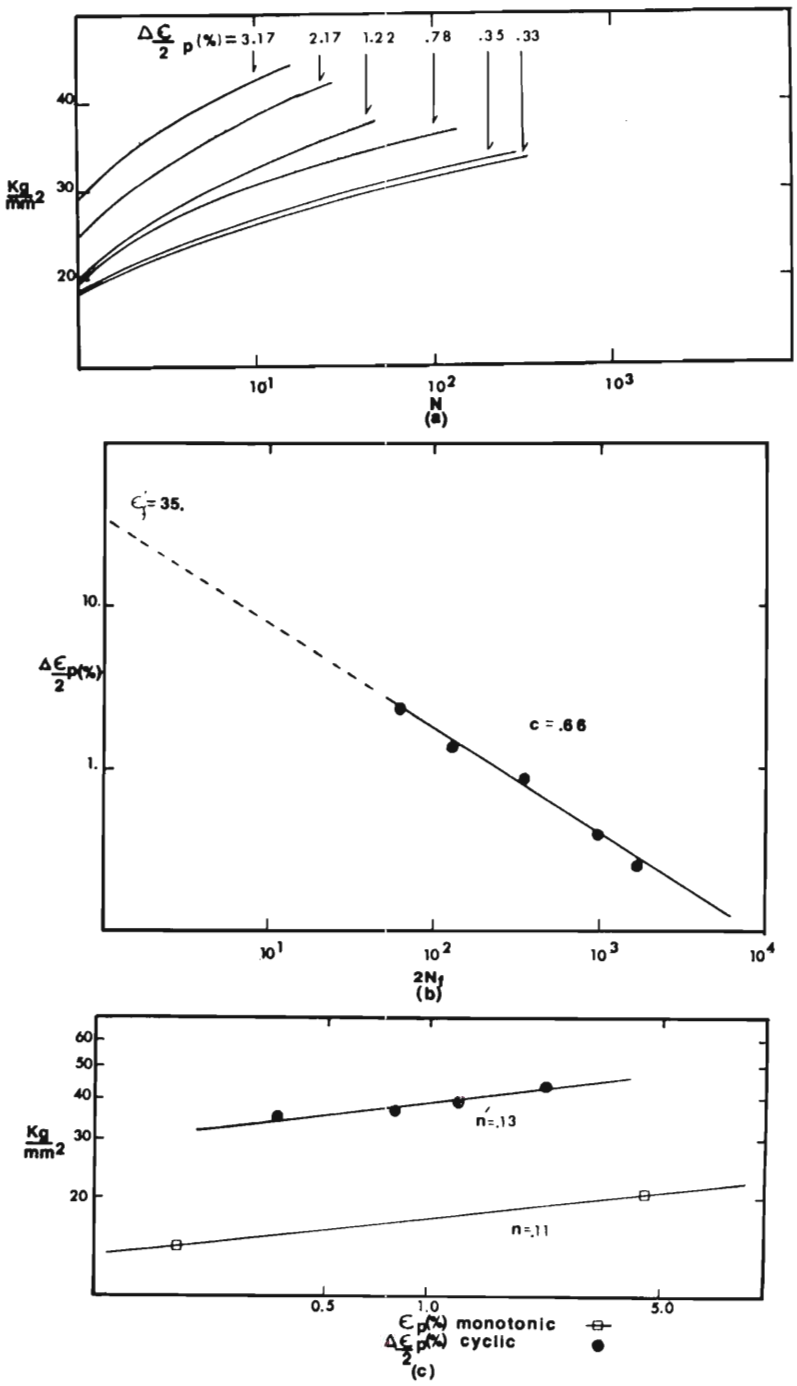

Figure 48. Low Cycle Fatigue Behavior of Al-Zn-Mg Aged at 150°C for 0.25 Hours: (a) Stress Amplitude Versus Cycles, (b) Coffin-Manson Plot, and (c) Cyclic and Monotonic Stress-Strain.

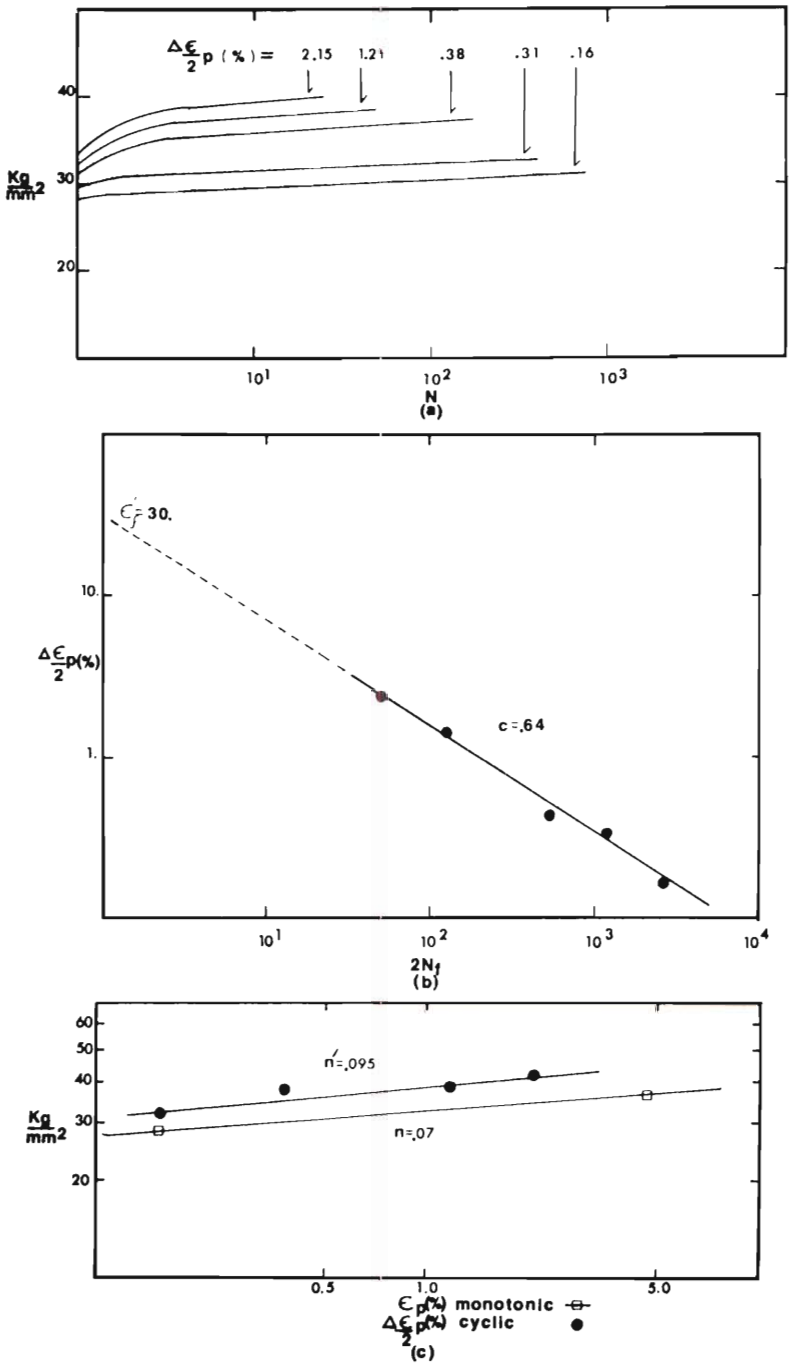

Figure 49. Low Cycle Fatigue Behavior of Al-Zn-Mg Aged at 150°C for 4.0 Hours: (a) Stress Amplitude Versus Cycles, (b) Coffin-Manson Plot, and (c) Cyclic and Monotonic Stress-Strain.

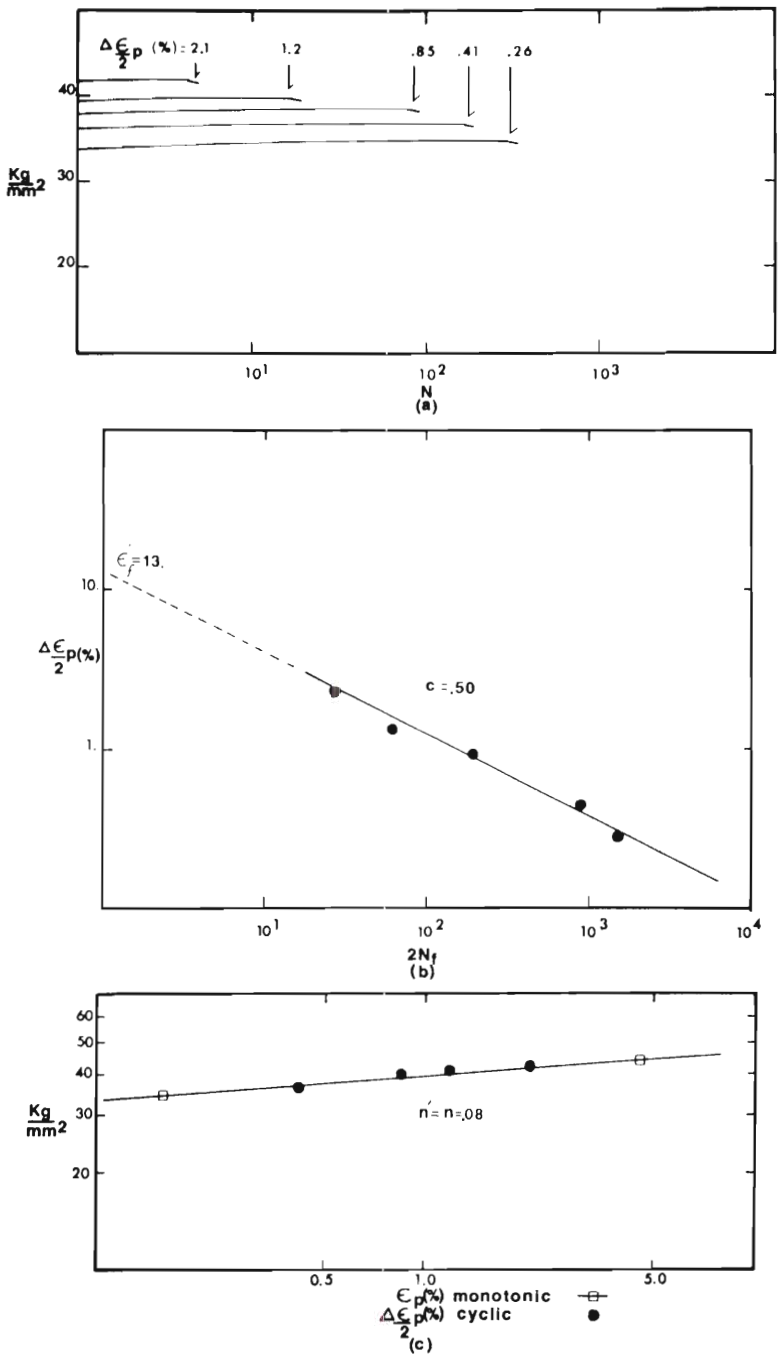

Figure 50. Low Cycle Fatigue Behavior of Al-Zn-Mg Aged at 150°C for 9.0 Hours: (a) Stress Amplitude Versus Cycles, (b) COffin-Manson Plot, and (c) Cyclic and Monotonic Stress Strain.

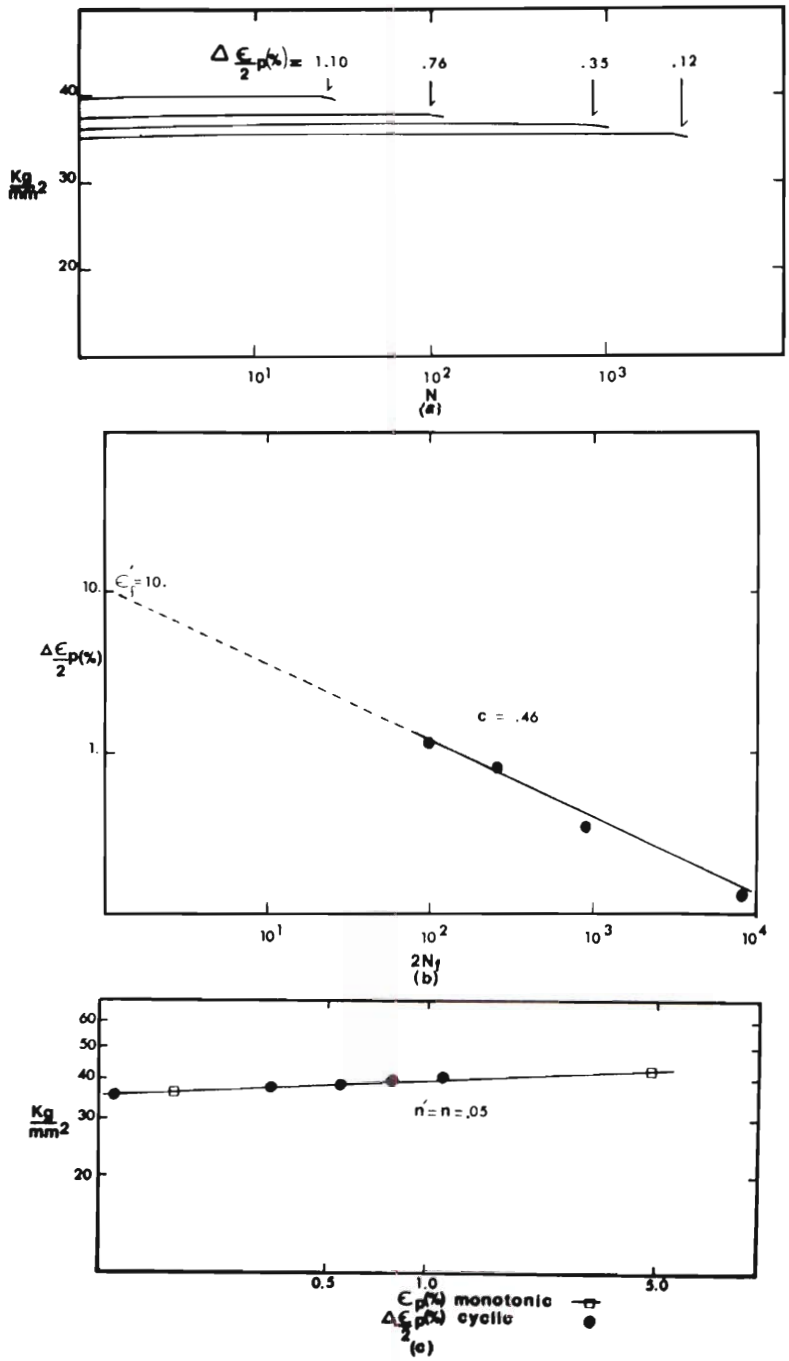

Figure 51. Low Cycle Fatigue Behavior of Al-Zn-Mg Aged at 150°C for 24 Hours: (a) Stress Amplitude Versus Cycles, (b) Coffin-Manson Plot, and (c) Cyclic and Monotonic Stress Strain.

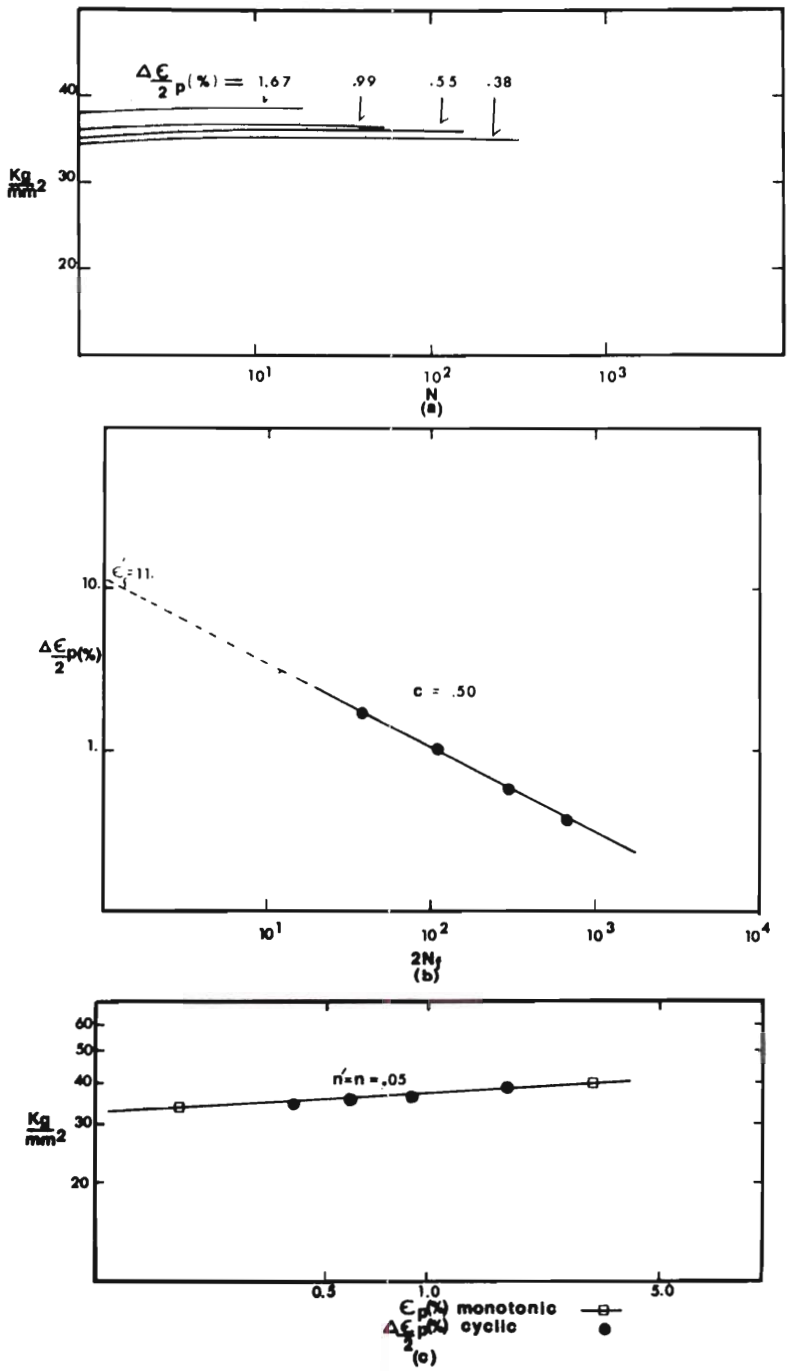

Figure 52. Low Cycle Fatigue Behavior of Al-Zn-Mg Aged at 150°C for 96 Hours: (a) Stress Amplitude Versus Cycles, (b) Coffin-Manson Plot, and (c) Cyclic and Monotonic Stress Strain.

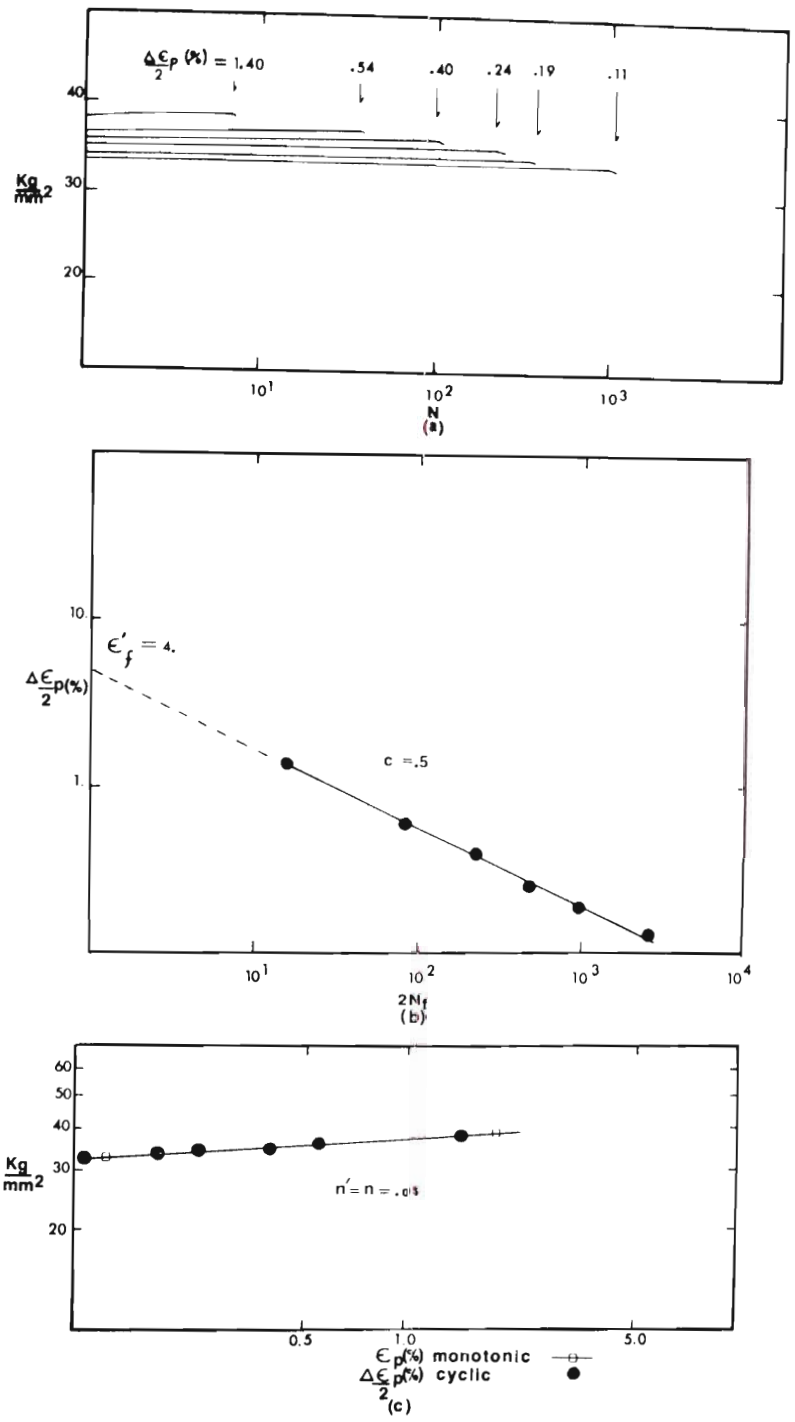

Figure 53. Low Cycle Fatigue Behavior of Al-Zn-Mg Double Aged at 120°C for 4.0 Hours. Followed by 24 Hours at 150°C.

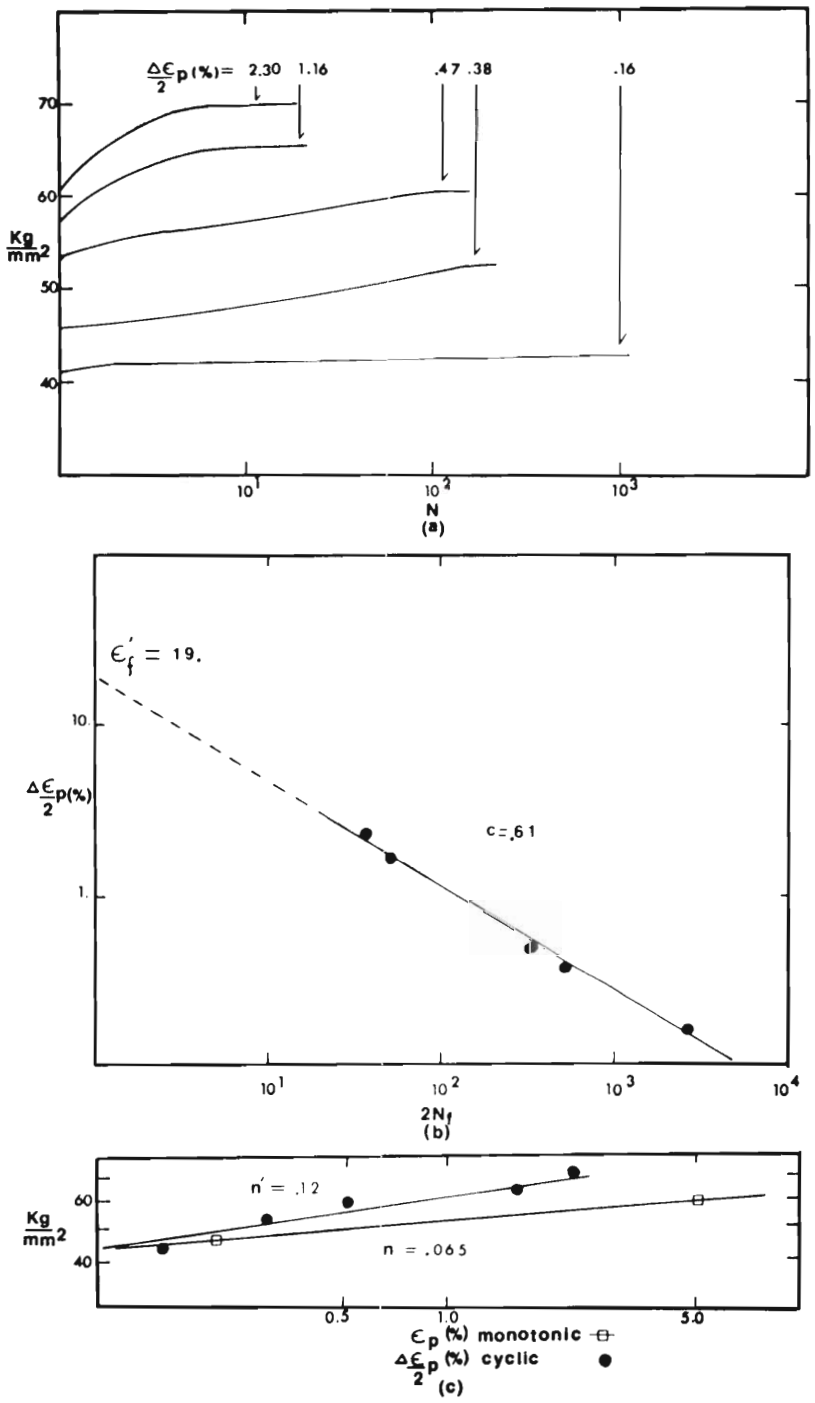

Figure 54. Low Cycle Fatigue Behavior of 7050 Aged at 120°C for 4 Hours: (a) Stress Amplitude Versus Cycles, (b) Coffin-Manson Plot, and (c) Cyclic and Monotonic Stress Strain.

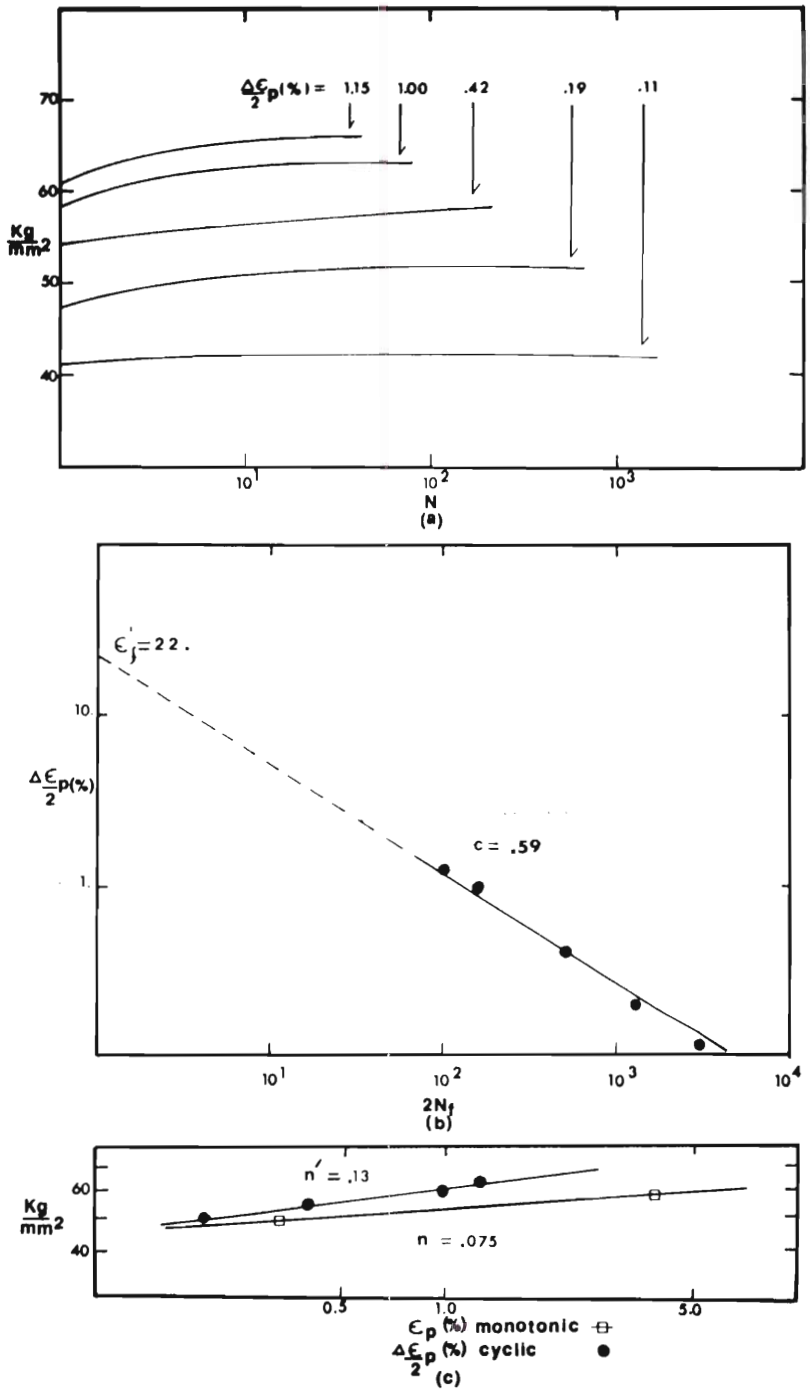

Figure 55. Low Cycle Fatigue Behavior of 7050 Aged at 120°C for 24 Hours: (a) Stress Amplitude Versus Cycles, (b) Coffin-Manson Plot, and (c) Cyclic and Monotonic Stress Strain.

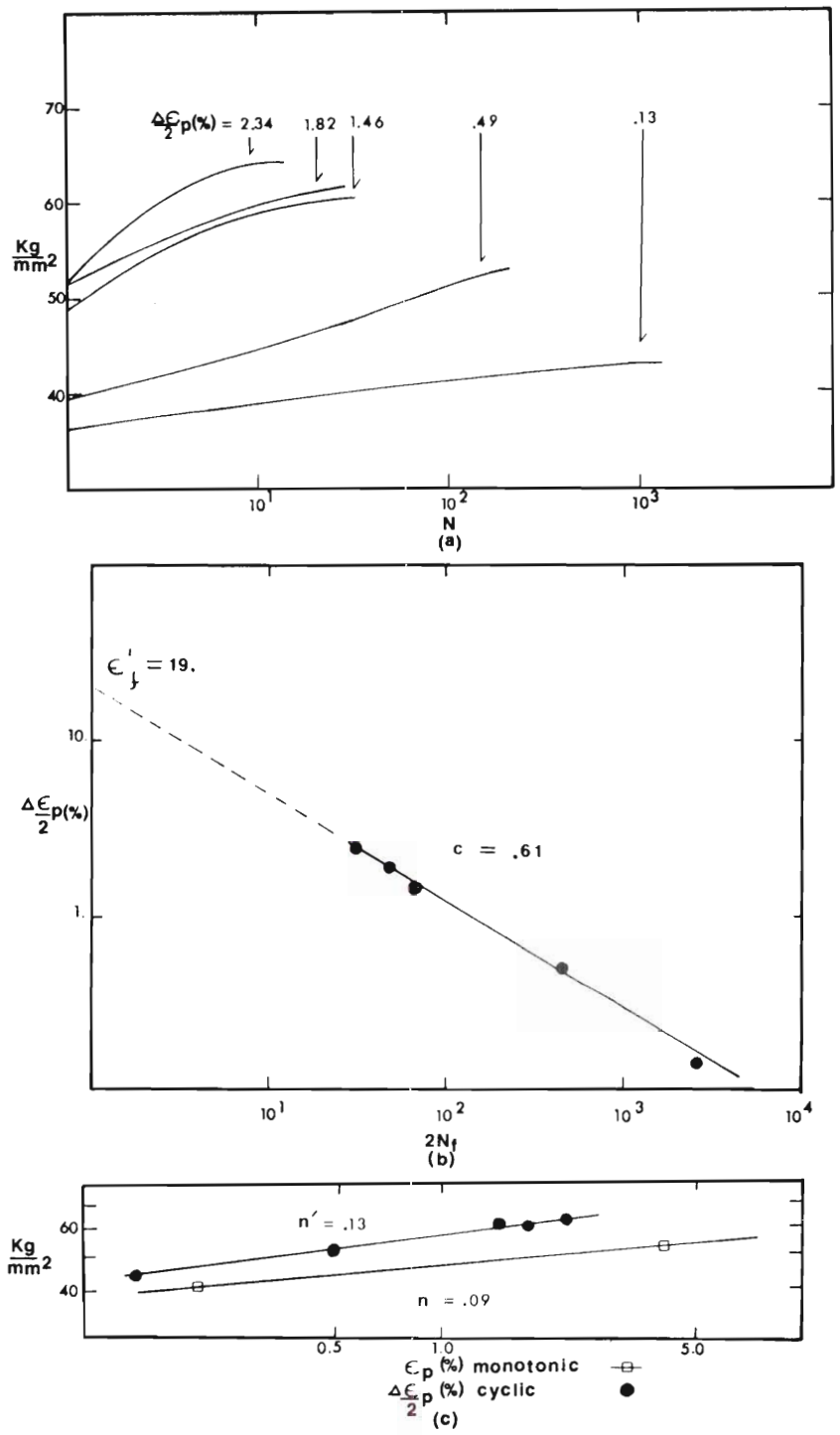

Figure 56. Low Cycle Fatigue Behavior of 7050 Aged at 150°C for 0.25 Hours: (a) Stress Amplitude Versus Cycles, (b) Coffin-Manson Plot, and (c) Cyclic and Monotonic Stress Strain.

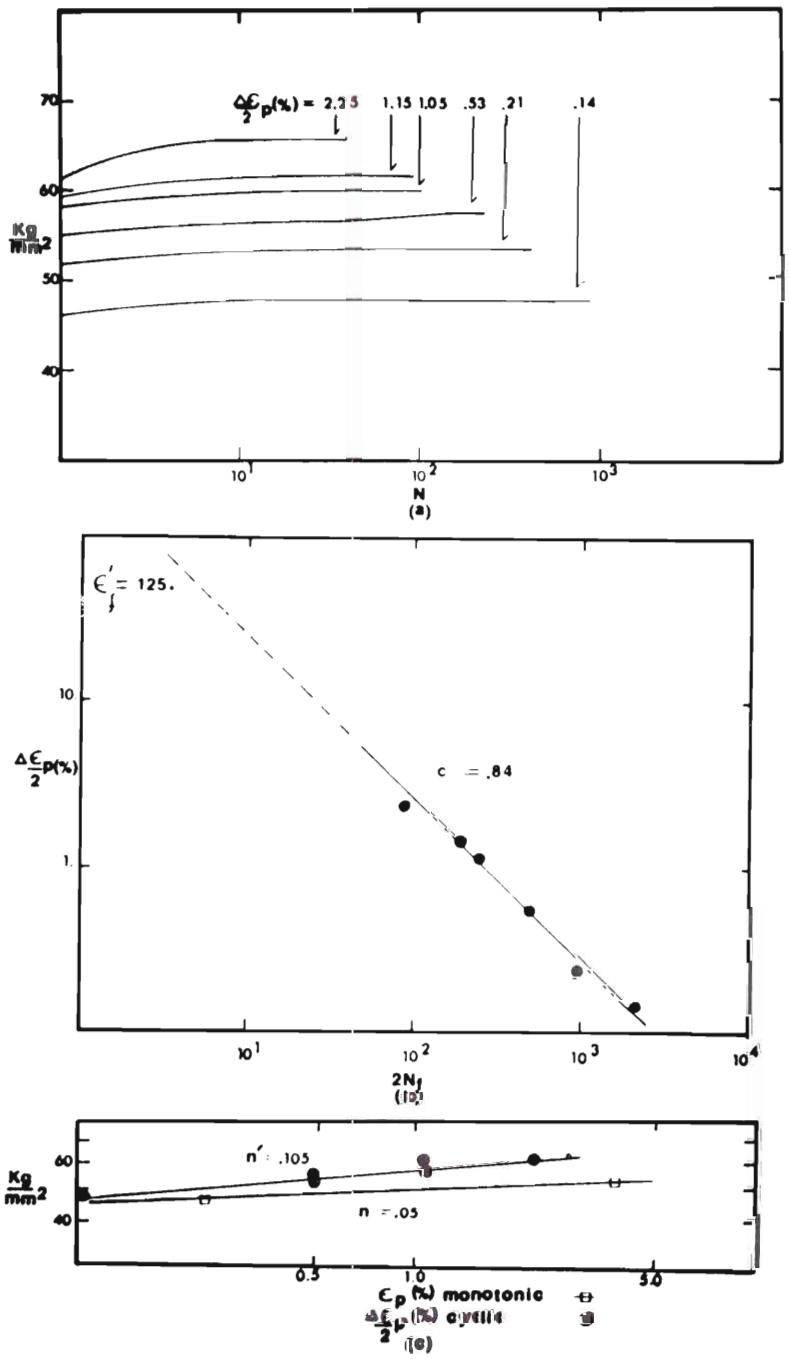

Figure 57. Low Cycle Fatigue Behavior of 7050 Aged at 150°C for 4 Hours: (a) Stress Amplitude Versus Cycles, (b) Coffin-Manson Plot, and (c) Cyclic and Monotonic Stress Strain.

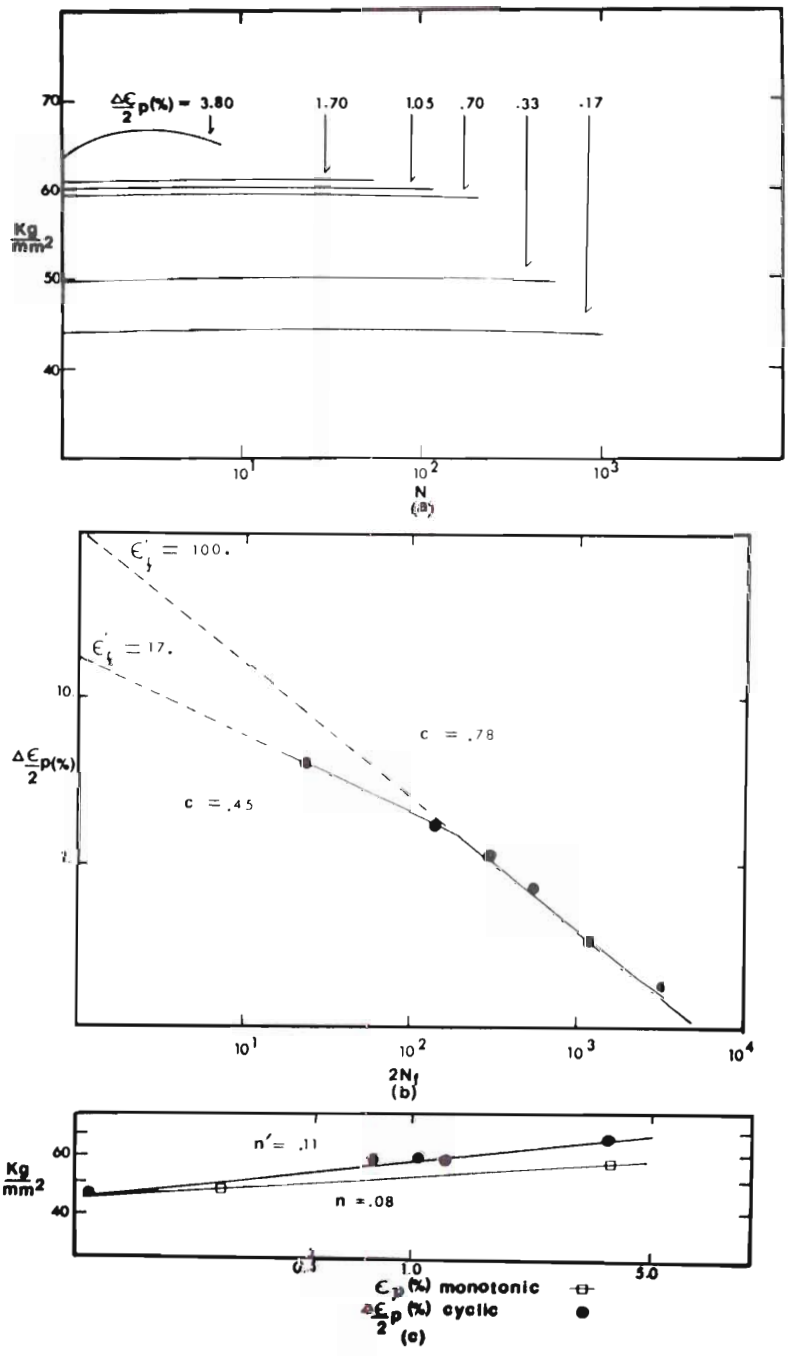

Figure 58. Low Cycle Fatigue Behavior of 7050 Aged at 150°C for 24 hours: (a) Stress Amplitude Versus Cycles, (b) Coffin-Manson Plot, and (c) Cyclic and Monotonic Stress Strain.

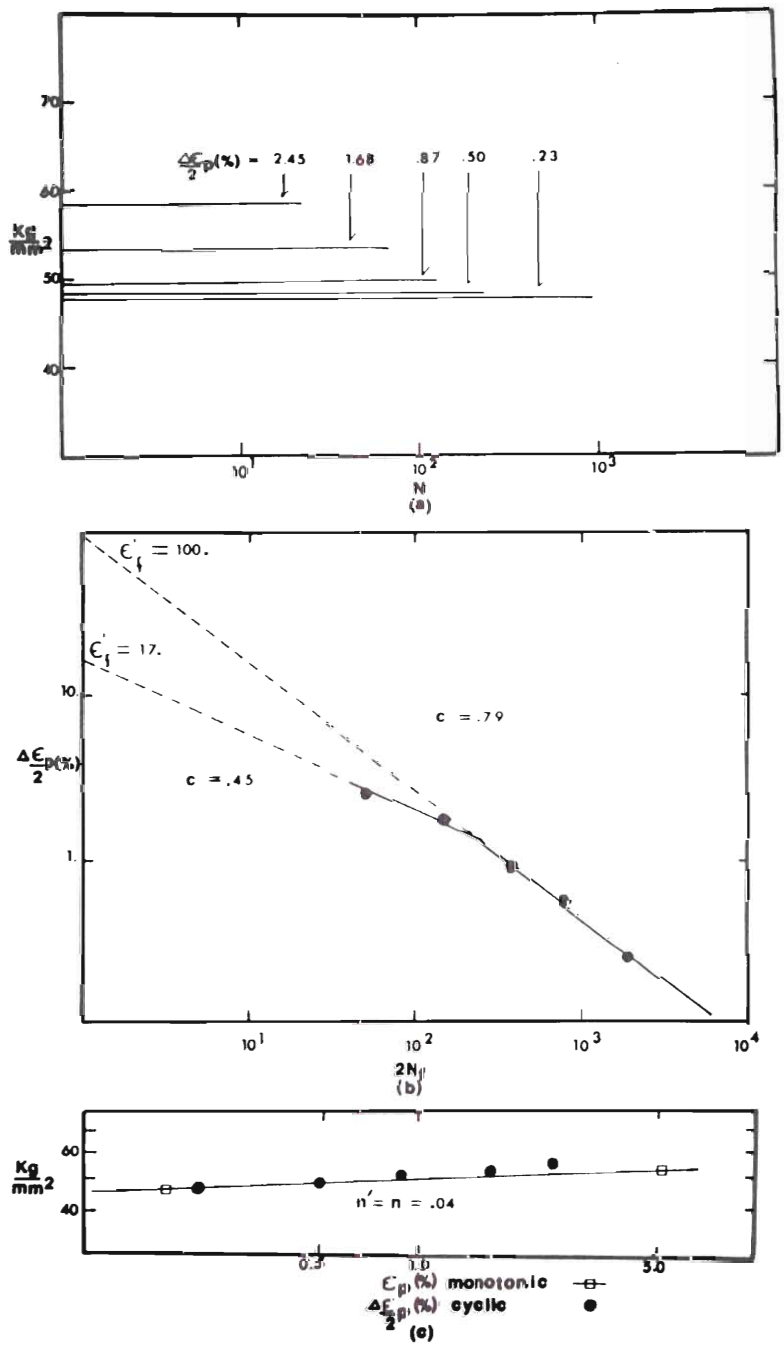

Figure 59. Low Cycle Fatigue Behavior of 7050 Aged at 150°C for 96 Hours: (a) Stress Amplitude Versus Cycles, (b) Coffin-Manson Plot, and (c) Cyclic and Monotonic Stress Strain.

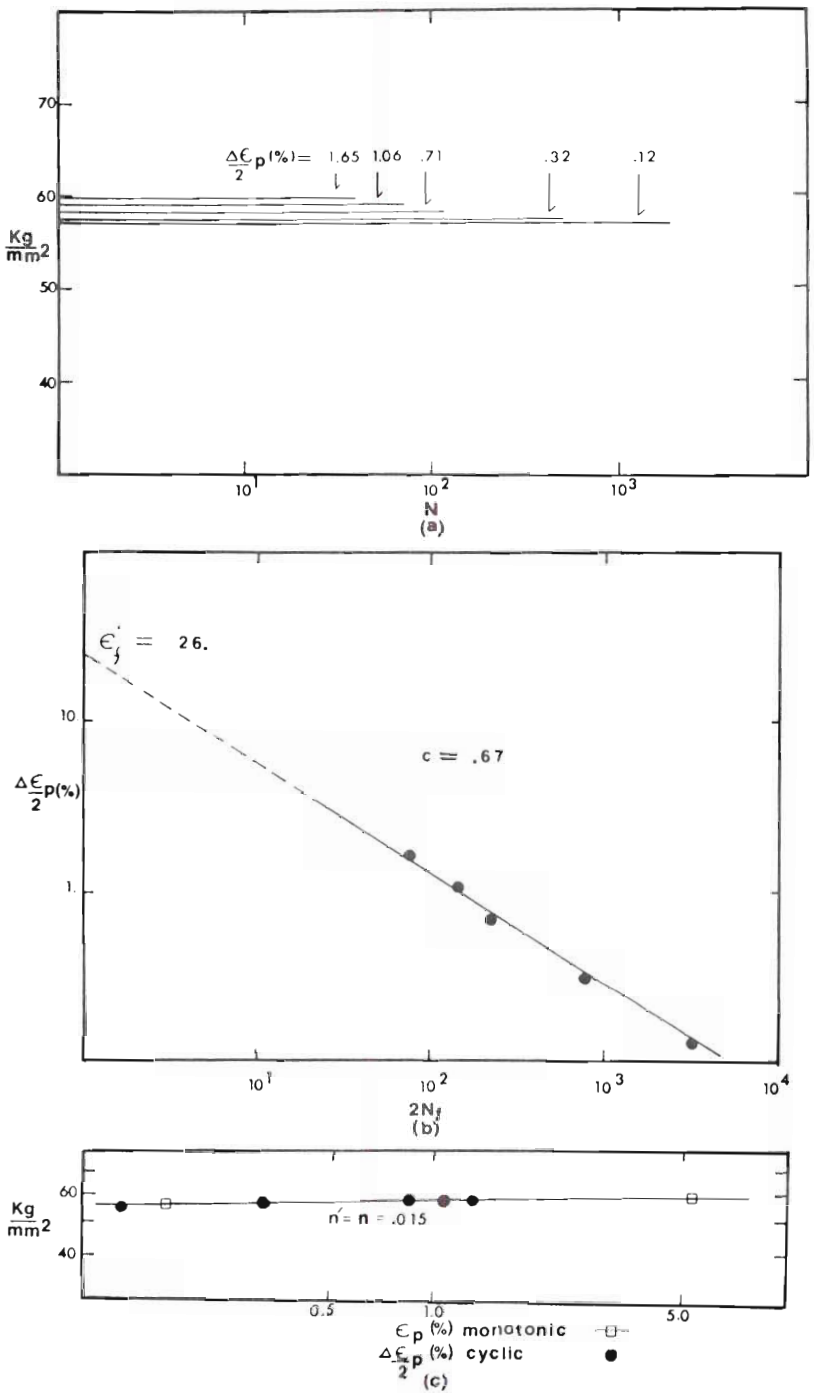

Figure 60. Low Cycle Fatigue Behavior of 7050 Double Aged 24 Hours at 120°C, Followed By 24 Hours at 150°C: (a) Stress Amplitude Versus N, (b) Coffin-Manson Plot, and (c) Cyclic and Monotonic Stress-Strain.

APPENDIX B

SELECTED AREA DIFFRACTION PATTERNS

Selected area diffraction (SAD) patterns that were observed under similar aging treatments in the ternary and 7050 alloys were found to be similar in the arrangement of precipitate spots with respect to the matrix reflections, Figures 61 and 62. Streaking was not found to occur in <100> directions, a condition which is generally associated with the presence of Al_2Cu Mg (S) or Al_2 Cu (θ). The presence of copper was therefore, not found to alter the precipitation sequence by the addition of another type of precipitate at the aging temperatures investigated in this research.

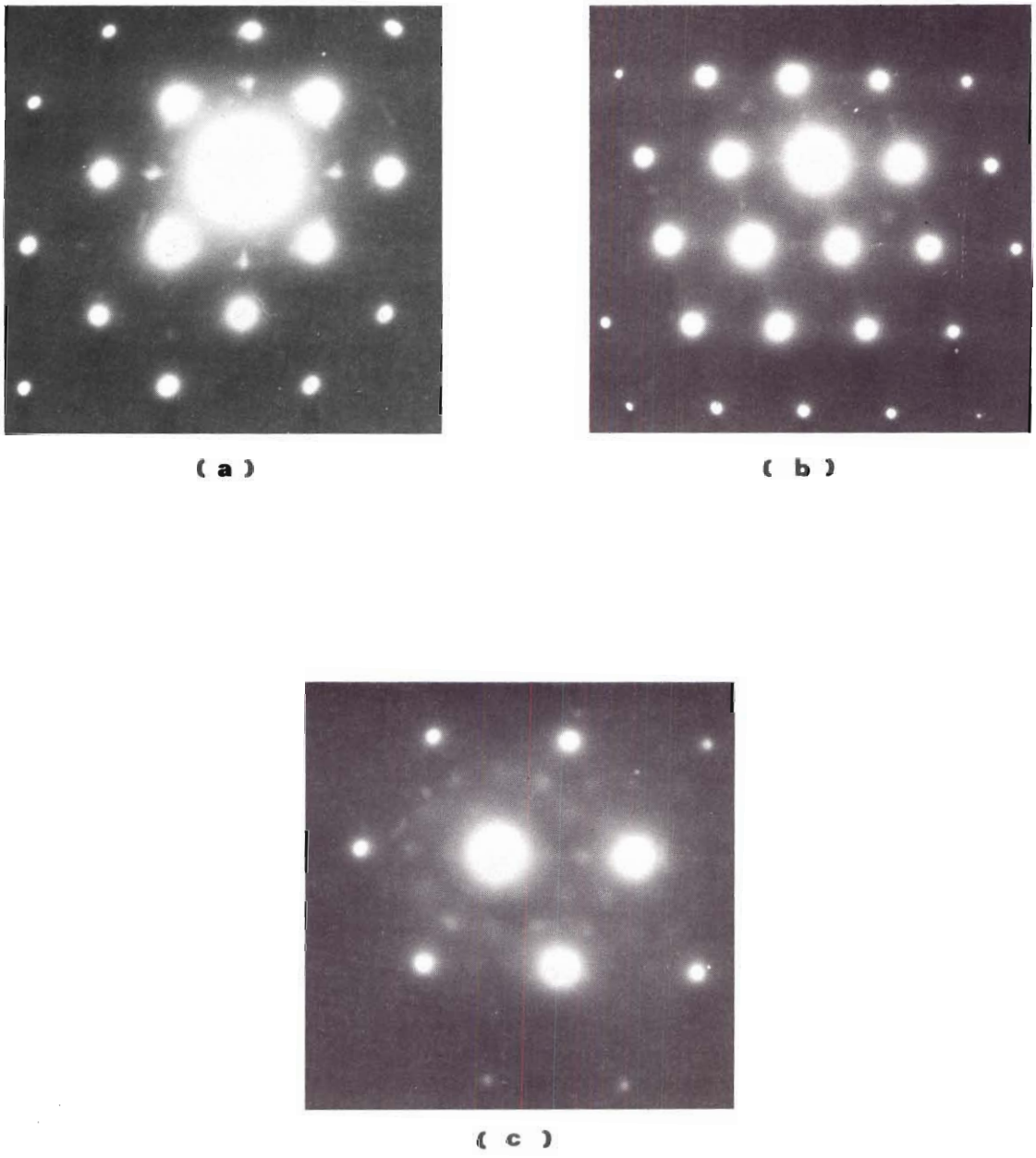

Figure 61. Selected Area Diffraction Patterns for Al-Zn-Mg Alloy Aged 24 Hours 150°C: (a)(200),(b) (220) and (c) (111) Reflections.

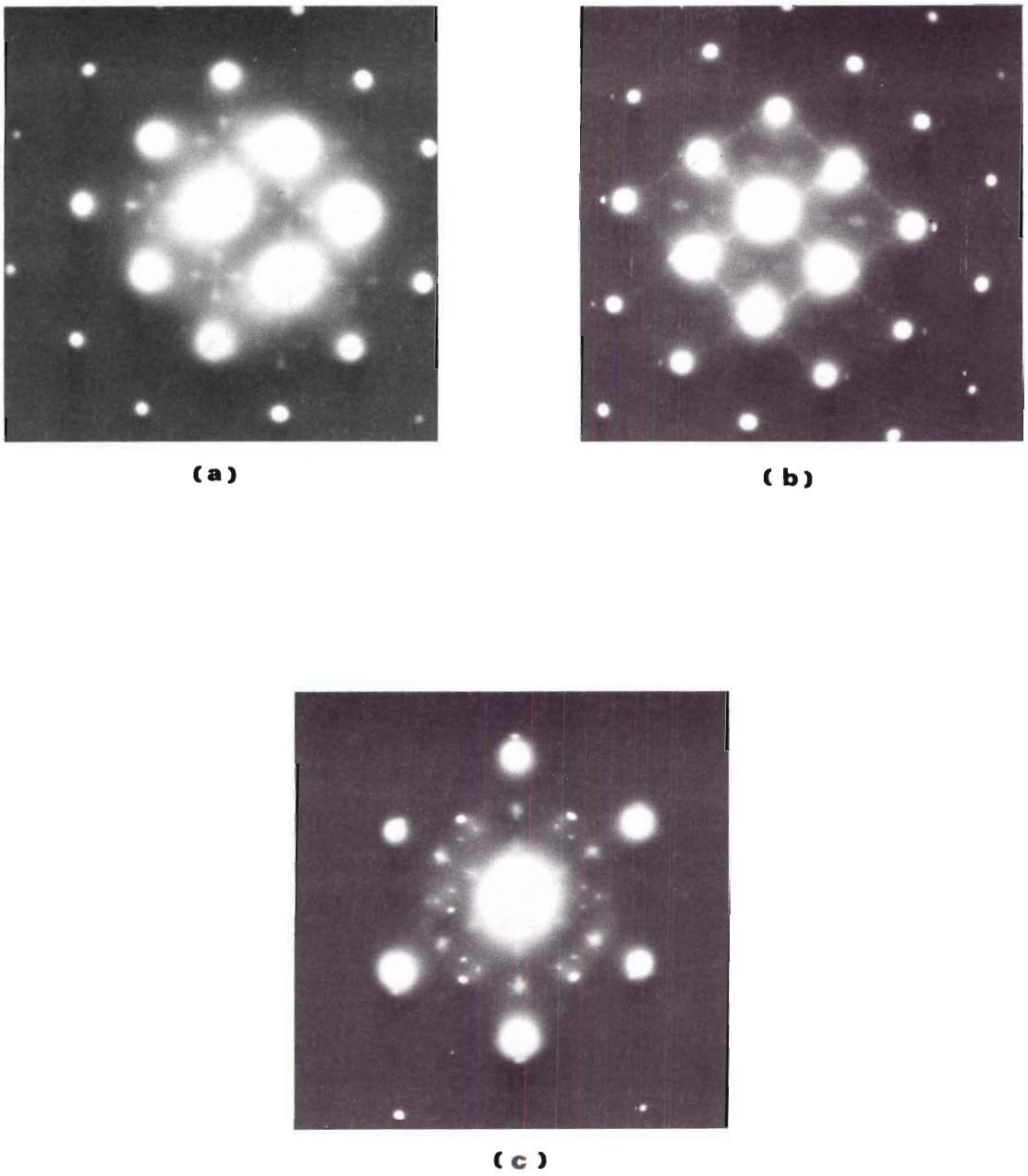

Figure 62. Selected Area Diffraction Patterns for 7050 Aged 24 Hours: (a) (200), (b) (220), and (c) (111) Reflections.

BIBLIOGRAPHY

1. W. Koster and W. Dullenkorpf, Z. Metallkunde, 28 (1936), 309.

2. D. O. Sprowls, and R. H. Brown, "Stress Corrosion Mechanisms for Aluminum Alloys," International Conference on Fundamental Aspects of Stress-Corrosion Cracking, Columbus, Ohio, (1967).

3. M. O. Speidel, "Stress Corrosion of Aluminum Alloys," Invited lecture for "Advances in the Physical Metallurgy of Aluminum Alloys II," Spring IMD Meeting, May 29, 1973. To be published in Met. Trans.

4. M. V. Hyatt, and M.O. Speidel in "Stress-Corrosion Cracking in High Strength Steels and in Titanium and Aluminum Alloys," Edited by B. F. Brown, Naval Research Laboratory, Washington, D.C. (1972).

5. S. P. Lynch, Met. Sci. J., 7 (1973) 93.

6. Morris E. Fine, "Precipitation hardening of Aluminum Alloys," Keynote Lecture for "Advances in the Physical Metallurgy of Aluminum Alloys I," Spring IMD Meeting, May 29, 1973. To be published in Met. Trans.

7. W. E. Anderson, "Fatigue of Aircraft Structures," International Met. Rev. 17 (1972) 240.

8. J. T. Staley, Alcoa Research Laboratory Report on "Exploratory Development of High Strength Stress Corrosion Resistant Alloys Usable in Thick Alloy Sections," AFML Contract F-33615-69-C-1644, and Investigation to Develop a High Strength, Stress-Corrosion Resistant Aluminum Aircraft Alloy," Naval Air Systems Command Contract N00019-70-C-0118 and N00019-69-C-0292 (1969-1974).

9. D. S. Thompson, S. A. Levy and G. E. Spangler, Metallurgical Research Division, Reynolds Metals Company Reports on "A Program to Improve the Fracture Toughness and Fatigue Resistance of Aluminum Sheet and Plate for Aircraft Applications," AFML Contract TR-73-24211. (1973).

10. M. V. Hyatt, "Program to Improve the Fracture Toughness and Fatigue Resistance of Aluminum Sheet and Plate for Airframe Applications," Technical Report AFML-TR-73-224, September, 1973.

11. F. Ostermann, Met. Trans. 2, (1971) 2897.

12. W. H. Reimann, and D.J. Deyne, "Fatigue Crack Initiation in Aluminum Alloys," Paper presented at Advancesin the Physical Metallurgy of Aluminum Alloys II, Spring IMD Meeting, Philadelphia, Pa., May, 1973.

13. W. Schutz, Aluminum 50 (1974) 271, 350.

14. W. Koster and W. Dullenkorpf, Z. Metallkunde, 28 (1936), 309.

15. W. Koster and W.Wolf, ibid, 28 (1936), 155.

16. W. L. Fink and L. A. Silley, Trans. Amer. Inst. Min. Met. Eng., 124 (1937), 78.

17. E. Butchers, G. V. Raynor, and W. Hume-Rothery, J. Inst. Metals, 69 (1943), 209.

18. A.T. Little, G. V. Raynor, and W. Hume-Rothery, ibid., 69 (1943), 423, 467.

19. E. Butchers and W. Hume-Rothery, ibid., 71 (1945) 291.

20. D. J. Strawbridge, W. Hume-Rothery, and A. T. Little, ibid., 74 (1948), 191.

21. G. Siebel, Z. Electrochem., 49, (1943), 218.

22. P. C. Varley, M. K. B. Day, and A. Sendorek, J. Inst. Metals, 86 (1958), 337.

23. M. Van Lancker, Metallurgy of Aluminum Alloys, William Clowes and Sons, Ltd., London and Beccles, 1967.

24. I. J. Polmear, J.Inst. Metals, 86 (1957), 113.

25. I. J. Polmear, ibid., 76 (1958), 24.

26. I. F. Mondolfo, N. A. Gjostein, and D. W. Levinson, Trans. AIME, 206 (1956), 1378.

27. W. Sander, and K. L.Meissner, Z. Metallkunde, 15 (1923), 181.

28. W. Sander and K. L. Meissner, ibid., 16 (1924), 12.

29. R. C. Evans, An Introduction to Crystal Chemistry, Cambridge University Press, London, 1966, 87.

30. N. F. Mott, J. Inst. Metals, 60 (1937), 267.

31. J. B. Cohen, H. Herman, Nature, 91 (1961), 63.

32. J. Gjonnes, and G. Simenson, Acta. Met., 18 (1960).

33. R. W. Gould, and E. A. Starke, Jr., Advances in X-ray Analysis, Plenum Press, Vol. 9 (1966), 57.

34. P. A. Thackery, J. Inst. Metals, 96 (1968), 228.

35. J. B. Friauf, J. Amer. Chem. Soc., 49, (1927a), 3107.

36. J. B. Friauf, Phys. Rev., 29, (1927), 35.

37. F. Laves and H.Witte, Metallwirtschaft, 14, (1935), 645.

38. F. Laves and H. Witte, Metallwirtschaft, 15 (1936), 15.

39. Y. Komura, M. Mitarai, I. Nakatari, H. Iba and T. Shimizu, Acta Cryst., B26, (1970), 668.

40. J. H. Wernick, "Structure and Properties of Some Intermediate Phases," in Physical Metallurgy, R. W. Cahn, ed., American, Elsevier, New York, (1970), pp. 229-280

41. G. B. Brook, G.I. Williams, E.M. Smith, J. Inst. Metals, 83 (1954-55), 271.

42. J. Herenguel and G. Chaudron, Metaux et Corrosion, 16 (1941), 33.

43. J. Herenguel and G. Chaudron, ibid., 18 (1943), 30.

44. J. Herenguel, Rev. Metaux, 44 (1947), 77.

45. W. A. Anderson: Precipitation fromSolid Solution, ASM, (1959), 150.

46. J. P. A. Jacquet, Compt. Rend., 228 (1949), 1027.

47. G. Bergman, J. T. Waugh, and L. Pauling, Nature, 169 (1952), 1057.

48. A. Saulnier and G. Cabane, Rev. Met., 46 (1949), 13.

49. H. Nishimura, Y. Murakani and H. Otsuji, Suiyokwai-Shi, 12 (1950), 47.

50. I. J. Polmear and P. Scott-Young, J. Inst. Metals, 87 (1958-59), 47.

51. I. J. Polmear, J. Inst. Metals, 89 (1960-61), 51.

52. W. F. Smith and N. J. Grant, Met. Trans. AIME, 2 (1970), 1333.

53. S. N. Singh and M. C. Flemings, Met. Trans. AIME, (1969), 1803.

54. L. A. Willey, "Phase Diagrams," Aluminum, Vol. I., K. R. Van Horn (ed), ASM (1967), 359-396.

55. E. Orowan, in Symp. on Internal Stress in Metals and Alloys, Inst. Metals, London (1948), 451.

56. E. Orowan, in M. Cohen (ed) Dislocation in Metals, AIME, New York (1954).

57. V. Gerold, "Precipitation Hardening" to appear in Dislocation Theory - A Collective Treatise (ed. R.F.N. Nabarro) Marcel Dekker Inc., New York, (to be published).

58. H. Haberkorn and V. Gerold, Phys. Stat. Sol. 15 (1966), 167.

59. M. Witt and V. Gerold, Z. Metallkunde, 60 (1969), 482.

60. M. Witt and V. Gerold, Scripta Met., 3, (1969), 371.

61. V. A. Phillips, Acta Met., 14 (1966), 1533.

62. L. M. Brown and R. K. Ham, Strengthening Methods in Crystals, Ed. by A. Kelly and R. B. Nicholson, Elsevier 9 (1971).

63. D. Raynor and J. M. Silcock, Metal Science J., 4 (1970), 121-130.

64. H. A. Holl, Corrosion, 23, (1967), 173.

65. N. Ryum, Acta Met., 17 (1969), 821.

66. S. P. Lynch, Metal Science J., 7 (1973), 93.

67. P. T. N. Unwin and G. C. Smith, J. Inst. Metals, 97 (1969), 299.

68. N. Ryum, Acta Met., 16 (1968), 327.

69. P.T.N. Unwin, ibid., 17 (1969), 1379.

70. I. J. Plmear and I. F. Bainbridge, Phil. Mag., 4 (1959), 1293.

71. A. J. McEvily and J. B. Clark, E. C. Utley and W. H. Herrstein, Trans. Met. Soc., AIME, 227 (1963), 1093.

72. P. J. E. Forsyth, J. Aus. Inst. Met., 8, (1963), 52.

73. C. A. Stubington, Acta. Met., 12 (1964), 931.

74. C. A. Stubington, and P. J. E. Forsyth, ibid., 14 (1966), 5.

75. A. Abel and R. K. Ham, ibid., 14 (1966), 1495.

76. H. Gleiter, ibid., 16 (1968), 455.

77. S. P. Lynch, and D. A. Ryder, Aluminum, 49, (1973), 748.

78. C. Calabrese and C. Laird, Matl. Sci. Eng., 13 (1974), 141.

79. R. F. Hanstock, J. Inst. Metals, 83, (1954-55).

80. T. Broom, J. H. Molineux, and V. N. Whittaker, ibid., 84, (1955-56), 357.

81. T. Broom, J. A. Mazza, and V. N. Whittaker, ibid., 86 (1957-58),17.

82. T. Broom, and V. N. Whittaker, Nature, 177, (1956), 486.

83. F. Seitz, Advances in Physics, 1 (1952), 43.

84. T. Broom, ibid., 3 (1954), 26.

85. D. Turnbull, in Reb. Conf. on Defects in Crystalline Solids, Physical Society (1955), 203.

86. J. B. Clark, and A. J. McEvily, Acta. Met., 12 (1964), 1359.

87. B. L. Averback, Trans. Amer. Soc. Metals, 41 (1949), 262.

88. C. Laird and G. Thomas, Intern. J. Fracture Mec., 3 (1967), 81.

89. Bela I. Sandor, Fundamentals of Cyclic Stress and Strain, University of Wisconsin Press, Madison, Wisconsin, (1972).

90. R. W. Hendricks

91. V. Gerold, "Applications of Small-Angle X-ray Scattering to Problems In Physical Metallurgy and Metal Physics," in X-Ray Small Angle Scattering, ed., by H. Brumberger, Gordon and Breuch, Publishers, New York, (1967), 277-317.

92. S. B. Chakrabortty, private communications.

93. S. N. Singh and M. C. Flemings, Trans. of the Met. Soc. of AIME, 245 (1969), 1803.

94. P. Bardhan, E. A. Starke, Jr., J. Mat. Sci., 3, (1968), 577.

95. L. Green, unpublished results.

96. J. M. Silcock, J. Inst. of Metals, 89, (1960-1961), 203.

97. G. Thomas and J. Nutting, ibid., 88 (1959-1960), 81.

98. E. H. Hollingsworth and G. C. English, ALCOA Research Laboratory Report on "Investigation of the Mechanism of Stress Corrosion of Aluminum Alloys," Naval Air Systems Command Contract N00019-67-C-0481, (1969), 29.

99. I. J. Polmear, J. Inst. Metals, 87, (1958-59), 24.

100. E. A. Starke, Jr., J. Of Metals, January, 1970.

101. P.T.N. Unwin, G. W. Lorimer and R. B. Nicholson, Acta Met., 13, (1965), 403.

102. P.T.N. Unwin and R. B. Nicholson, ibid., 1379.

103. J. D. Embury and R. B. Nicholson, ibid., 13 (1965), 403.

104. S. P. Lynch, Metal Science Journal, 7 (1973), 93.

105. N. Ryun and K. Baardseth, J. Inst. Metals, 96 (1968), 92.

106. A. J. Cornish and M.K.B. Day, ibid., 99 (1971), 377.

107. P.T.N. Unwin and G. C. Smith, ibid., 97 (1969), 299.

108. C. E. Feltner and P. Beardmore, "Achievement of High Fatigue Resistance in Metals and Alloys," ASTM STP 467, (1970), 77.

109. B. Tompkins, Phil. Mag., 18 (1968), 1041.

110. J. R. Hancock and J. P. Grosskreutz, Acta Met., 17 (1969), 77.

111. G. Kralik and H. Scheniderhan, Scripta Met., 6 (1972), 843.

112. B. Tomkins, Phil. Mag., 23 (1971), 687.

113. Morris E. Fine, private communication.

114. A. Saxena and S. D. Antolovich, to be published.

115. T. Endo and JoDean Marrow, J. of Materials, JMLSA, 4 (1969), 159-175.

116. JoDean Marrow in "Cyclic Plastic Strain Energy and Fatigue of Metals", ASTM STP, 378 (1965), 4.

117. D. J. Duquette, and P. R. Swann, "An Electron Microscopic Examination of Pre-Crack Fatigue Damage in Age Hardened Al-5.Zn-2.5Mg," Office of Naval Research Tec. Rept. 3, Contract N00014-67-A-0117-0012, NR036-093, Feb. 1974.

VITA

Thomas Henry B. Sanders, Jr. the son of Mr. and Mrs. T. Henry B. Sanders was born in Fishtown, Philadelphia, Pennsylvania on July 23, 1944. He was graduated from Atlantic City High School in Atlantic City, New Jersey and entered the Georgia Institute of Technology in January, 1963. In June, 1966 he received a Bachelor's degree in Ceramic Engineering. After graduation Mr. Sanders was employed by the Advanced Casting Technology Section of the Materials Development Laboratory of Pratt and Whitney Aircraft in East Hartford, Connecticut.

In September, 1967 he returned to Georgia Tech to persue graduate study in the department of Ceramic Engineering. While completing the research requirements Mr. Sanders enrolled in the Advanced ROTC program. In September 1970 he was awarded the Master's Degree and was subsequently commissioned a Reserve Second Lieutenant in the Chemical Corps of the U. S. Army. During the ensuing years he entered the Department of Chemical Engineering and Metallurgy to study and conduct research in the area of Physical Metallurgy. He attended the Chemical Officers Basic Course at Fort McClellan, Alabama and was platoon leader for the 401st Chemical Company, USAR, Chamblee, Georgia. Currently, he is an engineer with the Physical Metallurgy Division of Alcoa Laboratories.

Mr. Sanders has actively participated in the student chapters of the American Ceramic Society, Keramos (Ceramic Engineering Honorary)

and A.S.M.-A.I.M.E. He is also a member of Sigma Xi and the American Crystallographic Society. As an undergraduate he was a member of the Fraternity of Phi Gamma Delta.